APATITE AND ZIRCON (U-TH)/HE CONSTRAINTS ON THE EXHUMATION HISTORY OF PUERTO RICO

by

Yomayra A. Román Colón

A thesis submitted in partial fulfillment of the requirements for the degree of

MASTER OF SCIENCE
in
GEOLOGY

UNIVERSITY OF PUERTO RICO
MAYAGÜEZ CAMPUS
2014

Approved by:

_____	_____
Aaron Cavosie, Ph.D. Graduate Committee, chair	Date
_____	_____
Daniel Stockli, Ph.D. Graduate Committee, member	Date
_____	_____
Hernán Santos, Ph.D. Graduate Committee, member	Date
_____	_____
Ivette Cruzado, Ph.D. Office of Graduate Studies Representative	Date
_____	_____
Lizzette A. Rodríguez Iglesias, Ph.D. Department of Geology, Director	Date

ABSTRACT

The island of Puerto Rico preserves a complex volcanic arc history. Paleogeographic reconstructions of Puerto Rico during the evolution of island arc magmatism have been illustrated in diverse models as a combination of complex multi-stage volcanism, eustatic fluctuations and tectonic changes across the three main igneous provinces; southwest, central and northeast. However, the timing of their accretion, the temporal and thermal interaction of the three igneous provinces, and the upper crustal response to paleo-stress fields produced by subduction and collision during the Late Eocene to Early Miocene are not well constrained. In order to better understand and constrain these fundamental processes this research employs an (U-Th)/He low temperature thermochronometric approach using accessory minerals like zircon and apatite from different plutonic bodies strategically located along the three igneous provinces of Puerto Rico and also from neighboring islands. (U-Th)/He zircon data suggest that the earliest major exhumation phase started during the Early Eocene in southwestern Puerto Rico at ~55 Ma and at ~49 Ma in the northern and central section of Puerto Rico. This exhumation phase may be recording the collision of the Caribbean plate with the Bahamas Bank. A smaller thermal signature is recorded by zircon at ~41 Ma during the Middle Eocene and was identified on both the east and the west sides of the island where exhumation reached maximum rates. During the Middle Eocene exhumation, cooling ages are progressively younger to the south. This suggests that the paleo-north section of the island experienced faster cooling and similar exhumation rates due to the proximity to the northern collisional arc boundary. Calculated exhumation rates vary by location and time. Assuming a typical geothermal gradient (20°C/km) calculated exhumation rates range from 0.34-0.15 km/Myr. Islands east of Puerto Rico (Culebra, Vieques and the British Virgin Islands) record apatite cooling ages of ~20 Ma (Early Miocene), younger than most apatite He ages in Puerto Rico. These younger cooling ages may be explained by either the final stages of arc magmatism in the eastern Greater Antilles, or alternatively, an early episode of rifting by right-lateral transtension in the Virgin Islands platform. These findings provide new insights on post volcanic tectono-thermal events marked by the Eocene collision of the Caribbean plate with the Bahamas Bank, the eastward migration of volcanism, later island structural arrangements and the onset of the Muertos Trough southern subduction zone.

RESUMEN

La isla de Puerto Rico preserva una compleja historia de arco volcánico. Las reconstrucciones paleogeográficas de Puerto Rico durante la evolución del arco de isla han sido ilustradas en diversos modelos, como una combinación de múltiples etapas volcánicas, fluctuaciones eustáticas y cambios tectónicos ocurridos a través de las tres principales provincias ígneas; suroeste, centro y noreste de la isla. Sin embargo, el tiempo de acresión, la interacción temporal y termal de estas provincias y la respuesta de la corteza superior al paleo-estrés producido por la subducción y colisión durante el Eoceno Tardío al Mioceno Temprano no han sido bien determinadas. Para poder entender y delimitar estos procesos, este proyecto presenta un nuevo enfoque utilizando minerales accesorios como el zircón y la apatita provenientes de los distintos cuerpos plutónicos que se encuentran estratégicamente localizados a lo largo de las tres provincias ígneas. La data obtenida por el método de (U-Th)/He en cristales de zircón sugiere que el primer episodio de exhumación comenzó en el suroeste de Puerto Rico durante el Eoceno Temprano hace ~55 millones de años y hace ~49 millones de años en la sección norte y central. Esta fase de exhumación pudiera estar grabando la collisión de la placa del Caribe y el Banco de las Bahamas. Una señal más pequeña fue grabada en el zircon durante el Eoceno Medio y fue identificado en ambos extremos de la isla (este y oeste) donde la exhumación alcanzó su razón máxima cerca de los ~41 millones de años. Durante el Eoceno Medio, las edades de exhumación por enfriamiento son más jóvenes hacia el sur de la isla. Esto sugiere que la región paleo-norte de Puerto Rico experimentó rápido enfriamiento y razones similares de exhumación como resultado a la proximidad a la collisión al norte de la isla. La razón de exhumación varían por localidad y tiempo. Asumiendo un gradiente geotérmico de (20°C/km) se obtuvieron rangos de exhumación de 0.34-0.15 km/Myr. Las islas al este de Puerto Rico (Culebra, Vieques y las Islas Vírgenes Británicas) grabaron edades de ~20 millones de años (Mioceno Temprano) más jóvenes que muchas de las edades de apatite en Puerto Rico. Estas edades más jovenes de enfriamiento pueden ser explicadas por etapas finales de arco magmático en el este de las Antillas Mayores ó por un episodio temprano de “rifting” por transtensión en la plataforma de las Islas Vírgenes. Estos descubrimientos proveen un nuevo ángulo en los eventos volcánicos y tectónico-termales ocasionados por la collisión de la Placa del Caribe con el Banco de las Bahamas durante el Eoceno,la migración del volcanismo hacia el este y los cambios estructurales de la isla y el comienzo de la subducción al sur de la isla en Caja de Muertos.

DEDICATION

To my husband and family for their unconditional love and support.

ACKNOWLEDGEMENTS

I would like to thank many people who helped and supported me during my research project. First, my deepest gratitude goes to my research advisor, Dr. Aaron Cavosie, for this great opportunity and his encouragement and guidance for the past years. Special thanks to my committee members, Dr. Daniel Stockli and Dr. Hernán Santos for their collaboration and support during the writing process. My special thanks are extended to Dr. Johannes Schellekens (R.I.P.) for discussions and suggestions.

This research project was funded by several institutions including the Geology Department of the University of Puerto Rico-Mayaguez, the University of Kansas-Lawrence and the University of Texas-Austin. Special thanks to Dr. Luis González for funding my tuition at Kansas University. In addition, funding was also provided by Exxon Mobil for travel expenses to the University of Kansas during the spring of 2009. I am particularly grateful to the staff and graduate students of the Geology Department at the University of Kansas and the University of Puerto Rico for providing laboratory and field assistance, particularly to Roman Kislitsyn, Timmons Erickson, Raiza Quintero, Francis Pérez, Yadira Soto and Samuel Pacheco. I would like to extend my gratitude to Edgardo Pujols for his constant support and encouragement, discussions and assistance in the lab and the field. Finally, thanks to my parents for their unconditional support and sacrifices to ensure that I had an excellent education.

TABLE OF CONTENTS

Introduction

This Master Thesis contains one chapter that has been written in manuscript format for submission to a geologic scientific jounal. This study has several coauthors that have provide assistance with data interpretation and data analyses whereas I have completed the major analytical and writing components of the thesis myself. The coauthors are Dr. Aaron Cavosie (University of Puerto Rico-Mayaguez), Dr. Daniel Stockli (University of Texas-Austin) and Edgardo Pujols (University of Texas-Austin). The chapter provides new insights on the Cenozoic thermal history of Puerto Rico and nearby islands by taking advantage of He thermochronometric analysis performed on plutonic rocks. The motivations were to provide new information on the post-magmatic history of the northeastern Caribbean island arc by correlating the lower temperature cooling paths (~180-0^{o}C) to exhumational and hydrothermal events induced by tectonic drivers. In simple terms, this method can date uplift and cooling of rocks as they get closer to the surface of the Earth.

The modeled He data provided here refine current tectonic models and offer new constraints on the timing and rates of exhumation of the different igneous blocks, allowing for a more complete reconstruction and identification of structural heterogeneities by comparing thermal paths. A total of 29 samples from plutonic intrusions along the three main igneous provinces of Puerto Rico as well as samples from Culebra, Vieques and the British Virgin Islands were collected and analyzed using zircon and apatite He thermochronology. This technique takes advantage of the thermally activated diffusion of radiogenic ^{4}He out of apatite and zircon crystals. (U-Th)/He zircon data recorded multiple exhumational phases associated first with the Bahamas Bank

collision against the Caribbean plate in the Early Eocene at ~55 Ma in the southwestern region and ~49 Ma in the northern and central section of Puerto Rico. A second cooling phase in the Middle Eocene at ~41 Ma in the south central igneous province is recognized and can be associated with the last stages of collisional exhumation. Apatite, a lower temperature thermochronometer, records a cooling window (~30- 20 Ma) associated with subduction to the south during the Early Oligocene to Early Miocene and its possible northern flexural responses. Additionally this data set provides valuable information for hydrocarbon maturation in the island since the temperatures recorded by apatite and zircon are near the catagenesis window.

The main technique used in this research to acquire the time-temperature paths from multiple rocks was Low-Temperature (U-Th-Sm)/He Thermochronology. It is called "Low-Temperature Thermochronology" because the minerals used as thermochronometers only cover a range of temperatures lower than 200^{o}C which are consider low compared to igneous and methamorphic processes. Radiogenic Helium is a by-product of the U-Th-Sm alpha decay schemes and the knowledge of the diffusion behavior as a function of temperature. The method takes advantage of the mineral (i.e. apatite or zircon) capacity to retain radiogenic Helium inside the crystal. The temperature range, which translates to a closure temperature (Tc), is determined by multiple step heating experiments in the laboratory and the linear relationship between temperature and diffusion (Arrhenius plot).

The geological applications of He thermochronology are many since the minerals present today at the surface experienced different temperatures in the past associated with plate tectonic interactions. The temperatures endured will range according to their

igneous crystallization and metamorphic history and ultimately the rock's path to the surface. The two thermochronometers used, apatite and zircon, record different "helium ages", when the temperature is lowered enough for helium retention. This allows both time and temperature information from these minerals to be determined. When the two thermochronometers are combined (apatite Tc = 70^{o} C and zircon Tc =180^{o} C) the different temperatures and time recorded and inferred geologic processes calculated cooling rates. Assuming that the rate of cooling the rock experienced was constant, the path between two thermocronometers or any other two-time temperature constraints is known as monotonic-cooling.

Many processes can heat or cool the crust and therefore reset the He age of minerals, like exhumation (vertical movement and erosion of a rock mass) and the intrusion of dikes and plutons in the crust that can lead to hydrothermal events and can change regional temperature gradients. These processes tend to occur at fairly distinctive cooling rates. For example, faulting has cooling rates an order of magnitude higher than passive erosion or isostatic re-equilibration. Cooling rates of plutonic rocks depend on their composition and volume but are usually extremely fast compared to the other process mentioned above. Calculated cooling rates (^{o}C/My) can be translated to exhumation rates (km/My) by means of assuming a geologically reasonable geothermal gradient (^{o}C/km). As geothermal gradients can vary though time, we use a range of geothermal gradients to explore time-temperature paths. Temperature increases with depth in the crust by radioactive decay and primordial heat and it tends to do that mostly on a linear fashion (geothermal gradient). Therefore, a mineral experiencing temperatures above the He closure temperature would not retain radiogenic Helium until it stars

cooling or moving up in the crust by exhumational processes. A rock being exhumed will pass through different isotherms; the less sensitive minerals (high Tc) like zircon will record deeper levels and older ages and more sensitive minerals (low Tc) shallower levels and younger ages. The final result is a time-temperature history that can be used to infer reasonable tectonic processes according to cooling rates or exhumational rates.

CHAPTER 1

APATITE AND ZIRCON (U-TH)/HE CONSTRAINTS ON THE EXHUMATION HISTORY OF PUERTO RICO

1. INTRODUCTION

Puerto Rico is a complex island arc located in the northeastern Greater Antilles and forms part of the Puerto Rico-Virgin Islands microplate (PRVI) (Larue, 1994; Mann et al., 2005). The island arc has undergone significant tectonic and igneous modifications since its origin, which remains controversial (Erikson et al., 1990; Jolly et al., 2007). There is general agreement that after the Eocene oblique-collision of the eastern Greater Antilles with the Bahamas Bank, igneous activity in Puerto Rico ceased and a different phase of deformation in the island initiated (Erikson et al., 1990; Mann et al., 2005).

Paleogeographic reconstructions of Puerto Rico during the evolution of island arc magmatism have been shown in various models that feature subduction polarity reversals, multiple stages of volcanism, eustatic fluctuations and tectonic changes across the three main structural provinces of the island (Dolan et al., 1991; Pindell, 1994; Jolly et al., 2007). However, many aspects of the active arc and post-arc history of Puerto Rico remain poorly constrained, including the timing of province accretion, their temporal interactions, and how the three provinces responded to upper crustal stress fields and subduction from the Eocene to the Miocene.

The motivation of this work is to provide constraints on the timing of the major tectonic events that affected Puerto Rico in the final stages of island arc evolution. This study applies the apatite and zircon He thermochronometers to a variety of plutonic and volcanic rocks in the three igneous provinces of Puerto Rico and neighboring islands to establish the low temperature thermal history of the island, and more broadly the northeastern Greater Antilles. These thermochronometric systems provide new temporal

and thermal insights on the tectonic variations and interactions of the three main provinces.

The objectives of this study are to use these new data to explore the post-volcanic history of Puerto Rico to provide new insights on: (1) the timing of exhumation and block interaction along the three igneous provinces, (2) the tectonic history of the island as a whole using the thermal and temporal data in a spatial context, (3) thermal signatures recorded in plutonic rocks derived from major tectonic events, and (4) the timing and rates of cooling of intrusive rocks in the island as determined by an array of 1-D cooling models.

2. GEOLOGIC BACKGROUND

2.1. Tectonic models for the origin of Puerto Rico

Puerto Rico is formed from subduction-related volcanism in a Cretaceous island arc located in the eastern Pacific (Pindell, 1993; Jolly et al., 2007). The history of the arc is often explained as a consequence of a subduction polarity reversal event that transformed a north-dipping subduction system in the eastern Pacific to a southwestern-dipping subduction system, although the timing of this event is debated (Pindell, 1993; Fig.1). Island arc volcanism began in the Aptian and continued until the Early Eocene, when subduction was interrupted at the northern part of the island arc (Jolly et al., 1998a). Larue (1994) and Smith et al. (1998) suggested a change in plate motion direction and tectonic evolution of the Caribbean Plate by the Paleogene. Regardless of the paleogeographic location of Puerto Rico during the initiation of arc magmatism, it is generally accepted that the cessation of arc volcanism was caused by the Eocene collision

of the Caribbean Plate with the non-subductable thickened oceanic lithosphere of the Bahamas Bank (Glover, 1971; Speed et al., 1991; Pindell, 1994). The Bahamas Bank collision is recorded in Puerto Rico during the Late Eocene, where most of the deformation was localized along the Northern and Southern Puerto Rico fault zones (Mann et al., 2005; Fig. 2). Left-lateral motion and thrust faulting accommodated deformation throughout the Eocene. It was later followed by the deposition of a carbonate platform along the northern and southern margins of the island that marked the end of volcanism in Puerto Rico (Late Eocene) and the northern Virgin Islands (Late Oligocene to Late Miocene). Following the initial Hispaniola-Bahamas collision, western Puerto Rico experienced north-south extension accompanied by a 25° counterclockwise rotation of the Puerto Rico-Virgin Islands microplate and right lateral shear along the Anegada Passage (Mann et al., 2005). Different Caribbean tectonic models have been proposed to explain the collisional history in Puerto Rico during the Paleogene. Laó et al. (2012) proposed a thrust emplacement mechanism for the Monte del Estado and Río Guanajibo serpentinite belts in southwestern Puerto Rico, during the Maastrichtian-Paleocene based on structural and stratigraphic relations. In addition, evidence was presented for a younger transpressional event in the Cerrillos belt during Late Eocene-Early Oligocene (Laó et al., 2012). Deformation during Middle Eocene-Early Oligocene through the Southern Puerto Rico Fault Zone (SPRFZ) in central southern Puerto Rico by left-lateral transcurrent faulting has also been proposed (Erikson et al., 1990). Most deformational events during the Late Eocene to Middle Oligocene are associated with strike-slip motion along the Northern and Southern Puerto Rico fault zones (Mann et al., 2005). The ages of slip on these large fault systems are only constrained to Eocene or prior time using bio-

stratigraphic relationships (Glover, 1971; Erikson et al., 1990; Mann et al., 2005) (Fig. 2). More precise constraints are hindered by the lack of post-Oligocene deformation and the development of the northern transgressive carbonate sequence (Glover, 1971; Erikson et al., 1990; Jolly et al., 1998a).

2.2. Igneous Provinces of Puerto Rico

Puerto Rico preserves a ~80 Myr record of island arc construction from the Albian to Eocene (112-45 Ma) (Jolly et al., 1998a). The island consists of pre-arc Jurassic oceanic crust and Cretaceous-Eocene, volcaniclastic and sedimentary sequences, which were intruded by plutons during the Santonian to Eocene (85-38 Ma) (Smith et al., 1998; Pérez, 2008). The terminology of Schellekens (1998b) and Pérez (2008) was used for describing the three major structural blocks of Puerto Rico: The Southwestern, Central and Northeast Igneous Provinces. The three provinces are divided by two major left-lateral fault zones: the Northern Puerto Rico Fault Zone (NPRFZ) and the Southern Puerto Rico Fault Zone (SPRFZ) (Fig.2).

2.2.1 Southwestern Igneous Province (SIP)

The Southwestern Igneous Province is distinguished from the other igneous provinces due to the occurrence of a serpentinite-hosted mélange called the Bermeja Complex that predates the island arc (Schellekens, 1998a). The Bermeja Complex contains the oldest rocks reported in Puerto Rico, including radiolarian chert, serpentinized peridotite, amphibolite, mid-ocean rich basalt, and arc-related volcanic and sedimentary strata (Jolly et al., 1998a; Fig. 3). Pelagic cherts in the Bermeja Complex are interpreted to have originated in the eastern Pacific (Farallon plate) (Mattson, 1960; Montgomery et al.,

1994); radiolarian species found in the chert range in age from Pliensbachian to Turonian (Montgomery et al., 1994; Schellekens, 1998a). Radiometric ages from Bermeja Complex amphibolites yield a K-Ar hornblende age of 126 ± 3 Ma (Cox et al., 1977). Hornblende K-Ar ages of 110 ± 3.3 Ma, 86.3 ± 8.6 and 84.9 ± 8.5 Ma from the Bermeja Complex rocks were reported by Tobisch (1968) and interpreted as reset ages.

Volcanic strata of southwestern Puerto Rico are composed of plagioclase-augite-hornblende-bearing tuff, basaltic andesite and andesite lavas (Jolly et al., 2007; Fig. 3). The earliest onset of arc volcanism is recorded by the Maguayo porphyry, an andesite stock (Fig. 2) yielding K-Ar and Ar-Ar hornblende ages of 86.1 ± 2.1 Ma (Cox et al., 1977; Schellekens, 1998b). Jolly et al. (2007) proposed that southwest Puerto Rico represents an arc fragment with an origin unrelated to the Central and Northeastern Igneous Provinces, and further, that the polarity of subduction in southwest Puerto Rico was northeast-dipping. This interpretation is based on the presence of high-Mg andesites and hornblende-bearing lavas, which require the incorporation of a slab melt component (Jolly et al., 2007).

2.2.2 Central Igneous Province (CIP)

The Central Igneous Province is characterized by volcanic strata and plutons; it contains the most extensive area of exposed igneous rocks in Puerto Rico (Smith et al. 1998). The province preserves a record of magmatism ranging in age from Early Cretaceous to Eocene, and is bounded by the largest granitoid intrusions on the island, the San Lorenzo and Utuado batholiths (Fig. 2). Pérez (2008) reported U-Pb zircon ages and oxygen isotope ratios ($\delta^{18}O$) for whole rock, zircon, quartz and titanite for most of the

plutonic rocks in the CIP. According to Pérez (2008), plutonism in the province began during the Santonian (Coamo Arriba stock, 85.6 ± 1.3 Ma; Morovis and Ciales stocks, 85.3 ±1.8 Ma and 83.9 ± 1.7 Ma, respectively). The San Lorenzo and Utuado batholiths were intruded along opposite sides along the margins of the CIP during the Campanian-Maastrichtian. The San Lorenzo batholith yields zircon (U-Pb) ages of 75.1 ± 2.1 Ma (granodiorite) and 74.1 ± 1.4 Ma (quartz diorite) while Utuado granodiorite yields a slightly younger age of 70.8 ± 1.2 Ma. Two granodiorite plutons near the San Lorenzo batholith, the Vieques and Caguas plutons (67.1 ± 1.6 Ma and 66.8 ± 1.2 Ma) were identified as belonging to the CIP based on geochemical and age similarities (Fig. 2) (Pérez, 2008). Igneous activity in the CIP ended in the Eocene with the intrusion of the Cuyón and Barranquitas stocks at 47.6 ± 0.8 Ma and 47.7 ± 1.6 Ma, respectively (Pérez, 2008).

2.2.3 Northeastern Igneous Province (NIP)

The northeastern province is characterized by a volcanic sequence ranging from Late Cretaceous to Early Paleogene and contains few plutonic rocks. It is separated from the CIP by the southeast trending Northern Puerto Rico Fault Zone (NPRFZ) (Jolly et al., 1998a; Fig. 2). During the Santonian, left-lateral faulting assembled the Central and Northeastern provinces; the Santonian displacement age of the San Francisco-Cerro Mula fault was established by geochemical similarities of the volcanic rocks of both provinces (Jolly et al., 1998a). The NIP is highly folded and faulted; additionally a number of strike-slip faults are present dividing the block in three domains (Jolly et al., 1998b). Younger units are located toward the west in the NIP, consisting of volcaniclastic

successions with a variety of compositions ranging from basalt to rhyolite. The volcanic rocks were intruded by the Río Blanco pluton at 47.7 ± 2.1 Ma (Pérez, 2008), the only large pluton in the NIP.

3. SAMPLES AND METHODOLOGY

(U-Th)/He thermochronology is a powerful tool with multiple geomorphic and tectonic applications (House et al., 1999; Farley, 2000; Reiners, 2005; Stockli, 2005). The technique analyzes ^{4}He emitted from parent isotopes ^{238}U, ^{235}U, ^{232}Th, and ^{147}Sm in minerals and the understanding of thermally-activated volume diffusion of alpha decay particles from different thermochronometers (Dodson, 1973; Zeitler, 1987; Farley, 2000; Reich et al., 2007). A cooling history, once modeled, can provides ages that are dependent on a variety of geologic processes, such as exhumation, cooling, and hydrothermal alteration (Dunai, 2005; Ehlers et al., 2005; Ketcham, 2005).

3.1. Sample description

The zircon and apatite He thermochronometers were employed because these minerals are common in intermediate to felsic plutonic rocks and they have low (U-Th)/He closure temperatures (i.e. zircon ~180°C and apatite ~ 70°C), which makes them highly sensitive to thermal changes in the upper crust (Farley, 2000; Reiners et al., 2004). In order to understand one-dimensional time-temperature paths in exhumed rocks, this study includes igneous rock samples distributed among the three igneous provinces. Twenty-nine samples representing twenty-four igneous rocks from the SIP, CIP, and NIP of Puerto Rico, and also samples from the neighboring islands of Culebra, Vieques and

the British Virgin Islands (BVI) were collected for mineral separation (Fig. 2; Table 1). The samples are distributed as followed: Puerto Rico (n=22); [SIP (n=9), CIP (n=12), NIP (n=1)], Culebra (n=2), Vieques (n=1), and BVI (n=4). Of the 29 samples, 18 yielded sufficient material to be able to analyze both zircon and apatite. Eight samples only yielded zircon, and three samples only yielded apatite. In Summary, (U-Th)/He ages from 26 zircon and 21 apatite samples were obtained. The error in age assigned to each aliquot is 6% for apatite and 8% for zircon. This is based on the ages and the number of aliquots (*N*). Age standards used are the Fish Canyon Tuff (FCT) zircon with an age of 27.9 Ma ± 8% and the 05XIE87 Xainza rift apatite (Southern-Tibet) with an age of 7.5 Ma ± 6% (Villeneuve et al., 2000; Reiners et al., 2002). The error applied for the final (U-Th)/He age in zircon or apatite ages is 2 standard error (SE) by the equation ($2*SE = 2*\sigma/\sqrt{N}$).

3.2. He Thermochronology

At least three zircon and apatite grains were analyzed from each sample to evaluate reproducibility of He age; individual crystals constitute a single measurement. Inclusion free-crystals of approximately 75-150 μm in width with a proportional surface to volume ratio were photographed for subsequent alpha ejection correction and inserted into 1mm Pt tubes (Farley et al., 1996; Reiners et al., 2001; Hourigan et al., 2005). Aliquots were degassed by a Nd-YAG and diode laser at temperatures over 1000°C in a vacuum. The ^{4}He extracted is spiked with ^{3}He and passed through a cryogenic trap where it is purified and concentrated; He with a known ^{4}He/^{3}He ratio is then added. The remaining sample is analyzed by a quadrupole mass spectrometer after ^{4}He-degassing. Concentrations of parent isotopes ^{238}U, ^{335}U, ^{232}Th and ^{147}Sm were measured by an Element2 HR-ICP-MS.

Aliquots in a diluted state are spiked with known quantities of ^{235}U, ^{230}Th and ^{147}Sm and analyzed in solution. Mineral separation and analytical work were conducted at the University of Kansas in the Isotope Geochemistry Laboratory (IGL) and the University of Texas at Austin in the (U-Th)/He Geo- and Thermochronometry Laboratoy. Various aliquots were excluded from the analysis due to analytical procedure errors, broken or loss grains, visible and suspected inclusions (high He ncc counts) and under- or over-spiking (lower or higher ^{235}U, ^{230}Th and ^{147}Sm ratios) of the solution. Other grains were unsuitable because of their high Ue concentrations (metamict grains) and small grain size (small ESR values) both proven to have an effect on diffusion kinetics (Nasdala et al., 2001; Farley, 2000), and therefore were not representatives of the closure temperature of the general population.

3.3. Inverse Modeling of (U-Th)/He ages

Inverse modeling was done using the *He*lium *M*odeling *P*rogram (HeMP) developed at the University of Kansas by Hager (2009). The software uses a series of statistical and numerical solutions to predict the evolution of a thermochronometric system as a function of time and temperature (Ketcham, 2005). One useful approach in thermochronology for thermal history identification is to fit a modeled time-temperature path to the obtained (U-Th)/He ages. This can be accomplished by vertical profiling along a fault slip direction using a single thermochronometer for fault initiation and exhumation. If two thermochronometers are available (i.e. zircon and apatite) from a single rock sample, such as the 18 samples from this study, one-dimensional inverse modeling can provide

feasible time-temperature paths for a particular area. Other thermal and temporal constraints from U-Pb or Ar-Ar ages can be added for a complete thermal reconstruction.

4. RESULTS

4.1. (U-Th)/He zircon and apatite ages

Southwestern Igneous Province

The oldest (U-Th)/He ages for the SIP are recorded in arc-related rocks in the Bermeja Complex (Fig. 9; Table 2). Zircons from Lajas Formation andesite (55.5 ± 4.4 Ma), Maguayo Porphyry (54.3 ± 4.3 Ma), detrital zircons in the Cotui limestone (50.1 ± 4.0 Ma, Hormigueros Porphyry (51.4 ± 4.1 Ma) and Las Tunas stock (49.2 ± 3.9 Ma) all yielded similar Early Eocene (U-Th)/He ages ranging from 55-49 Ma (Fig. 5; Fig. 7; Fig. 9). The Tibes pluton and a felsic dike near Mayagüez (Bo. Río Cañas) record zircon He ages of 43.3 ± 3.5 Ma and 38.9 ± 3.1 Ma, respectively.

^{4}He ages for apatite are more variable in the SIP. The Maguayo Porphyry yielded the oldest apatite He age in this study (52.2 ± 3.1 Ma), and also the only Early Eocene apatite age. Two other samples from the SIP, the Tea Road diorite (34.0 ± 2.0 Ma) and the Mayagüez felsic dike (34.4 ± 2.1 Ma), yielded ages at the Eocene-Oligocene boundary; the Las Tunas stock (31.0 ± 1.9 Ma) and the Hormigueros Porphyry (29.8 ± 1.8 Ma) both yielded Early Oligocene ages (Fig. 6; Fig 8; Fig; 9).

Central Igneous Province

The CIP records a progressive decrease of zircon He ages from north to south, including ages of 56.5 ± 4.5 Ma (Morovis stock), 49.0 ± 3.9 Ma (Ciales stock), 49.0 ± 3.9 Ma, 43.5 ± 3.5 Ma and 41.5 ± 3.3 Ma (Rio Grande pluton: 08RG-02; 08RG-01; 08RG-03), 40.2 ± 3.2 Ma (Caguas stock), 34.7 ± 2.8 Ma (San Lorenzo batholith; 06SL-03) and 33.9 ± 2.7 Ma (Cuyón stock) (Fig. 5; Fig. 7; Fig. 9). Three samples from the Utuado Batholith (Fig. 4) yielded ages of (47.8 ± 3.8 Ma; 08UP-03), 42.3 ± 3.4 Ma (06UP-02) and 41.6 ± 3.3 Ma (09UP-07). In contrast to the SIP, all apatite ages from the CIP are Oligocene or younger; no Eocene apatite He ages were found in the CIP. Five apatite samples from across the CIP yielded a narrow range of Oligocene ages from 32.1 -29.3 Ma. An additional six apatite ages from the CIP range from 26.1-10.4 Ma. These younger ages are interpreted as cooling ages that record localized deformation events rather than regional tectonics, as the samples that yielded "young" He apatite ages are all from rocks that preserve deformation or were sampled from plutons that locally record older He ages in other samples from the same intrusion.

Northeastern Igneous Province

The Rio Blanco pluton, located in the NIP yielded an Eocene zircon cooling age of 40.5 ± 3.2 Ma and an age of 25.9 ± 1.6 Ma for apatite (Fig. 9).

Culebra and Vieques Islands

The islands of Vieques and Culebra recorded Oligocene and Miocene He ages. The Vieques pluton has a zircon He age of 29.4 ± 2.3 Ma and the Culebra stock has an age of

33.1 ± 2.6 Ma; (09IC-23) (Fig. 7). For apatite, Culebra yielded ages of 29.7 ± 1.8 Ma; (07IC-04) and 19.0 ± 1.1 Ma; (09IC-23) (Fig. 8).

British Virgin Islands

The youngest zircon He ages in this study were recorded from the Virgin Islands batholith, where all ages were Late Oligocene (27.1-23.5 Ma). Tortola and Norman Island yielded zircon He ages of 25.0 ± 2.0 Ma and 27.1 ± 2.2 Ma (Fig. 9). A granodiorite from Virgin Gorda yielded ages of 23.5 ± 1.9 Ma and 24.9 ± 2.0 Ma, respectively (Fig. 2; Fig. 9). Virgin Gorda and Tortola granitoids record Miocene apatite ages of 21.6 ± 1.3 Ma and 17.7 ± 1.1 Ma, respectively (Fig. 9).

4.2. Inverse Modeling of (U-Th)/He ages

The cooling history of a particular sample is presented as a "field" on the HeMP modeled data, showing all viable time/Temperature paths constrained by the two thermochronometers (apatite and zircon) with their respective closure temperatures. Figures 13 illustrates the upper portion of the modeled data (<400°C) since this shows the most recent thermal history. Initial age constraints were set according to U-Pb zircon and K-Ar ages (Cox et al., 1977; Pérez, 2008). Final boundary constraints were set to 10°-0°C at the surface today. The inverse modeling graph for the Maguayo Porphyry in the SIP show a path of fast cooling between ~54-52 Ma (Fig. 13). Las Tunas and Hormigueros samples both share the same cooling history from ~ 50 Ma to 30 Ma which average a cooling rate of ~5.5°C/Myr (Fig. 9; Fig. 12). The CIP shows an even cooling history along the main bounding northeastern fault or Northern Puerto Rico Fault zone

(NPRFZ). There, (Utuado, Ciales, Morovis, Rio Grande and Coamo pluton) cooling rates (~5.8°C/Myr) overlapped from ~49 Ma (Early Eocene) to ~30 Ma (Early Oligocene). The cooling histories of the other samples in the southern CIP do not seem to overlap temporally or spatially. On the British Virgin Islands, fast cooling rates tend to overlap from Middle Oligocene to Early Miocene (Fig. 9).

The HeMP one-dimensional modeling was used because it provides every possible time-temperature path for a given rock. The modeling fills the unknown time-temperature gap between thermochronometers, providing a complete viable cooling history. A geothermal gradient is added to this cooling history to interpret the rock depths and how long it took for the rock to reach certain isotherms (cooling/exhumation rates) and ultimately the surface. In other words, it records where and at what temperature the rock was at for particular point in time. The cooling then is associated with exhumation if no other reheating event reset the thermochronometers. Finally, the exhumation is linked to a geological process, like active faulting and/or flexure. Not all the samples were modeled because they shared the same cooling history as other rock samples that were already modeled.

5. DISCUSSION

5.1. (U-Th)/He ages for the NE Caribbean

The zircon (U-Th)/He data indicate that the last major regional exhumation phase in the northeastern Greater Antilles started in the Early Eocene. In Puerto Rico, Eocene is associated with a flexural response of the collision of the Caribbean plate with the

Bahamas Bank (Erickson et al., 1990; Mann et al., 2005) (Fig. 7). Consistent E-W trending exhumation patterns can be delimited in the SIP and CIP where the oldest cooling ages and their spatial distribution record syn-collision arching at ~ 49 Ma during the Middle Eocene (Fig. 9; Fig. 11). A second phase of exhumation and cooling at ~41 Ma is recorded by zircon across the island (Fig. 6; Fig. 9). During this cooling phase exhumation seems to get younger to the south (Fig. 9). This suggests that the northern part of the island experienced faster cooling and similar exhumation rates due to the proximity to the northern arc boundary (Fig. 10; Fig. 12). The southern part of the island seems to record a major second pulse of cooling in the Early Oligocene (Fig. 6; Fig. 9). (U-Th)/He ages may constrain the time when movement initiated on the Muertos Trough at ~34 Ma (Byrne et al., 1985). At the northern part of the island, apatite (U-Th)/He ages record cooling a few Myr later, related to active subduction to the south and its possible northern flexural response. These data are consistent with the Late Eocene to Middle Oligocene unconformity at the northern part of the island that allowed the transgressive carbonate sequence to develop (Larue et al., 1994). Rocks from the eastern-most part of this study area (Culebra, Vieques and the British Virgin Islands) record apatite ages of ~20 Ma (Early Miocene), significantly younger than for the rest of Puerto Rico. An early episode of rifting in the Anegada Passage by right lateral transtension in the Virgin Islands platform may have cooled the rocks, thus preserving 20 Myr ages (Mann et al., 2005). Additionally, discrepancies in the thermal history between the British Virgin Islands and Puerto Rico block suggest that the islands diverged in their deformation style during Late Oligocene-Early Miocene, more likely during an early episode of deformation along the Anegada passage (Fig. 14).

5.2. Significance of Eocene He ages

The age of the collision between the Caribbean arc and the Bahamas Bank has been classified as diachronous from west to east by Mann et al. (2005). The new thermochronometric data presented suggest that collision initiation by rapid cooling starting as early as Early Eocene near the Great Southern Puerto Rico fault zone, with continued exhumation through the Eocene, earlier that previously suggested by Dolan et al. (1991) and coeval with major contractional deformation in Cuba (Gordon et al., 1997).

Biostratigraphic ages of the Late Eocene to Middle Oligocene unconformity (Erikson et al., 1990; Glover, 1971) could not represent the exact age of collision but rather may correspond to differences in the amount of total exhumation between the north-west parts of the Caribbean plate (Cuba) and the northeastern part (Puerto Rico) due to their paleo-location and progressive strain accommodation. A test of this hypothesis would be to evaluate exhumation ages derived from the same thermocronometers in Cuba, which should match cooling ages from Puerto Rico. If that is not the case, then the collision could not have occurred earlier than late Paleocene, as biostratigraphic constraints suggest.

The SIP may have collided with the CIP earlier than models proposed by Jolly et al., (1998a) as evidenced by the (U-Th)/He zircon cooling ages provided here near the SIP-CIP fault boundary. There are two possible scenarios that may satisfy the cooling ages found in both blocks. The first scenario involves the suture of two rigid blocks before the Early Eocene (~49 Ma) and later uplift; the second scenario proposes the coeval suturing and cooling of the two provinces during Early Eocene (Fig. 14). Both

interpretations are feasible, since it is impossible to distinguish the mechanism of exhumation with the current structural and cooling data. Possible cooling mechanisms are instantaneous flexural exhumation (almost instantaneous, locally), delayed exhumation by left lateral shearing along the SPRFZ (diachroneous), or kinematically linked exhumation of both blocks induced by the Bahamas Bank collision (instantaneous, regionally). If the first scenario is correct, the fault connecting both provinces, the Southern Puerto Rico fault zone, may have been active as early as the Late Paleocene although consistency in kinematic data, stratigraphic facies and cross-cutting relations may shed more light on the matter.

5.3. Hydrocarbon implications

The closure temperature of apatite (~70^{o}C) and zircon (~180^{o}C) are both close to the lower and upper temperature boundaries of catagenesis, the process when organic kerogen in sedimentary rocks is converted into hydrocarbons. The distribution of ages in the northern and southern regions of the island so far has shown temperatures close to 180^{o}C during the Eocene and 70^{o}C from Oligocene to Early Miocene. During this period conditions were suitable for hydrocarbon maturation if a source was present. This suggests that the northern and southern carbonate platforms exposed today were not a hydrocarbon source since they were being deposited during the same time of possible catagenesis, but at cooler temperatures. Additionally, a source from the area analyzed seems unlikely since the bulk composition of the units in the central region of the island, which experienced catagenesis temperatures, ranged mainly from volcanoclastic rocks, plutonic rocks and a few Cretaceous carbonate deposits. It is improbable that the northern

carbonate platform and its lower members have served as a seal since they were starting to develop and were not well compacted and/or barely present during the Late Oligocene. If migration from an unknown source took place later, then it is most likely to be confined inland rather than offshore due to today's northern or southern structural grain (dipping offshore). Additional structural, stratigraphic and thermochronometric data is needed to analyze the possibility of hydrocarbon formation, migration and entrapment offshore since its thermal history may vary from the mainland.

6. CONCLUSIONS

(U-Th/He) data derived from apatite and zircon reveal the deformational and post-volcanic phase of the Puerto Rico and its variable cooling patterns. The earliest and main exhumation phase started from the Early to Middle Eocene and its spatial distribution suggests a syn-collision arching, where exhumation was concentrated along the east-west line. This event marked the end of magmatism and records the collision with the Bahamas Bank earlier than previous biostratigraphic data suggests. Younger Eocene ages in the CIP may record later exhumation due to proximity to the northern plate boundary. Data from the southern part of the island record an Early Oligocene cooling event, possibly related to the initiation of the Muertos Trough at ~34 Ma. At the northern part of the island, apatite (U-Th)/He ages recorded cooling a few million years later related to active subduction in the south and its possible northern flexural response. The eastern most areas (Culebra, Vieques and the British Virgin Islands) record Early Miocene apatite ages younger than in Puerto Rico. Puerto Rico and The British Virgin Islands show discrepancies in their thermal history, suggesting that both islands diverged

during the period of extension in the Anegada Passage (Fig. 14). The new thermochronometric data is supported by time-temperature path inverse models, where collision was initiated by a period of rapid cooling beginning during the Early Eocene and exhumation through the Eocene. The overlap of cooling rates from the ~49 Ma to ~30 Ma along and near the NPRFZ also suggests cooling triggered by the same processes governing exhumation around the island.

ACKNOWLEDGEMENTS

This research project was funded by the Exxon Mobil Diversity Grant, the Geology Department of the University of Puerto Rico, University of Kansas and University of Texas in Austin. I would like to give special thanks to Aaron Cavosie, Daniel Stockli, Hernán Santos, Hans Schellekens and Luis González for discussions and for providing funding for the development of this project. Also to Edgardo Pujols, Roman Kislitsyn, Timmons Erickson, Raiza Quintero, Francis Pérez, Yadira Soto and Samuel Pacheco for provide field and lab work assistance.

REFERENCES CITED

Byrne, D.E., Suarez, G., and McCann, W.R., 1985. Muertos Trough subduction; microplate tectonics in the northern Caribbean?: Nature, v. 317, p. 420-421.

Cox, D.P., Marvin, R.F., M'Gonigle, J.W., McIntyre, D.H., and Rogers, C.L., 1977. Potassium-Argon geochronology of some metamorphic, igneous, and hydrothermal events in Puerto Rico and the Virgin Islands. U.S. Geological Survey Journal of Research, v. 5, p. 689-703.

Dodson, M.H., 1973. Closure temperature in cooling geochronological and petrological systems. Contributions to Mineralogy and Petrology, v. 40, p. 259-274.

Dolan, J., Mann, P., de Zoeten, R., and Heubeck, C., 1991. Sedimentologic, stratigraphic, and tectonic synthesis of Eocene-Miocene sedimentary basins, Hispaniola and Puerto Rico, *in* Mann, P., Draper, G., and Lewis, J., eds., Geologic and Tectonic Development of the North America-Caribbean plate boundary in Hispaniola: Geological Society of America Special Paper 262, p. 217-264.

Dunai, T.J., 2005. Forward Modeling and Interpretation of (U-Th)/He Ages. In: P.W. Reiners and T.A. Ehlers, Editors, Low Temperature Thermochronology: Techniques, Interpretations and Applications, Reviews in Mineralogy and Geochemistry, v. 58, p. 259-274.

Ehlers, T.A., Chaudhri, T., Kumar, S., Fuller, C.W., Willet, S.D., Ketcham, R.A., Brandon, M.T., Belton, D.X., Kohn, B.P., Gleadow, A.J.W., Dunai, T.J., Fu, F.Q., 2005. Computational tools for low-temperature thermochronometer interpretation. In: P.W. Reiners and T.A. Ehlers, Editors, Low Temperature Thermochronology: Techniques, Interpretations and Applications, Reviews in Mineralogy and Geochemistry, v. 58, p. 589-622.

Erikson, J., Pindell, J., and Larue, D., 1990. Mid-Eocene-early Oligocene sinistral transcurrent faulting in Puerto Rico associated with formation of the Northern Caribbean plate boundary zone: Journal of Geology, v. 98, p. 365-384.

Farley K. A., Wolf R. A., and Silver L. T., 1996. The effects of long alpha-stopping distances on (U-Th)/He ages. Geochim. Cosmochim. Acta 60, p. 4223-4229.

Farley, K.A., 2000. Helium diffusion from apatite: General behavior as illustrated by Durango fluorapatite. Journal of Geophysical Research, v. 105, p. 2903-2914.

Glover, L., III, 1971. Geology of the Coamo area, Puerto Rico, and its relation to the volcanic arc-trench association: U.S. Geological Survey Professional Paper 636, p. 102.

Hager, C., 2009. A new Matlab©-based helium modeling package ("HeMP") for thermal history recovery from single and multi-thermochronometer (U-Th)/He data and data arrays. [unpublished work]

Hourigan J.K., Reiners P.W., and Brandon M.T., 2005. U-Th zonation-dependant alpha-ejection in (U-Th)/He chronometry. Geochim. Cosmochim. Acta 69, p. 3349-3365.

House, M.A., Farley, K.A., and Kohn, B., 1999. An empirical test of helium diffusion in apatite: borehole data from the Otway basin, Australia. Earth and Planetary Science Letters, v. 170, p. 463-474.

Jolly, W.T., Lidiak, E.G., Schellekens, J.H., and Santos, H., 1998a. Volcanism, tectonics, and stratigraphic correlations in Puerto Rico. Geology Society of America, Special Paper 322, p. 1-24.

Jolly, W.T., Lidiak, E.G., Dickin, A.P., and Wu, T-W., 1998b. Geochemical diversity of Mesozoic island arc tectonic blocks in eastern Puerto Rico. Geological Society of America, Special Paper 322, p. 67-98.

Jolly, W.T., Schellekens, J.H., Dickin, A.P., 2007. High-Mg andesites and related lavas from southwest Puerto Rico (Greater Antilles Island Arc): Petrogenetic links with emplacement of the Late Cretaceous Caribbean mantle plume. Lithos 98, p. 1-26.

Ketcham, R.A., 2005. Forward and Inverse Modeling of Low-Temperature Thermochronometry Data. In: P.W. Reiners and T.A. Ehlers, Editors, Low Temperature Thermochronology: Techniques, Interpretations and Applications, Reviews in Mineralogy and Geochemistry, v. 58, p. 275-314.

Laó-Dávila, D.A., Llerandi-Román, P.A., Anderson, T.H., 2012. Cretaceous-Paleogene thrust emplacement of serpentinite in southwestern Puerto Rico: Geological Society of America Bulletin, v. 124, p. 1169-1190.

Larue, D.K., 1994. Puerto Rico and the Virgin Islands: in Donovan S.K. and Jackson, T. A. (eds.) Caribbean Geology: An introduction, University of the West Indies Publishers Association/University of the West Indies Press, Kingston, Jamaica, p. 151-165.

Mann, P., Hippolyte, J.-C., Grindlay, N.R., and Abrams, L.J., 2005. Neotectonics of southern Puerto Rico and its offshore margin, in Mann, P., ed., Active tectonics and

seismic hazards of Puerto Rico, the Virgin Islands, and offshore areas: Geological Society of America Special Paper 385, p. 173-214.

Mattson, P.H., 1960. Geology of the Mayagüez area, Puerto Rico. Geological Society of America Bulletin, v. 71, p. 319-362.

Montgomery, H.M., Pessagno, E.A., Jr., and Pindell, J.L., 1994. A 195 Ma Terrane in a 165 Ma sea: Pacific origin of the Caribbean Plate: GSA Today, v.4, no. 1, 3-6.

Nasdala, L., Wenzel, M., Vayra, G., Wenzel, T., and Kober, B., 2001. Metamictization of natural zircon: accumulation versus thermal annealing of radioactive-induced damage. Contribution to Mineralogy Petrology, v. 141, p. 125-144.

Pérez, R., 2008. Oxygen Isotope Geochemistry of Plutonic Rocks from Puerto Rico [Master's Thesis]: Mayagüez, Puerto Rico, University of Puerto Rico, p.140.

Pindell, J.L., 1993. Evolution of the Gulf of Mexico and the Caribbean: in Donovan S.K. and Jackson, T. A. (eds.) Caribbean Geology: an introduction, University of the West Indies Publishers Association/University of the West Indies Press, Kingston, Jamaica, p. 13-39.

Reich, M., Ewing, R., Ehlers, T, Becker, U., 2007. Low-temperature anisotropic diffusion of helium in zircon: implications for zircon (U-Th)/He thermochronometry. Geochimica et Cosmochimica Acta, v. 71, p. 2119-3130.

Reiners, P.W., and Farley K. A., 2001. Influence of crystal size on apatite (U-Th)/He thermochronology: An example from the Bighorn Mountains, Wyoming. Earth Planet. Sci. Lett. 188, p. 413-420.

Reiners, P.W., Farley K. A., and Hickes, H.J., 2002. He diffusion and (U-Th)/He thermochronology of zircon: initial results from Fish Canyon Tuff and Gold Butte. Tectonophysics, v. 349, p. 297-308.

Reiners, P.W., Spell, T., Nicolescu, S., Zanetti, K., 2004. Zircon (U-Th)/He thermochronometry: He diffusion and comparisons with Ar-40/Ar-39 dating. Geochimica et Cosmochimica Acta v. 68, p. 1857-1887.

Reiners, P.W., 2005. Zircon (U-Th)/He Thermochronometry. In: P.W. Reiners and T.A. Elhers, Editors, Low Temperature Thermochronology: Techniques, Interpretations and Applications, Reviews in Mineralogy and Geochemistry v. 58, p. 151-179.

Schellekens, J.H., 1998a. Composition, Metamorphic grade, and origin of Metabasites in the Bermeja Complex, Puerto Rico. International Geology Review, v.40, p. 722-747.

Schellekens, J.H., 1998b. Geochemical evolution and tectonic history of Puerto Rico. Geological Society of America, Special Paper 322, p. 35-66.

Smith, A.L., Schellekens, J.H., and Muriel-Diaz, A., 1998. Batholiths as markers of tectonic change in the northeastern Caribbean. Geological Society of America, Special Paper 322, p. 99-122.

Speed, R.C., Larue, D.K., 1991. Extension and transtension in the plane boundary zone of the northeastern Caribbean: Geophysical Research Letters, v. 18, p. 573-576.

Stockli, D.F., 2005. Application of low-temperature thermochronometry to extensional tectonic settings. In: P.W. Reiners and T.A. Ehlers, Editors, Low Temperature Thermochronology: Techniques, Interpretations and Applications, Reviews in Mineralogy and Geochemistry, v. 58, p. 123-149.

Tobisch, O.T., 1968. Gneissic amphibolite at Las Palmas, Puerto Rico, and its significance in the early history of the Greater Antilles island arc: Geol. Soc. Amer. Bull., v. 79, p. 557-574.

Villeneuve, M., Sandeman H.A., Davis, W.J., 2000. A method for intercalibration of U-Th-Pb and ^{40}Ar-^{39}Ar ages in the Phanerozoic. Geochimica et Cosmochimica Acta, v. 64, p. 4017-4030.

Zeitler, P.K., Herczeg, A.L., McDougall, I., and Honda, M., 1987. U-Th-He dating of apatite: A potential thermochronometer. Geochimica et Cosmochimica Acta, v. 51, p. 2865-2868.

TABLE 1. NAME, ROCK TYPE, AND LOCATION OF ROCK SAMPLES COLLECTED FOR THIS STUDY.

Location	Sample	Rock Type	Latitude/Longitude
Southern Igneous Province			
Bermeja Complex, P.R.	06BC-01	amphibolite	17° 58'59.58"N 67° 08'06.42"W
Sabana Eneas, P.R.	06CL-06	andesite bomb in Cotui Limestone	18° 4'42.96"N 67° 5'17.58"W
Mayagüez, P.R.	07CF-06	felsic dike	18°14'29.91"N 67° 03'37.78"W
Hormigueros, P.R.	06HP-01	altered porphyry	18°08'47.35"N 67°07'22.40"W
Cabo Rojo, P.R.	09LF-04	andesite porphyry	18º02'58.81"N 67º09'36.82"W
Las Tunas stock	06LT-01	porphyritic diorite	18° 2'45.88"N 67° 7'12.05"W
Maguayo, P.R.	09MP-01	diorite porphyry	18º00'2.37"N 67º05'17.04"W
Tea Diorite	06TD-01	porphyritic diorite	18°03'30.96"N 67°00'35.40"W
Tibes stock	06TS-06	gabbro	18°04'41.58"N 66°38'10.92"W
Central Igneous Province			
Caguas stock	06CG-01	granodiorite	18°14'28.86"N 66°00'34.74"W
Ciales stock	06CS-01	granodiorite	18°20'10.38"N 66°27'47.94"W
Cuyon stock	06CY-01	quartz diorite	18°06'23.94"N 66°14'47.34"W
Morovis stock	06MS-01	granite	18°18'02.64"N 66°24'36.96"W
Río Grande Pluton	08RG-01	granodiorite	18°17'16.08"N 66°16'01.74"W
	08RG-02	granodiorite	18°17'12.12"N 66°15'59.16"W
	08RG-03	granodiorite	18°17'55.74"N 66°15'09.42"W
San Lorenzo Batholith	06SL-01	quartz diorite	18°04'17.70"N 65°59'30.66"W

Location	Sample	Rock Type	Latitude/Longitude
	06SL-03	granodiorite	18°09'00.30"N 65°58'48.60"W
Utuado pluton	06UP-02	granodiorite	18°16'03.90"N 66°42'30.84"W
	08UP-03	granodiorite	18°17'20.22"N 66°42'40.44"W
	09UP-07	granodiorite	18°16'53.58"N 66°38'38.82"W
Northeast Igneous Province			
Rio Blanco stock	06RB-01	granodiorite	18°17'7.56"N 65°47'23.88"W
Culebra			
Playa Resaca	07IC-04	diorite	18°19'56.40"N 65°18'21.12"W
Cayo Ratón	09IC-23	micro-diorite	18º18’51.96"N 65º21’.1179"W
Vieques			
Western Vieques	06IV-01	granodiorite	18°07'00.54"N 65°31'12.36"W
British Virgin Islands			
Tortola	09VI-02	granodiorite	18º23’01.50"N 64º40’23.40"W
Norman Island	09VI-05	silicified rhyolite (keratophyre)	18°19'15.71"N 64°36'48.57"W
Virgin Gorda	09VI-06	granodiorite	18°27'44.64"N 64°24'58.80"W
Virgin Gorda	09VI-12	Quatz diorite	18°25'57.54"N 64°25'37.74"W

Location refers to either name of pluton (where available) or closest geographical reference (usually a town name).

TABLE 2. SUMMARY OF HE AGES OF ROCK SAMPLES ANALYZED FOR THIS STUDY.

Sample	Location	Zircon U-Pb Age (Ma)[1]	Zircon He Age (Ma)	Apatite He Age (Ma)
Southern Igneous Province				
06BC-01	Bermeja Complex	131 ± 8[2]	40.5 ± 3.2	N.D.
09LF-04	Lajas Formation	N.D.	55.5 ± 4.4	N.D.
09MP-01	Maguayo Porphyry	N.D.	54.3 ± 4.3	52.2 ± 3.1
06HP-01	Hormigueros Porphyry	N.D.	51.4 ± 4.1	29.8 ± 1.8
06CL-06	volcanic clast in Cotui Limestone	N.D.	50.1 ± 4.0	N.D.
06LT-01	Las Tunas stock	79 ± 2.1	49.2 ± 3.9	31.0 ± 1.9
06TS-06	Tibes stock	60.5 ± 1.6	43.3 ± 3.5	N.D.
07CF-06	felsic dike Mayagüez, P.R.	N.D.	38.9 ± 3.1	34.4 ± 2.1
06TD-01	Tea Diorite	38.4 ± 0.8	N.D.	34.0 ± 2.0
Central Igneous Province				
06MS-01	Morovis stock	85.3 ± 1.8	56.5 ± 4.5	29.8 ± 1.8
08RG-02	Rio Grande Pluton	N.D.	49.0 ± 3.9	22.6 ± 1.4
08UP-03	Utuado pluton	N.D.	47.8 ± 3.8	10.4 ± 0.6
08RG-01	Rio Grande Pluton	N.D.	43.5 ± 3.5	26.1 ± 1.6
06UP-02	Utuado pluton	70.8 ± 1.2	42.3 ± 3.4	32.1 ± 1.9
09UP-07	Utuado pluton	N.D.	41.6 ± 3.3	18.9 ± 1.1
08RG-03	Rio Grande Pluton	N.D.	41.5 ± 3.3	21.9 ± 1.3
06CS-01	Ciales stock	83.9 ± 1.7	40.9 ± 3.9	31.5 ± 1.9
06CG-01	Caguas stock	66.8 ± 1.2	40.2 ± 3.2	31.3 ± 1.9
06SL-03	San Lorenzo Batholith	75.1 ± 2.1	34.7 ± 2.8	29.3 ± 1.8*
06CY-01	Cuyon stock	47.6 ± 0.8	33.9 ± 2.7	N.D.
06SL-01	San Lorenzo Batholith	74.1 ± 1.4	N.D.	15.1 ± 0.9

2 Appendix 4.1 Uncertainty in age listed as 2SD.

1 All U-Pb ages except 08BC01 are from Pérez (2008).

* Age based on a single aliquot analyzed. N.D. = not determined

Sample	Location	Zircon U-Pb age (Ma)[1]	Zircon Age (Ma)	Apatite Age (Ma)
Northeast Igneous Province				
06RB-01	Rio Blanco stock	47.7 ± 2.1	40.5 ± 3.2	25.9 ± 1.6
Culebra				
09IC-23	Cayo Ratón	N.D.	33.1 ± 2.6*	19.0 ± 1.1
07IC-04	Isla Culebra (Playa Resaca)	N.D.	N.D.	29.7 ± 1.8
Vieques				
06IV-01	Isla de Vieques	67.1 ± 1.6	29.4 ± 2.3	N.D.
British Virgin Islands				
09VI-05	Norman Island	N.D.	27.1 ± 2.2	N.D.
09VI-02	Tortola	N.D.	25.0 ± 2.0	17.7 ± 1.1
09VI-06	Virgin Gorda	N.D.	24.9 ± 2.0	N.D.
09VI-12	Virgin Gorda	N.D.	23.5 ± 1.9	21.6 ± 1.3

1 All U-Pb ages except 08BC01 are from Pérez (2008).
2 Appendix 4.1
* Age based on a single aliquot analyzed.
Uncertainty in age listed as 2SD.
#N.D. = not determined

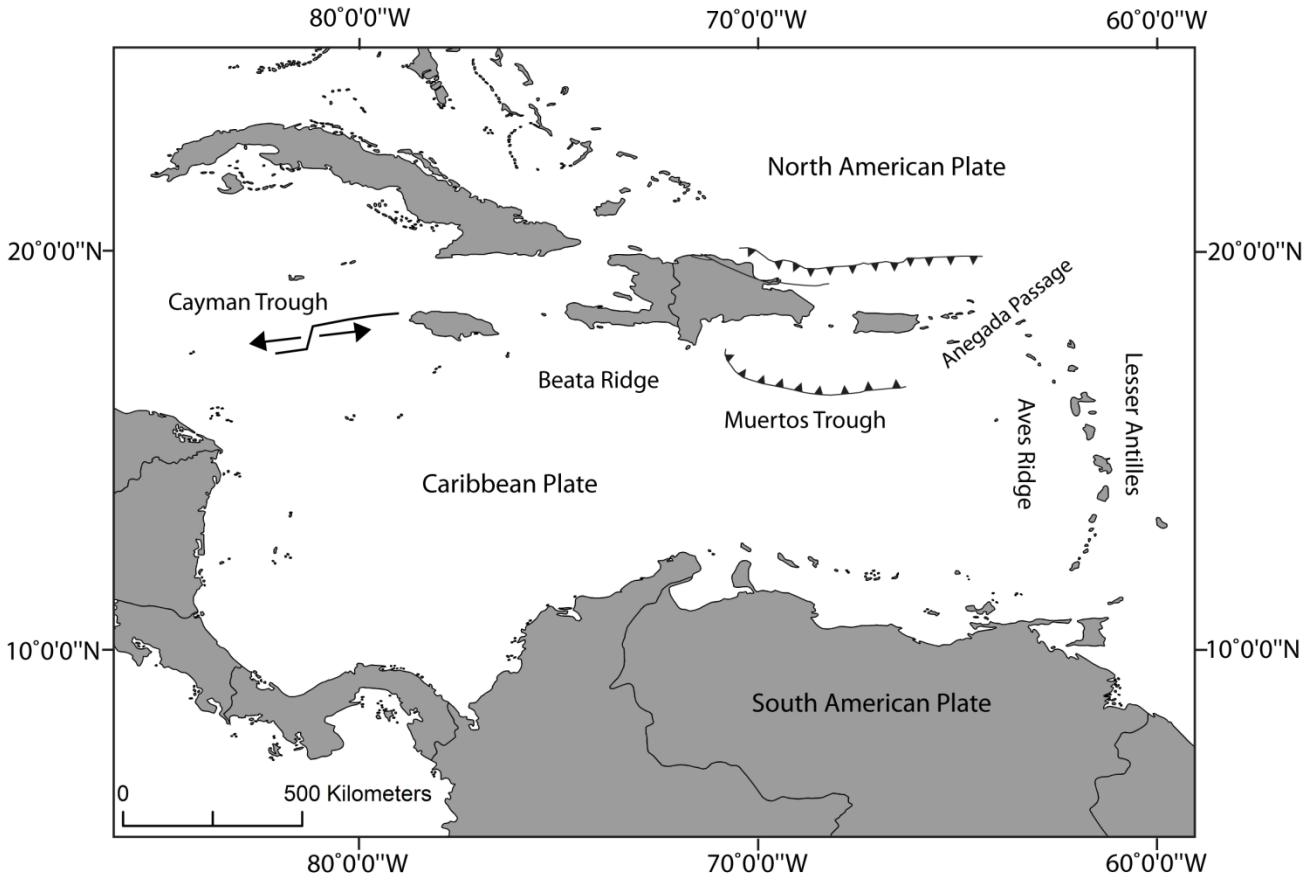

Figure 1. Location map showing the Greater and Lesser Antilles and their tectonic features. Bold lines represent faults and triangles the polarity of subduction. Modified from Jolly et al., 2007.

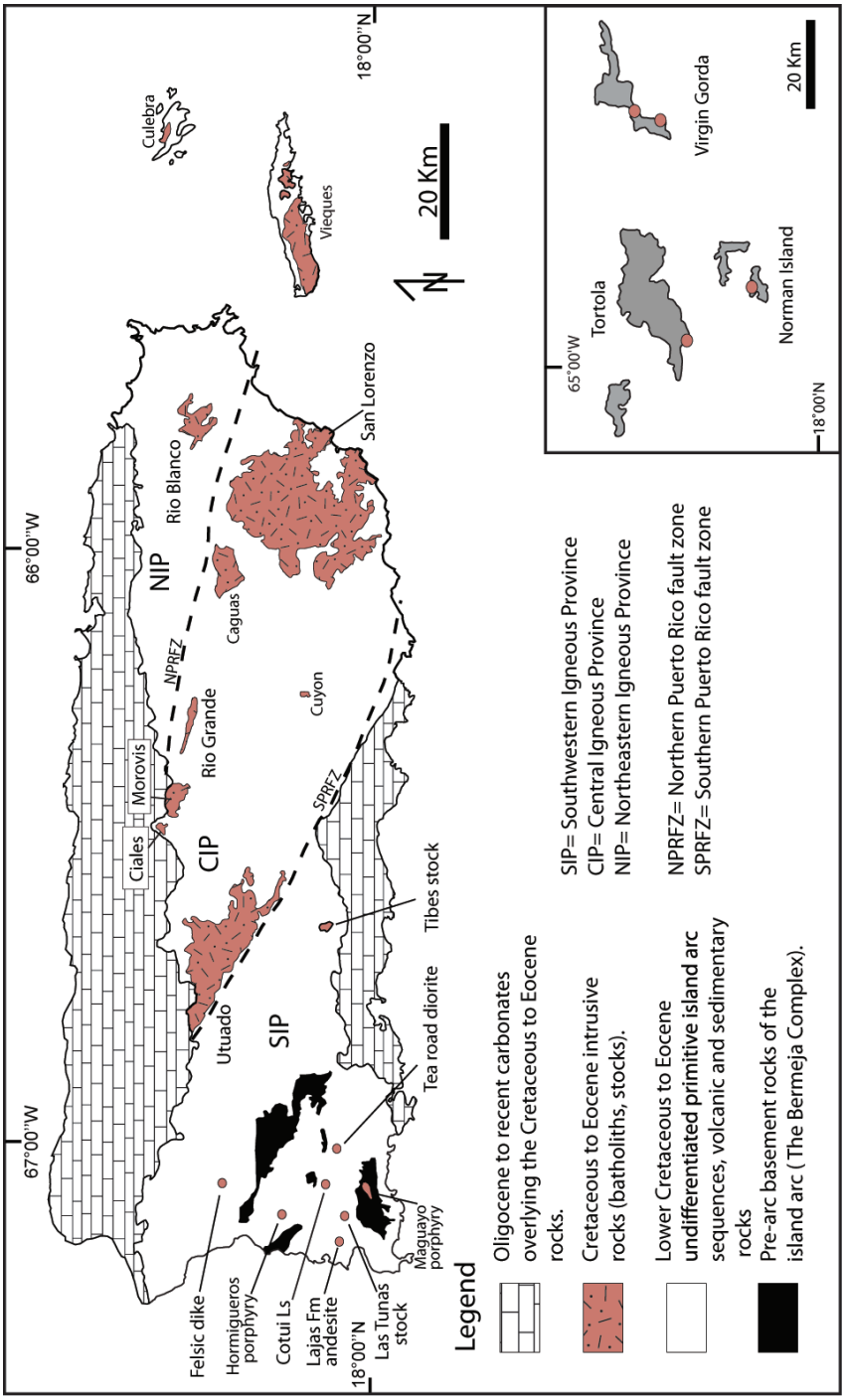

Figure 2. Geologic map of Puerto Rico showing the distribution of igneous intrusions analyzed in this study. Dashed lines represent the two left-lateral strike slip faults of the Northern and Southern Puerto Rico fault zone. Modified from Pérez, (2008).

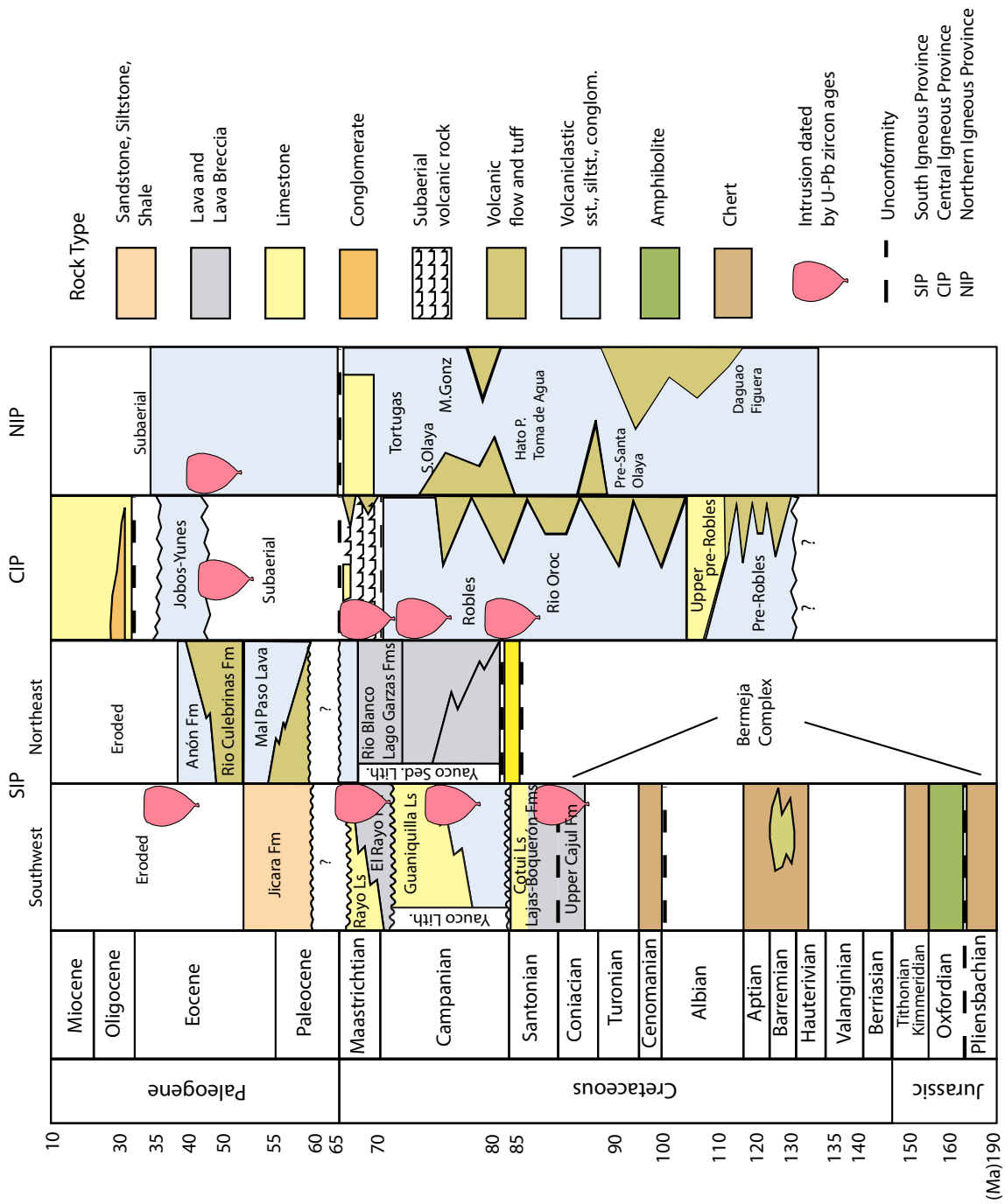

Figure 3. Stratigraphic correlations of the Southwestern, Central and Northeastern Igneous Provinces of Puerto Rico. Modified from Schellekens (1998a); Jolly et al., (2007). Some of the geologic formations of the Central Igneous Province described in the text are not explicitly identified in the figure.

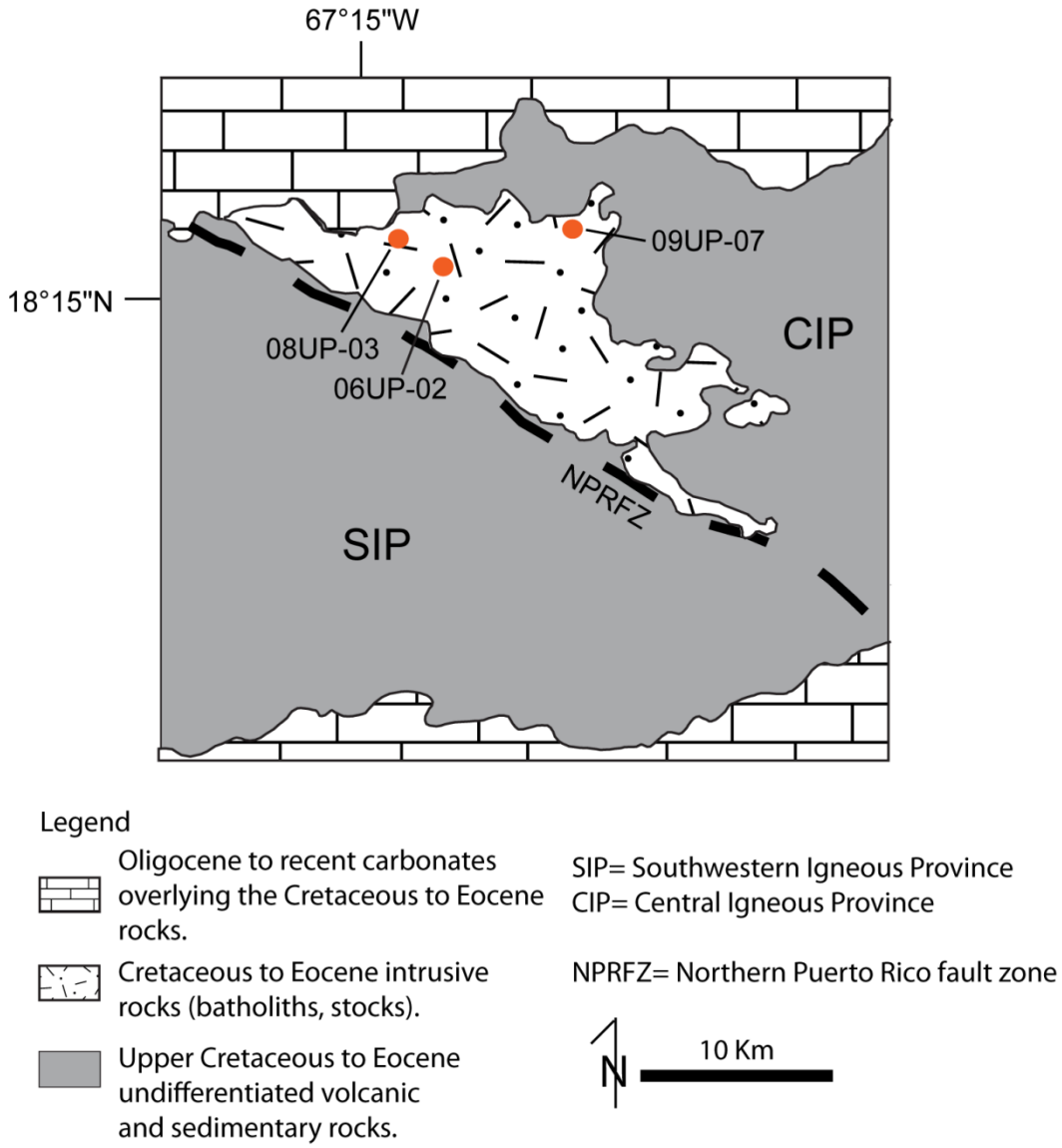

Figure 4. Geologic map of the Utuado Batholith in the Central Igneous Province showing sample locations.

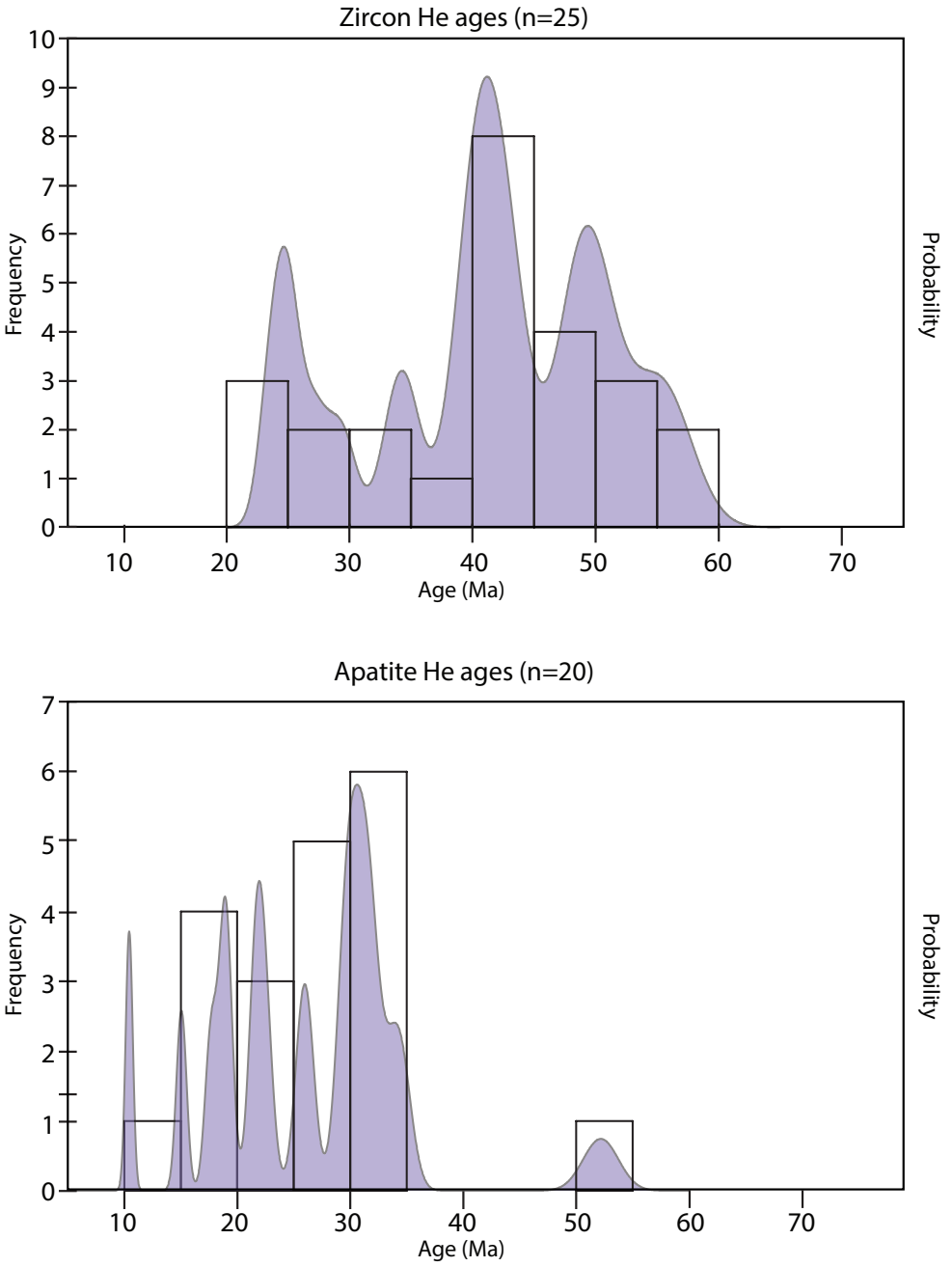

Figure 5. Frequency distribution of (U-Th)/He ages from zircon and apatite grains in the SIP, CIP, NIP, Vieques, Culebra and the British Virgin Islands.

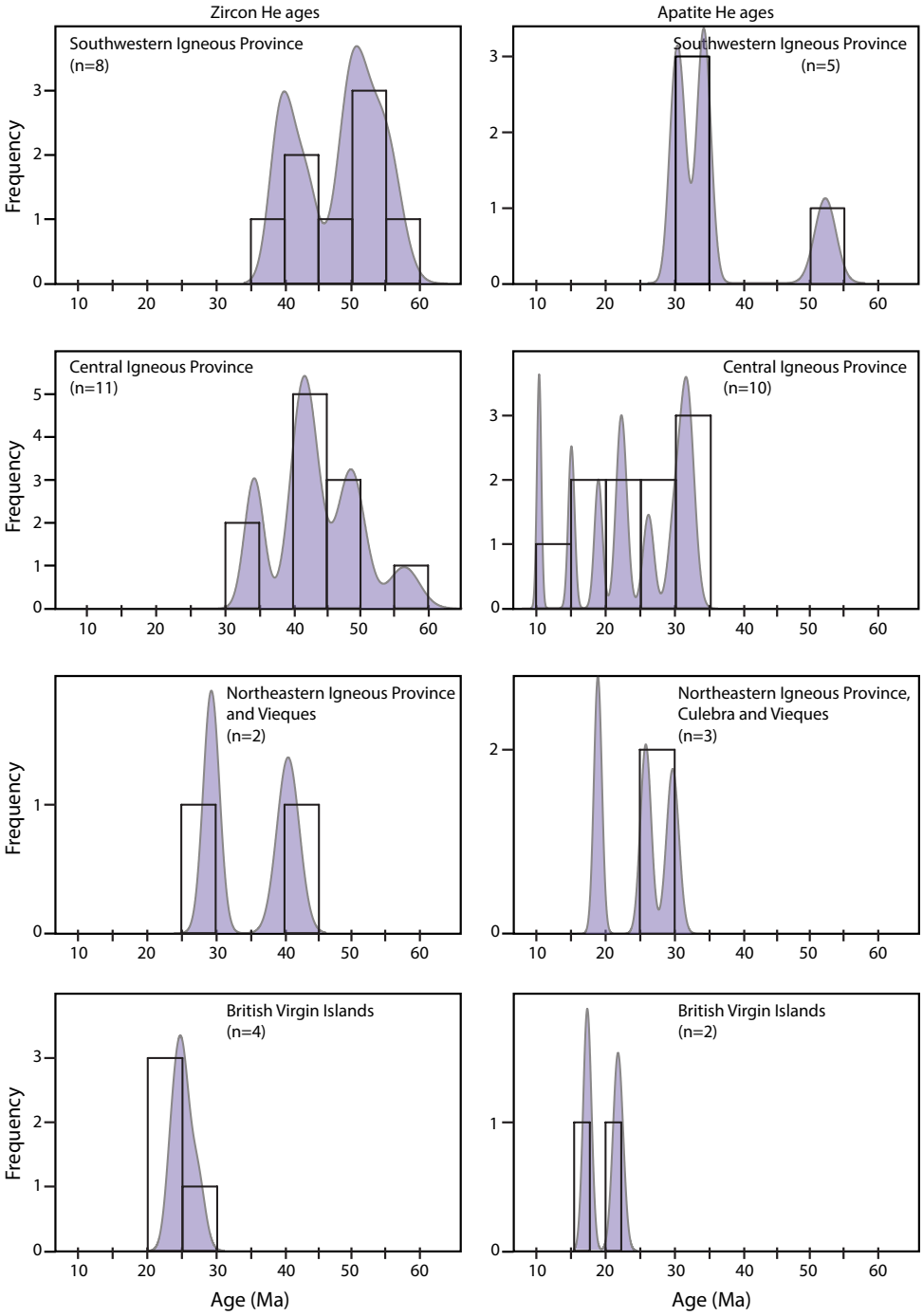

Figure 6. Frequency distribution of (U-Th)/He ages from zircon and apatite grains by igneous province.

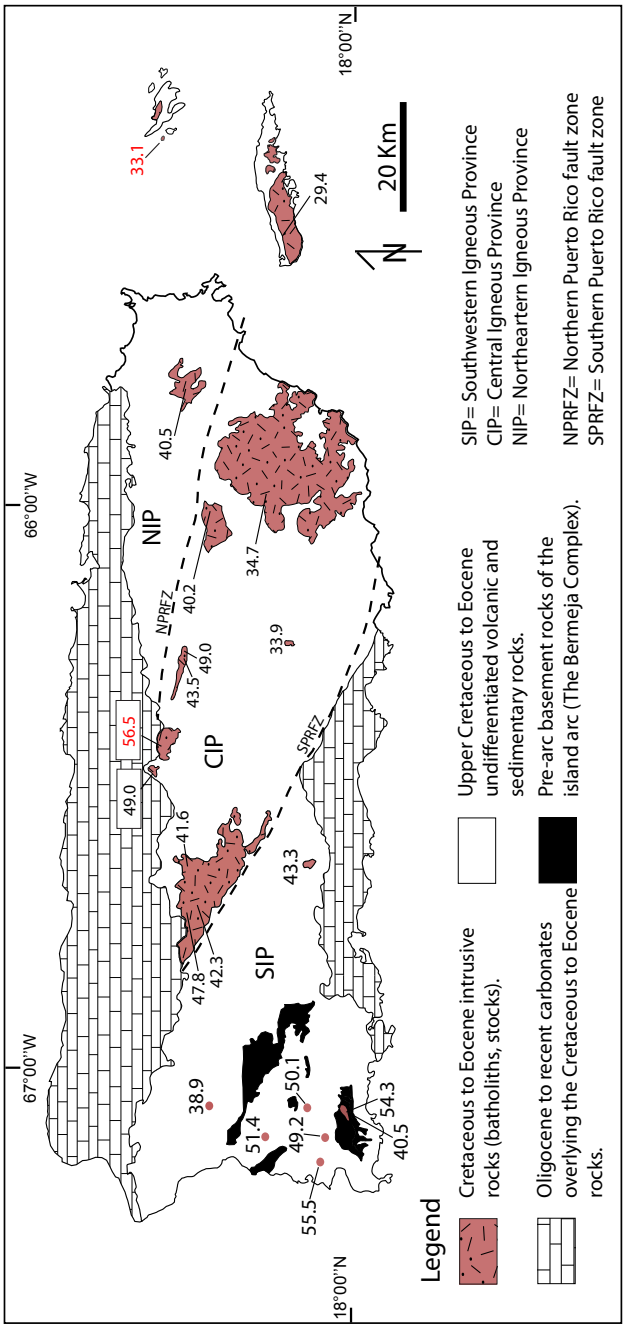

Figure 7. Map showing (U-Th)/He ages from zircon grains along the three igneous provinces of Puerto Rico. Values in red correspond to samples with a single aliquot analyzed.

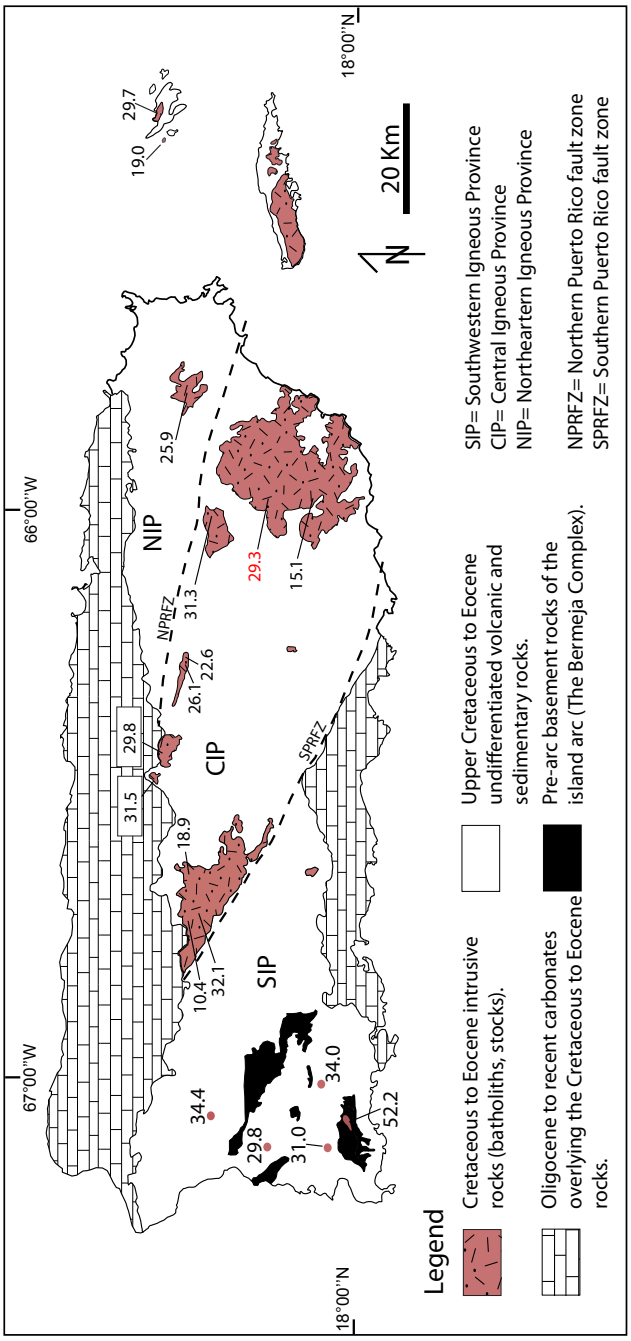

Figure 8. Map showing (U-Th)/He ages from apatite grains along the three igneous provinces of Puerto Rico.

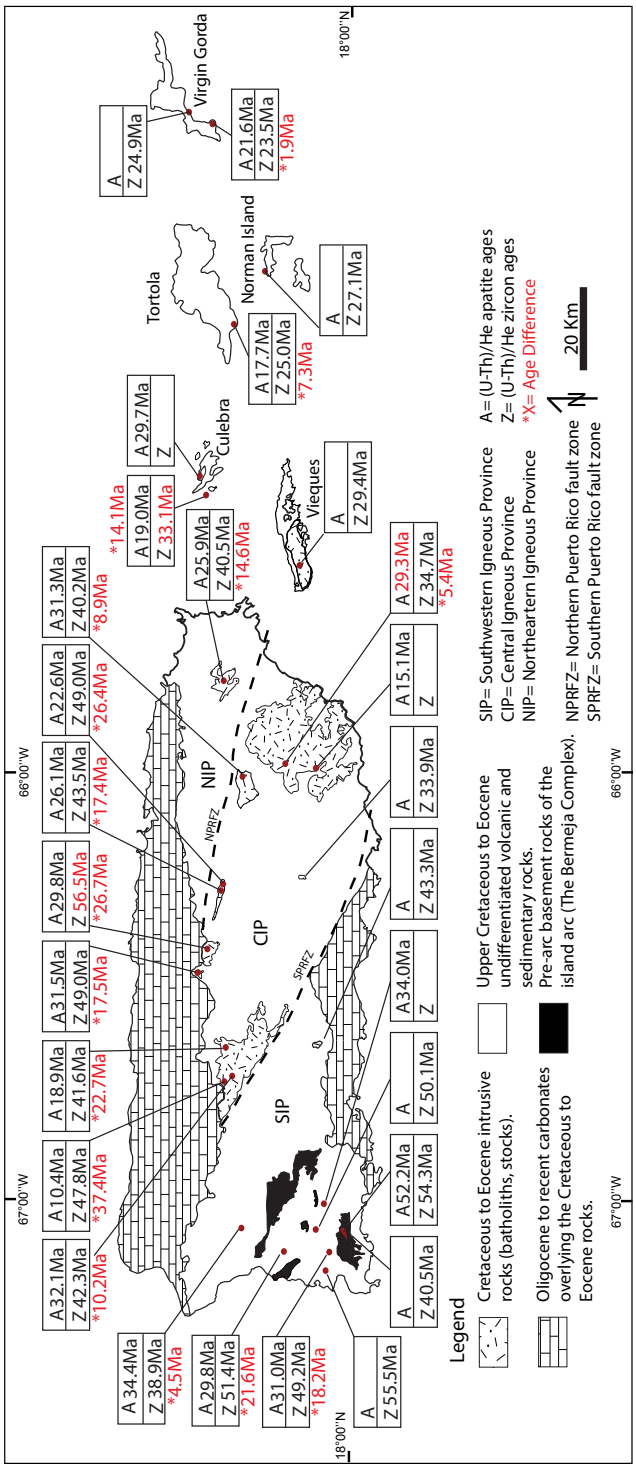

Figure 9. Map showing (U-Th)/He ages from zircon and apatite grains along the three igneous provinces of Puerto Rico and Vieques, Culebra and the British Virgin Islands. (In red is the time span between thermochronometers).

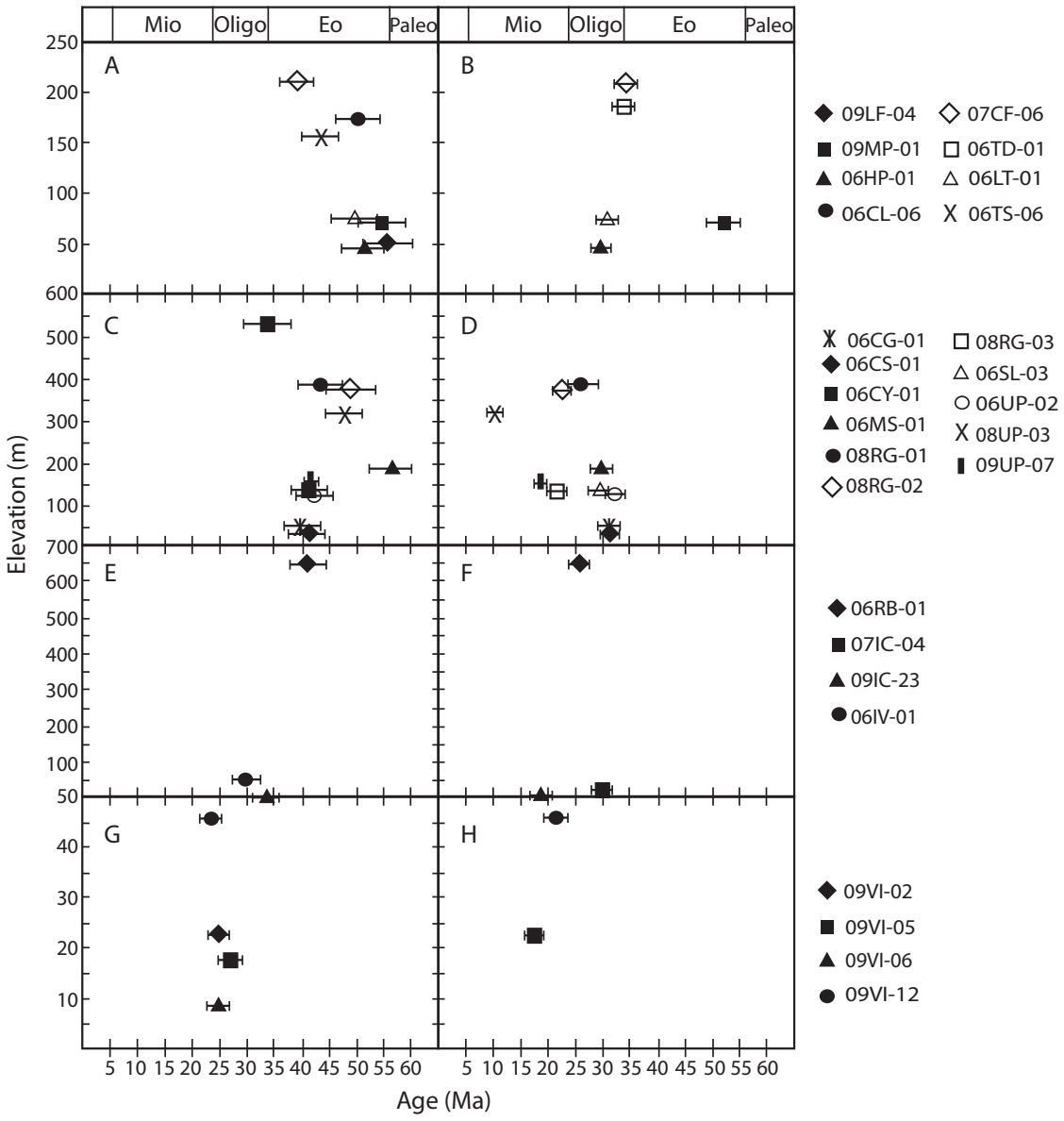

Figure 10. Graphs of elevation vs. age from the (U-Th)/He ages of zircon and apatite grains from the three igneous provinces of Puerto Rico including Vieques, Culebra and the British Virgin Islands. The abbreviation Mio, Oligo, Eo, and Paleo, indicate the epochs Miocene, Oligocene, Eocene and Paleocene respectively.

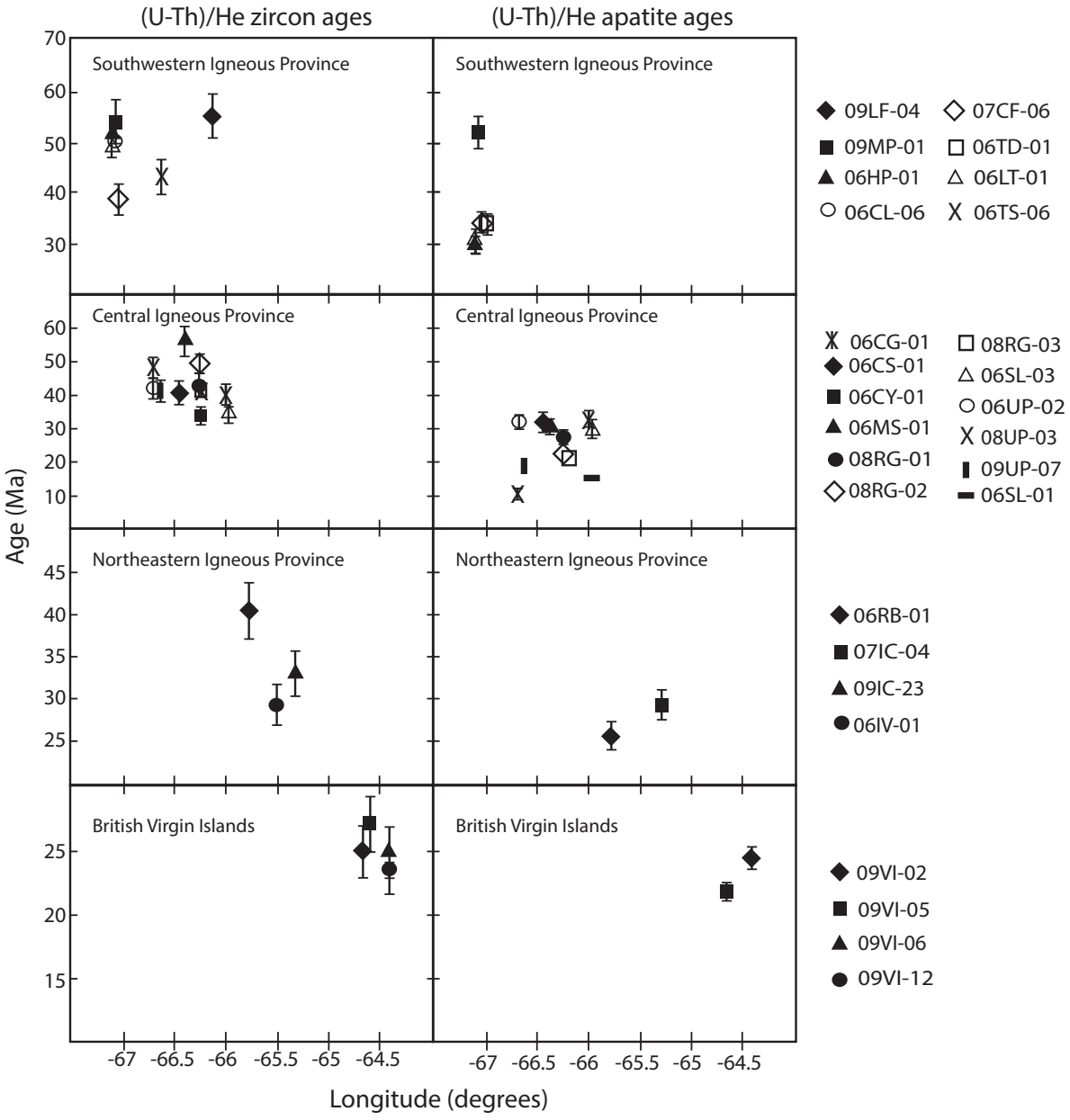

Figure 11. Graphs of age vs. longitude from the (U-Th)/He ages of zircon and apatite grains from the three igneous provinces of Puerto Rico including Vieques, Culebra and the British Virgin Islands.

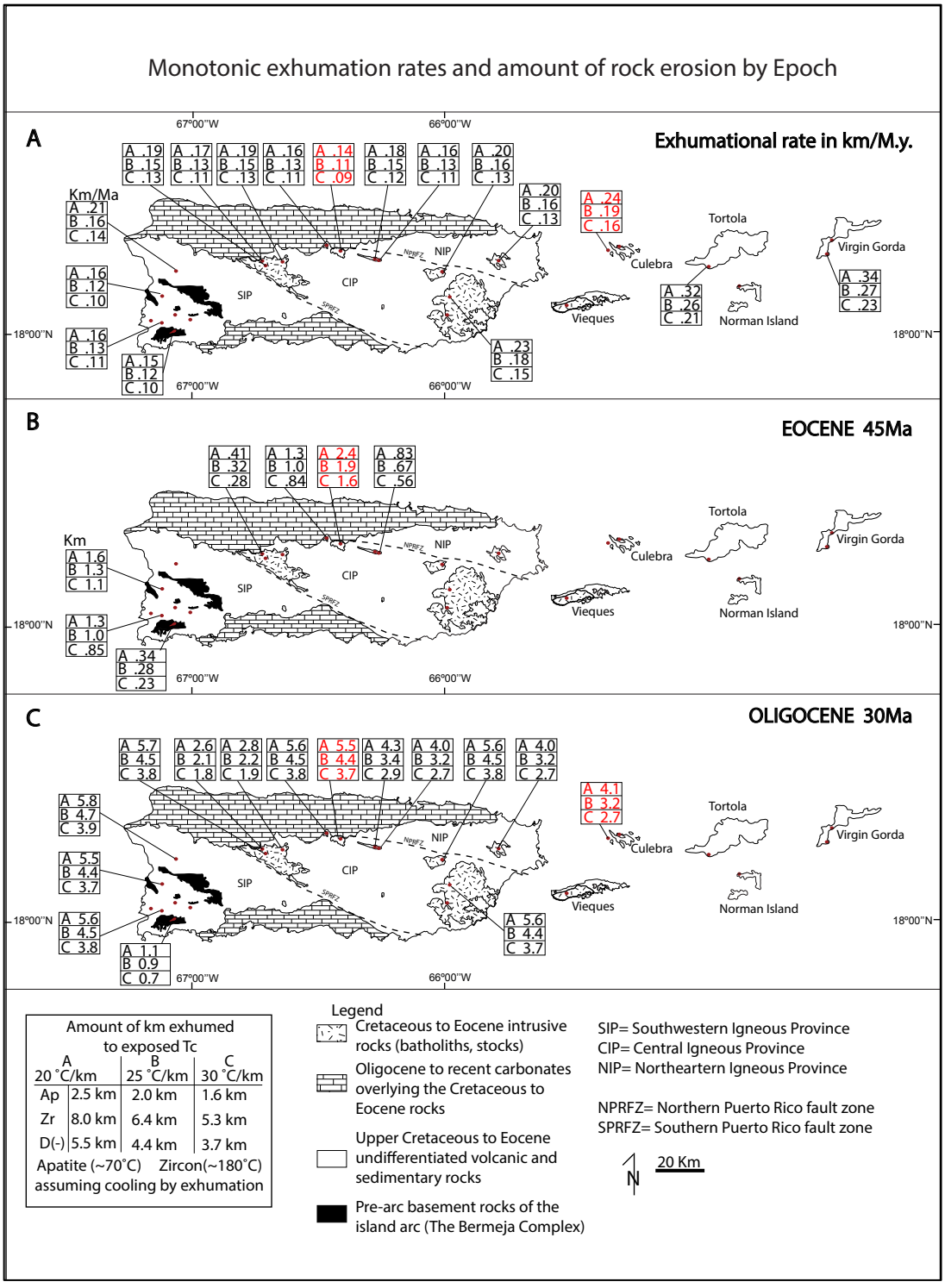

Figure 12. Map showing the exhumation rates and amount of rock erosion by epoch assuming a monotonic cooling at different geothermal gradient of 20ºC/km, 25ºC/km and 30ºC/km. Values in red correspond to samples with a single aliquot analyzed. See appendix for calculation formulas.

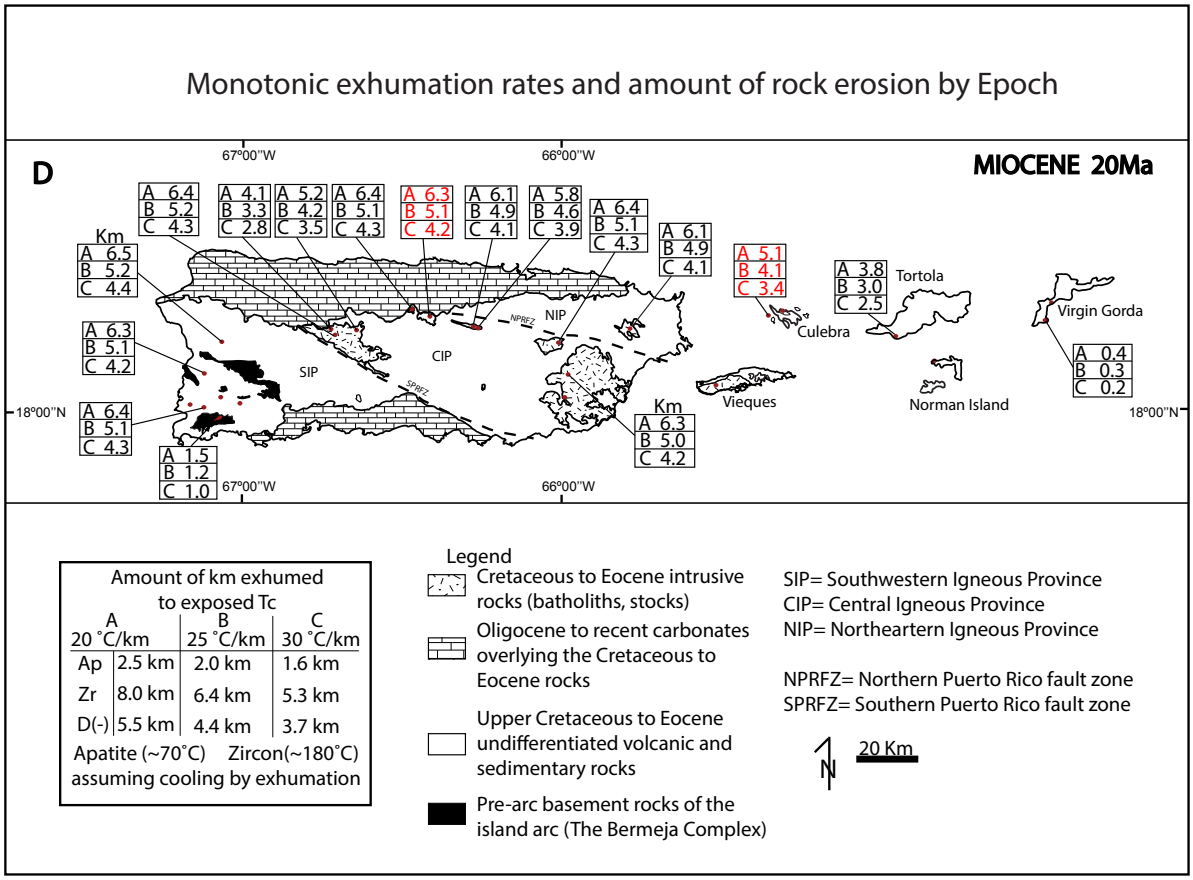

Figure 12. Map showing the exhumation rates and amount of rock erosion by epoch assuming a monotonic cooling at different geothermal gradient of 20ºC/km, 25ºC/km and 30ºC/km. Values in red correspond to samples with a single aliquot analyzed. See appendix for calculation formulas.

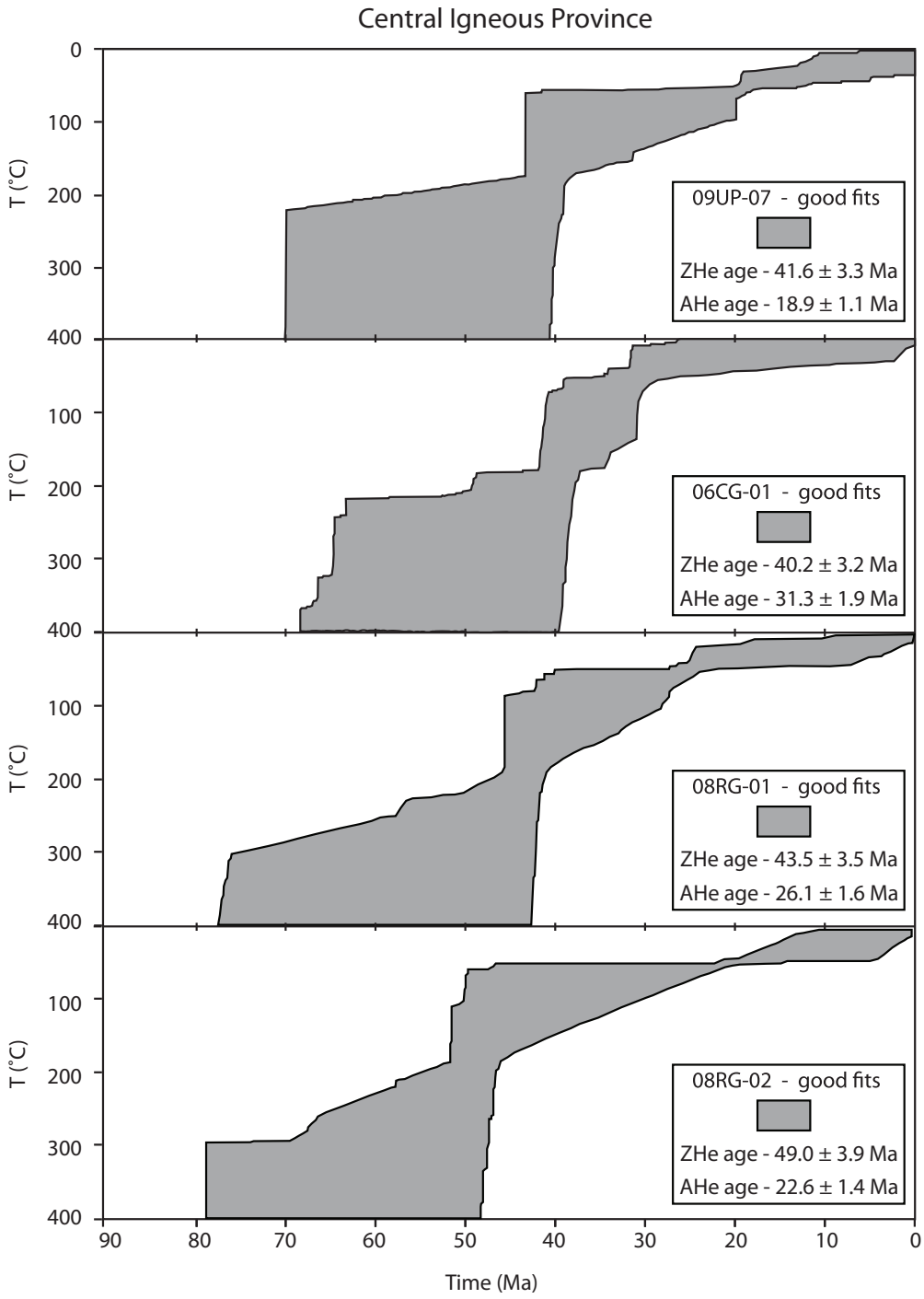

Figure 13. Modeled time-Temperature paths using HeMP for plutonic bodies in the Central Igneous Province (CIP), Southwestern Igneous Province (SIP), Northeastern Igneous Province (NIP) and the British Virgin Islands (BVI).

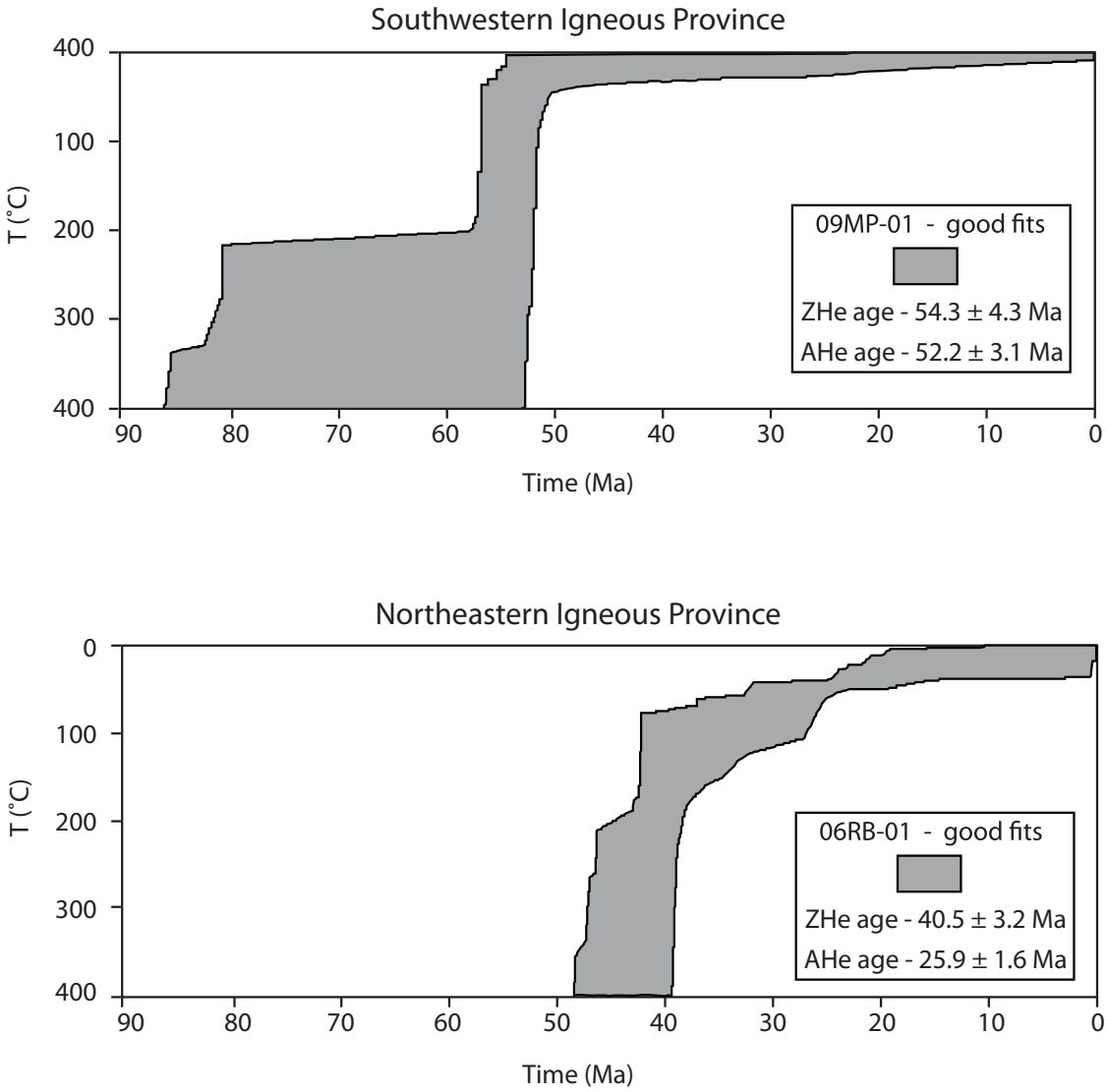

Figure 13. Modeled time-Temperature paths using HeMP for plutonic bodies in the Central Igneous Province (CIP), Southwestern Igneous Province (SIP), Northeastern Igneous Province (NIP) and the British Virgin Islands (BVI).

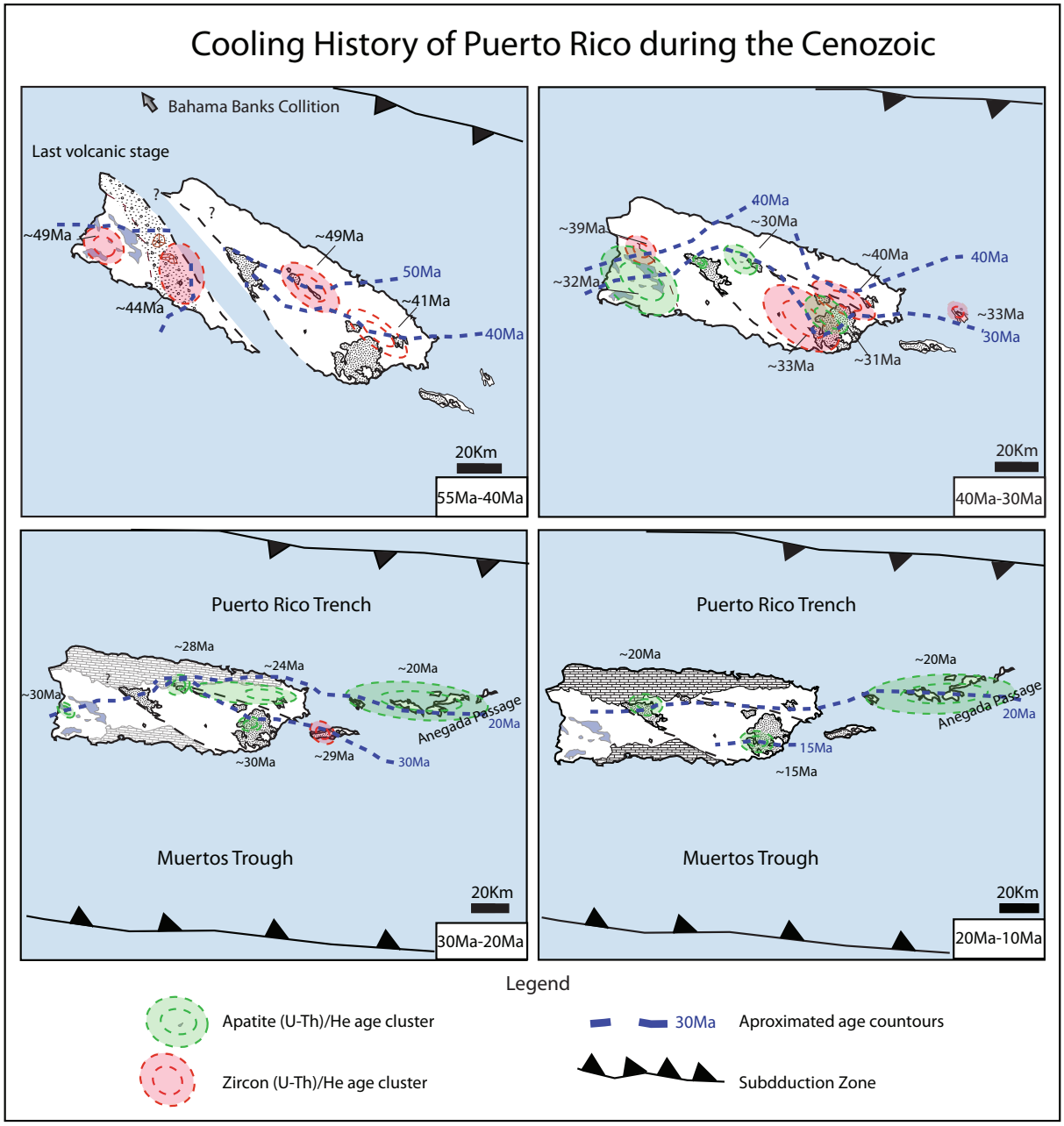

Figure 14. Tectonic model and contour map of the Puerto Rico-Virgin Island cooling history at different periods during the Cenozoic.

Appendix 1.1

Calculation of exhumation rates and amount of rock erosion by epoch assuming a monotonic cooling at different geothermal gradients of 20°C/km, 25°C/km and 30°C/km.

Tc = thermochronometer closure temperature

- **Tc (Zrc) – Tc (Ap) = Tc differential**

  180°C - 70°C = 110°C

- **Tc (Diff) / Geothermal Gradient = Amount of km exhumed to exposed Tc**

  110°C / 20°C/km = 5.5 km
  110°C / 25°C/km = 4.4 km
  110°C / 30°C/km = 3.7 km

- **Box A on figure 14**

  Km distance between isotherms = Rate of rock exhumed in M.y. period
  Δ Zrc-Ap (U-Th)/He ages

  Example: 07CF-06
  (U-Th)/He zircon age = 38.9 Ma
  (U-Th)/He apatite age = 34.4 Ma

  5.5Km = 1.2 km of exhumed material in a million year period under a geothermal
  4.5 Myr gradient of 20°C/km for a monotonic exhumation model.

- **Boxes B, C, D and E**
  - Only samples plotted are ones with zircon and apatite (U-Th)/He ages.
  - Values correspond to km of exhumed rock since Tc (Zrc)

  Exhumed rate from Box A **x** **Difference between (U-Th)/He zircon and time slice**

  Example: 07CF-06

  (1.2 km) x (38.9 Ma – 30 Ma) = 10.7 km of exhumation by 30 M.y.

APPENDIX 2.1 COTUI LIMESTONE (06CL-06) - PETROGRAPHIC DESCRIPTION

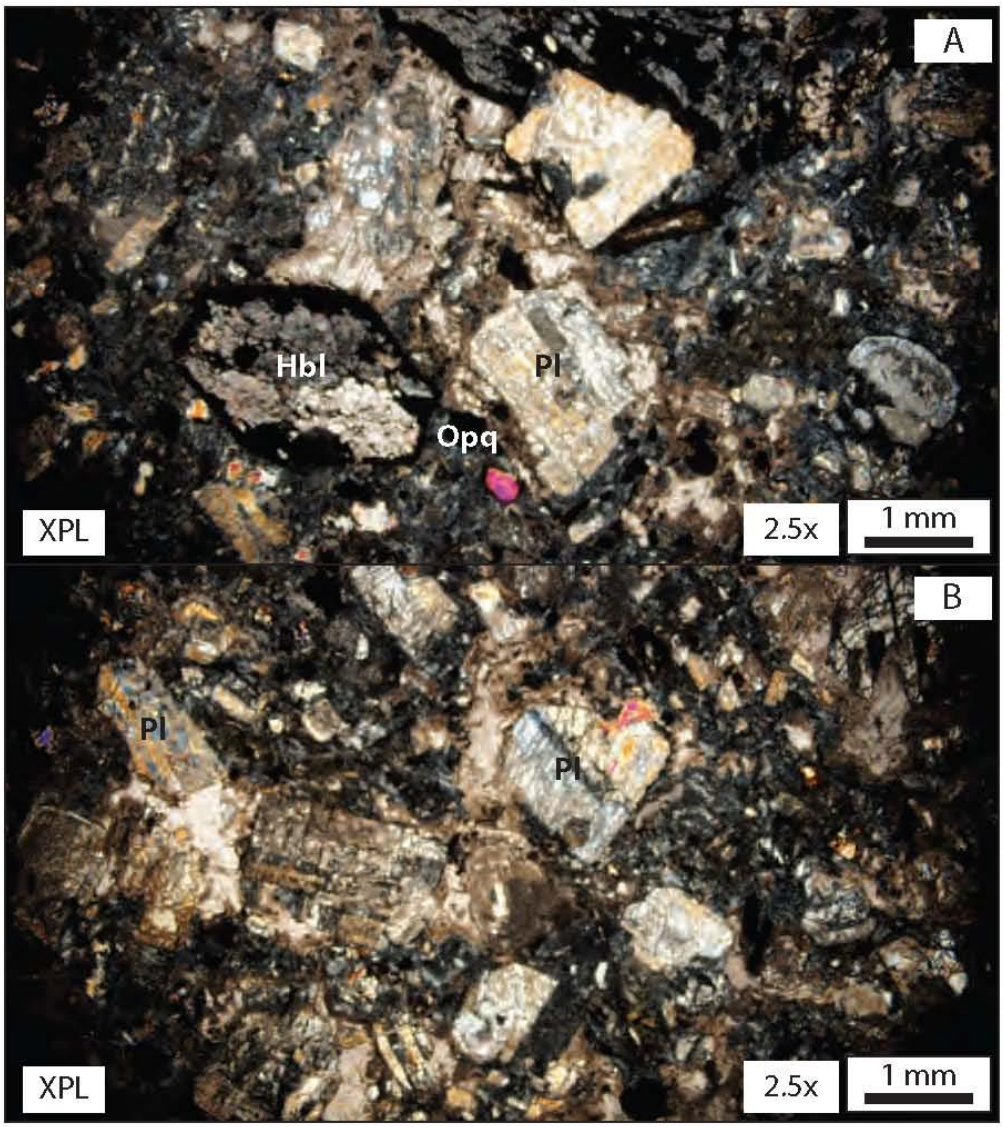

Thin section: 06CL-06
Location: Cotui Limestone
Rock name: andesite bomb in Cotui Limestone
Texture: holocrystalline, porphyritic
Grain size: medium-grained

Description

This highly altered rock is intermediate in composition and it has assimilated carbonate components from the Cotui Limestone. This porphyritic rock has euhedral plagioclase grains present in a microcrystalline plagioclase groundmass. Hornblende grains have been replaced by calcite but preserving their original habit. Calcite is present in a variety of sizes and it has irregular contacts with some visible alteration rims. Skeletal grains are also present.

Legend: Bt = biotite; Cal = calcite; Chl = chlorite; Kfs = K-feldspar; Hbl = hornblende; Opq = opaque mineral; Pl = plagioclase; Hbl = hornblende; Qz = quartz; Ser = sericite; Ttn = titanite; Zrn = zircon

APPENDIX 2.2 MAYAGUEZ (07CF-06) - PETROGRAPHIC DESCRIPTION

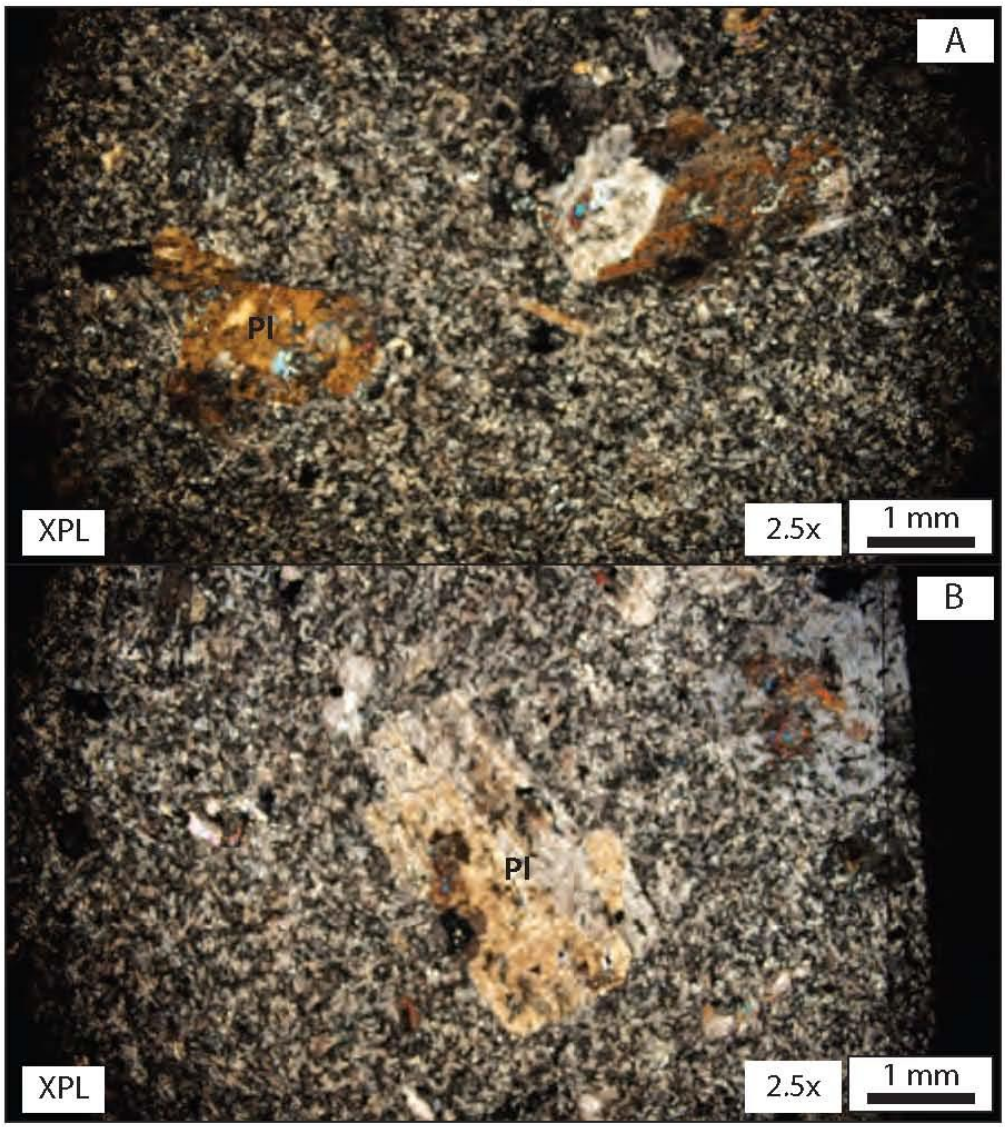

Thin section: 07CF-06
Location: Mayaguez
Rock name: felsic dike
Texture: holocrystalline, porphyritic
Grain size:

Description

This feldspar-rich aplitic dike is predominantly composed by a plagioclase and minor calcite groundmass with euhedral to anhedral plagioclase phenocrysts. Additionally, small amounts of anhedral calcite crystal **are visible. Quartz can also be identified.**

Legend: Bt = biotite; Cal = calcite; Chl = chlorite; Kfs = K-feldspar; Hbl = hornblende; Opq = opaque mineral; Pl = plagioclase; Hbl = hornblende; Qz = quartz; Ser = sericite; Ttn = titanite; Zrn = zircon

APPENDIX 2.3 HORMIGUEROS PORPHYRY (06HP-01) - PETROGRAPHIC DESCRIPTION

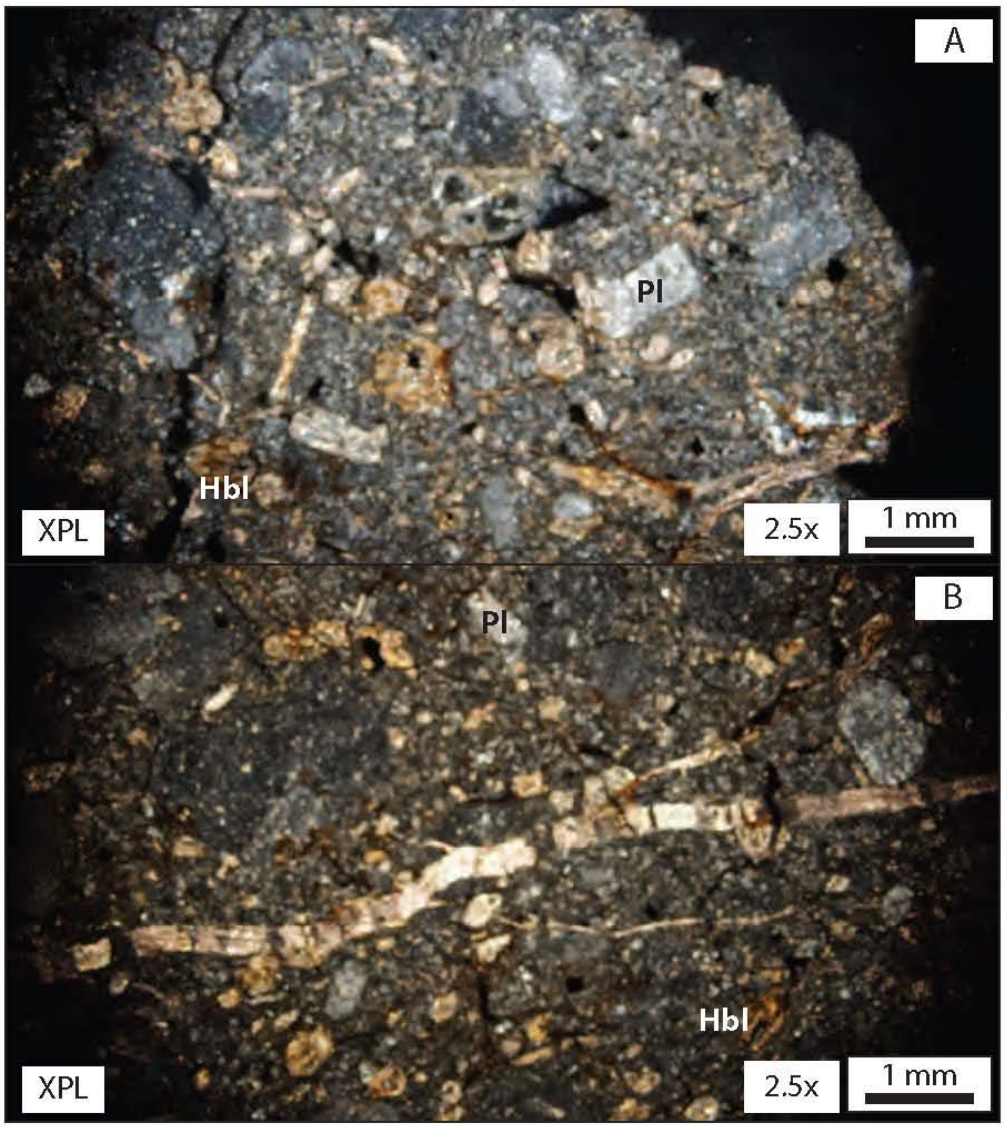

Thin section: 06HP-01
Location: Hormigueros porphyry
Rock name: diorite porphyry
Texture: holocrystalline, porphyritic
Grain size:

Description

This pervasively altered rock preserves an argellic texture. Some pseudomorphs of plagioclase and hornblende **grains can be identified but are very altered.**

Legend: Bt = biotite; Cal = calcite; Chl = chlorite; Kfs = K-feldspar; Hbl = hornblende; Opq = opaque mineral; Pl = plagioclase; Hbl = hornblende; Qz = quartz; Ser = sericite; Ttn = titanite; Zrn = zircon

APPENDIX 2.4 LAJAS FORMATION (09LF-04) - PETROGRAPHIC DESCRIPTION

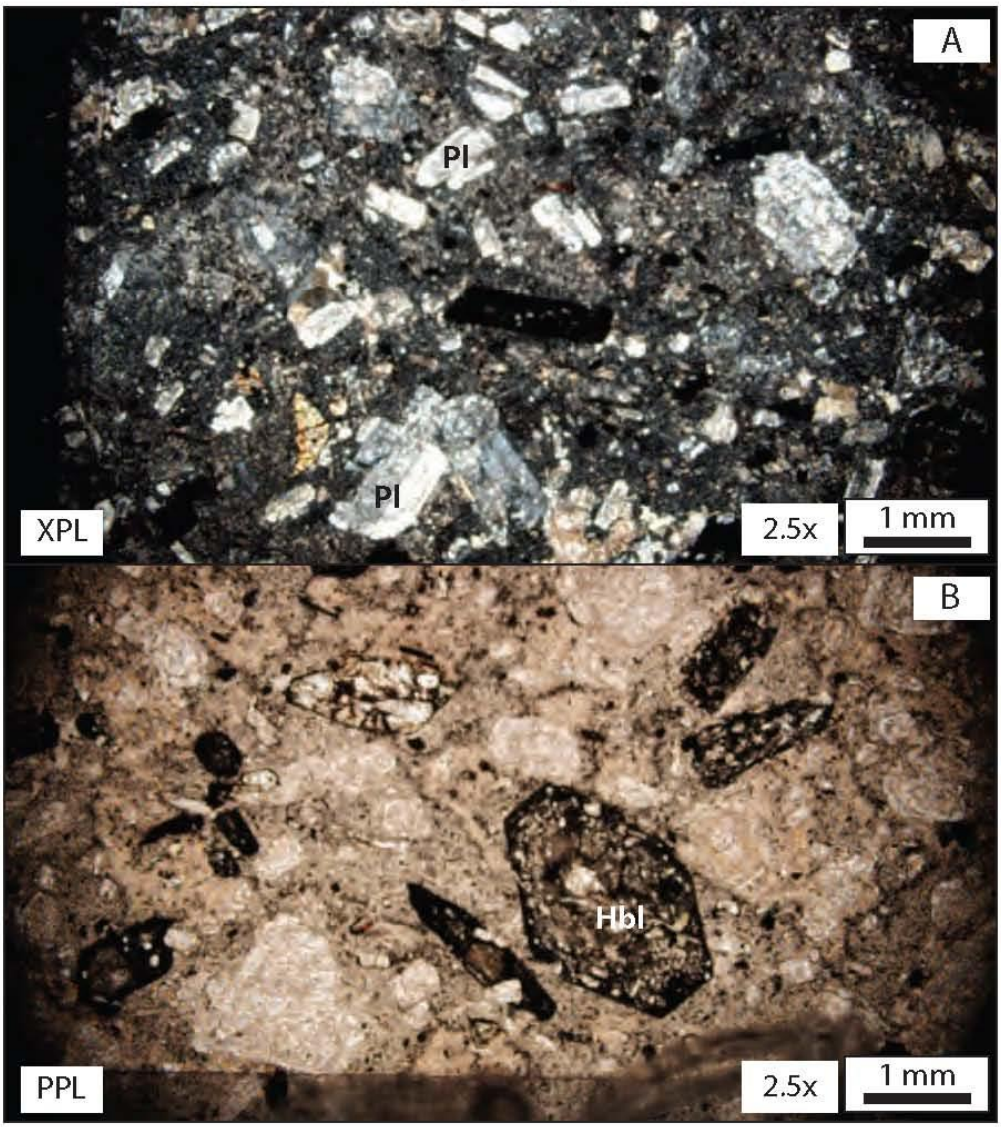

Thin section: 09LF-04
Location: Lajas Formation
Rock name: andesite porphyry
Texture: holocrystalline, porphyritic
Grain size:

Description

This porphyritic rock is composed of a plagioclase groundmass and euhedral to subhedral plagioclase and hornblende grains. Altered hornblende and plagioclase both show alteration rims. Opaque minerals are present in the groundmass.

Legend: Bt = biotite; Cal = calcite; Chl = chlorite; Kfs = K-feldspar; Hbl = hornblende; Opq = opaque mineral; Pl = plagioclase; Hbl = hornblende; Qz = quartz; Ser = sericite; Ttn = titanite; Zrn = zircon

APPENDIX 2.5 MAGUAYO PORPHYRY (09MP-01) - PETROGRAPHIC DESCRIPTION

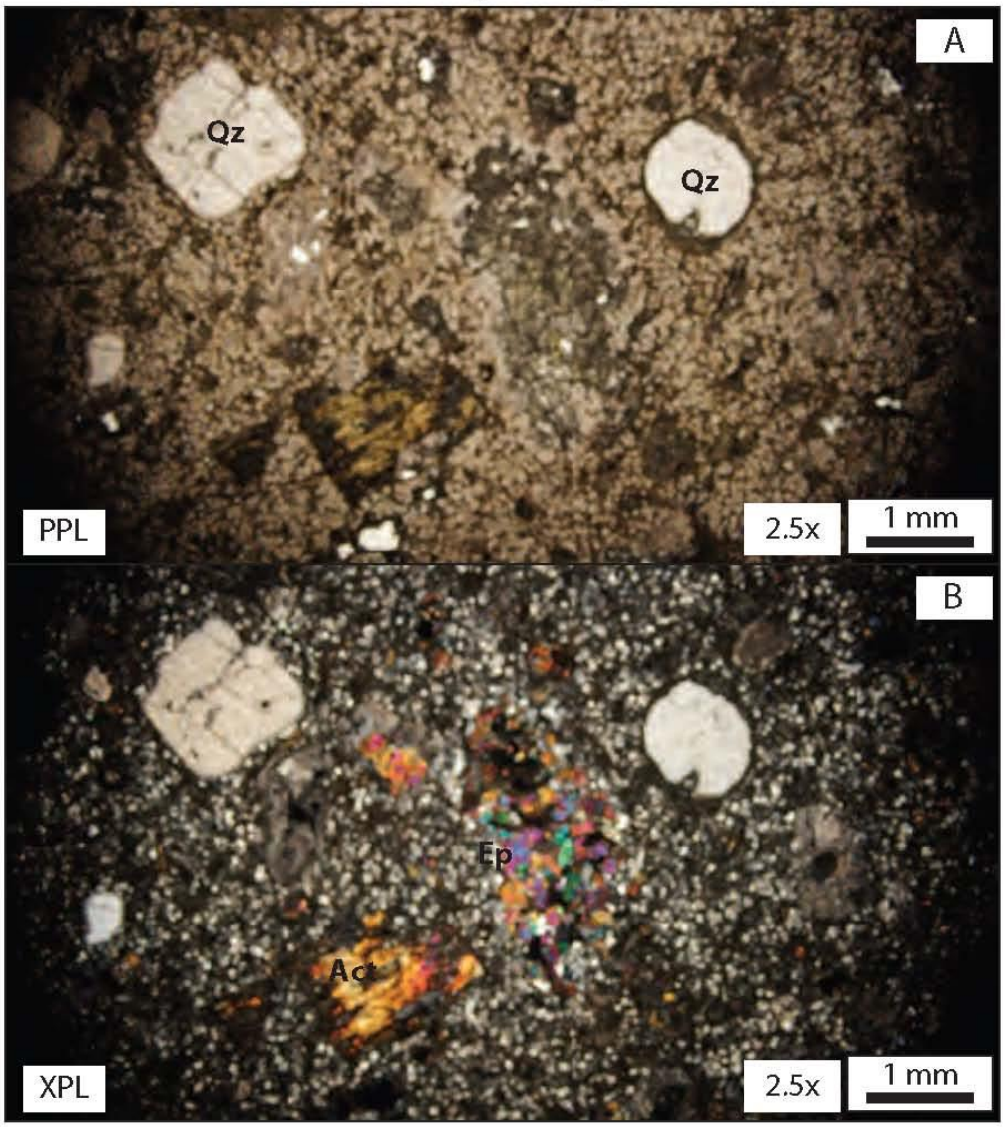

Thin section: 09MP-01
Location: Maguayo Porhyry
Rock name: diorite porphyry
Texture: holocrystalline, porphyritic
Grain size:

Description

This rock has a equigranular plagioclase groundmass with scatter-rounded quartz crystals. Additionally, propylitic **alteration as columnar aggregates of epidote and minor quantitires of fibrous actinolite are visible.**

Legend: Act = actinolite; Bt = biotite; Cal = calcite; Chl = chlorite; Cpx = clinopyroxene; Ep = epidote; Kfs = K-feldspar; Hbl = hornblende; Qz = quartz; Ser = sericite; Ttn = titanite; Zrn = zircon

APPENDIX 2.6 RIO GRANDE PLUTON (08RG-01) - PETROGRAPHIC DESCRIPTION

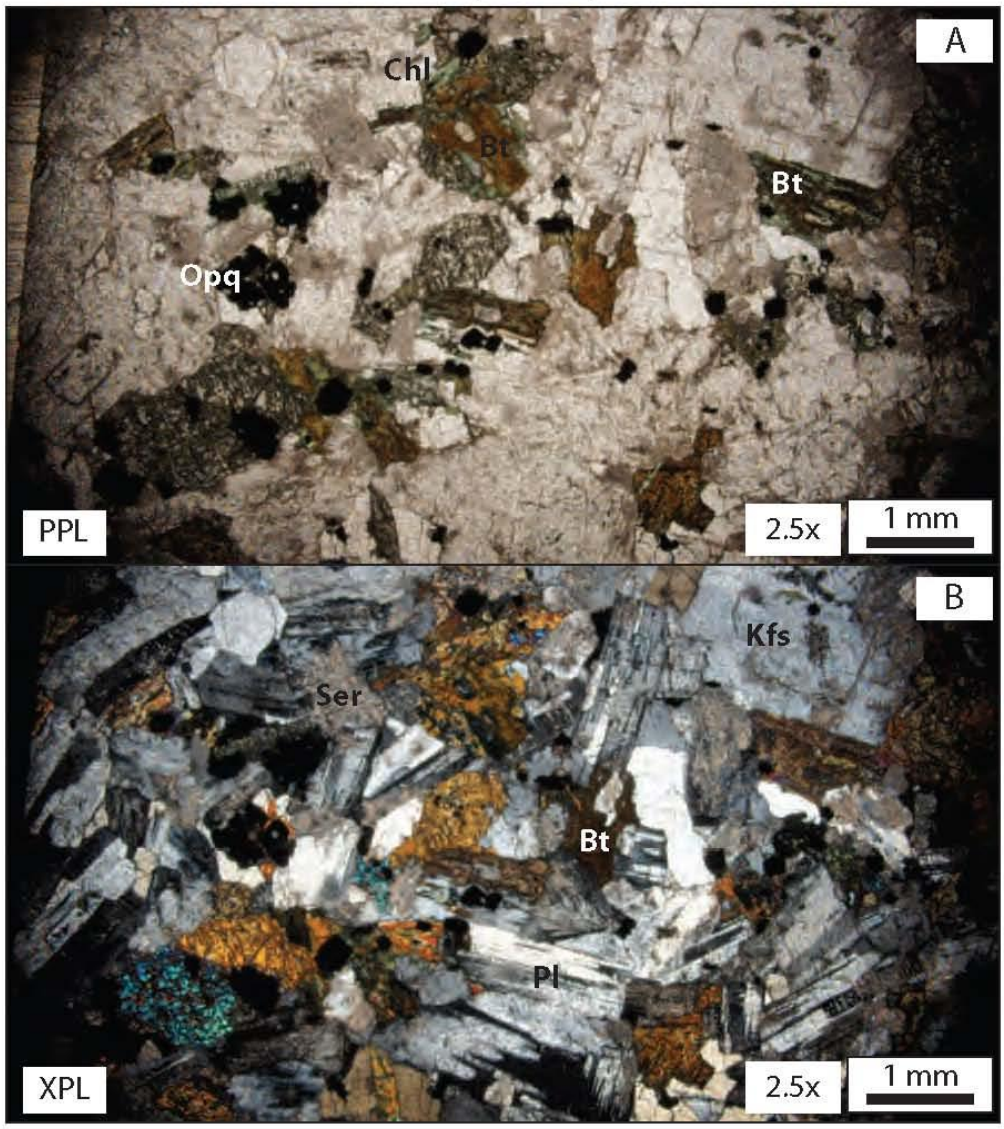

Thin section: 08RG-01
Location: Rio Grande Pluton
Rock name: hornblende diorite
Texture: holocrystalline, phaneritic
Grain size: medium-grained

Description

This rock is composed of plagioclase, quartz, K-feldspar, hornblende, and oxides. Plagioclase shows albite and Carlsbad twinning, alteration to sericite is also present. Hornblende grains show green pleochroism and secondary **alteration to chlorite, biotite, and actinolite. Oxides occur as inclusionsin hornblende. Quartz grains mostly fill** the interstices between plagioclase and K-feldspar. The mineral percentage is 45% plagioclase, 20% quartz, 15% K-feldspar, 10% hornblende, 2% biotite, 2% chlorite, 2% actinolite, 3% oxides, and 1% accesory minerals. According to Q-A-P modal percentage this rock is a hornblede diorite with 56% plagioclase, 25% quartz, and 19% K-feldspars.

Legend: Bt = biotite; Chl = chlorite; Kfs = K-feldspar; Hbl = hornblende; Opq = opaque mineral; Pl = plagioclase; Qz = quartz; Ser = sericite

APPENDIX 2.7 RIO GRANDE PLUTON (08RG-02) - PETROGRAPHIC DESCRIPTION

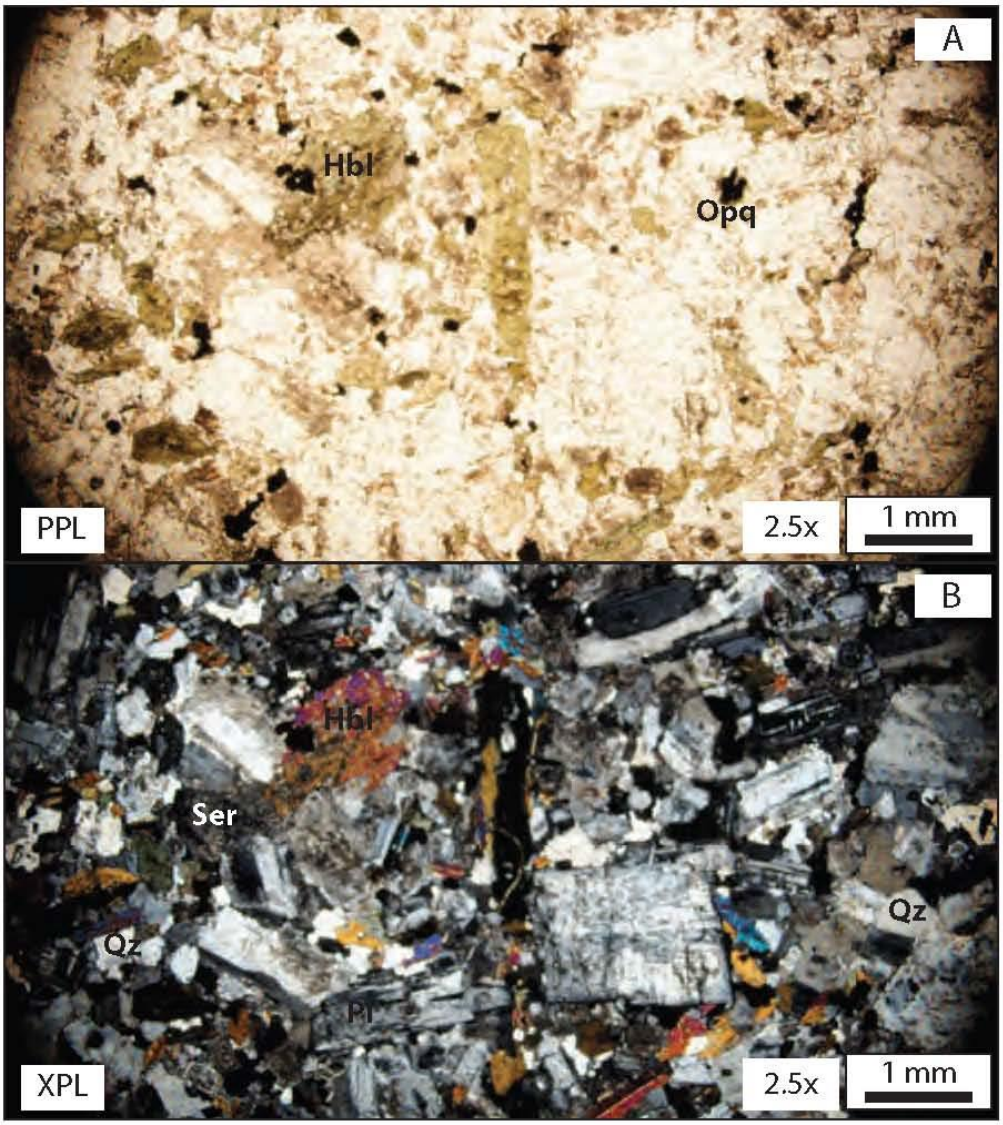

Thin section: 08RG-02
Location: Rio Grande Pluton
Rock name: hornblende diorite
Texture: holocrystalline, phaneritic
Grain size: medium-grained

Description

The mineral percentage in the rock is 40% plagioclase, 25% quartz, 20% K-feldspar, 12% hornblende, 2% oxides, and 1% accesory minerals (zircon and apatite). Subhedral to anhedral plagioclase grains show distinct oscillatory zoning and polysynthetic twinning. Plagioclase and K-feldspar show alteration to sericite. Plagioclase appears also as inclusions in hornblende grains. Hornblende grains show light-green pleochroism where oxide grains are present as inclusions and along their boundaries. Quartz occurs as anhedral intersticial grains. The Q-A-P modal percentage indicate that this rock is a hornblende andesite with 47% plagioclase, 29% quartz, and 24% K-feldspar.

Legend: Bt = biotite; Chl = chlorite; Kfs = K-feldspar; Hbl = hornblende; Opq = opaque mineral; Pl = plagioclase; Qz = quartz; Ser = sericite

APPENDIX 2.8 RIO GRANDE PLUTON (08RG-03) - PETROGRAPHIC DESCRIPTION

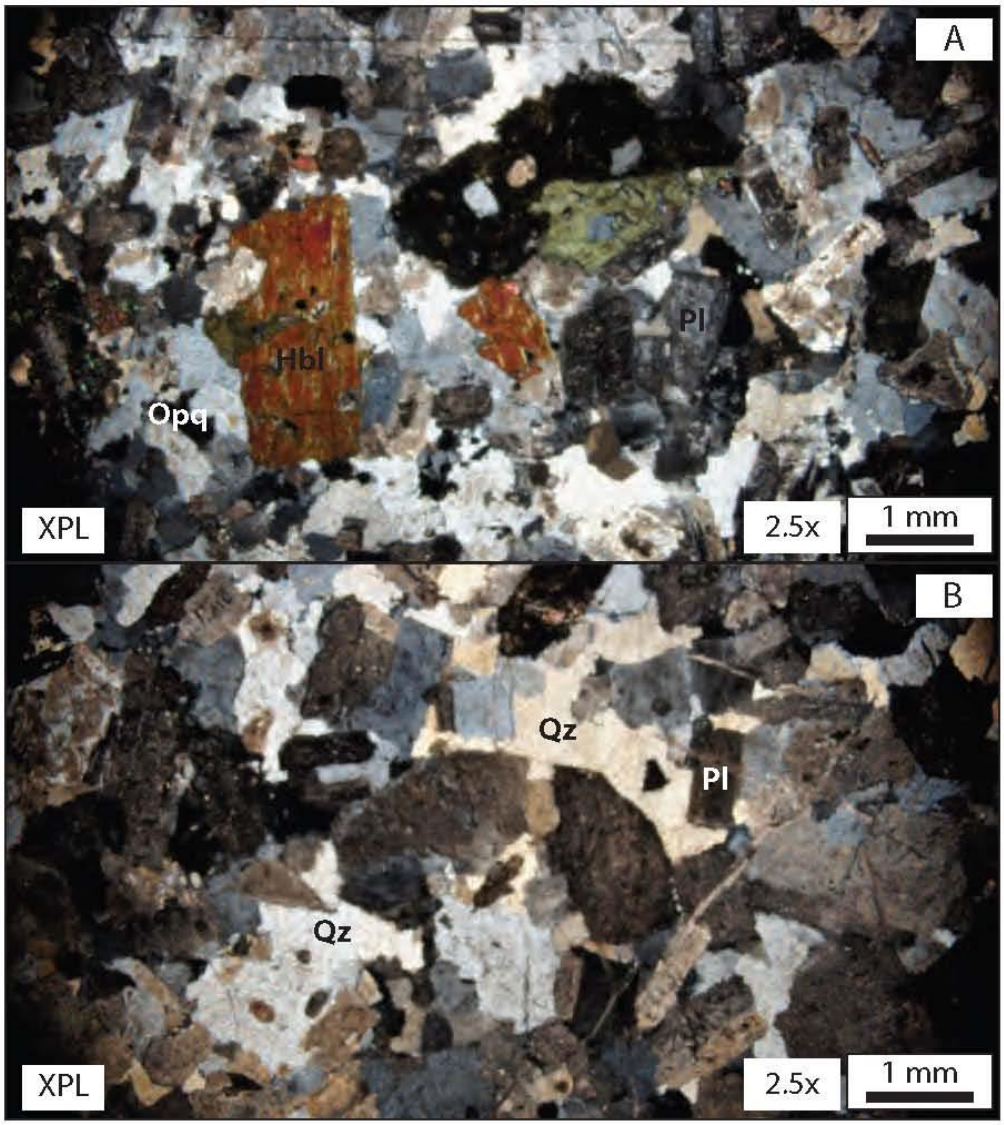

Thin section: 08RG-03
Location: Rio Grande Pluton
Rock name: hornblende diorite
Texture: holocrystalline, phaneritic
Grain size: medium-grained

Description

The rock is composed of 43% plagioclase, 20% quartz, 19% K-feldspar, 15% hornblende, 2% oxides, and 1% accesory minerals (zircon and apatite). The Q-A-P modal percentage of this rock is 53% plagioclase, 24% quartz, and 23% K-feldspar. Plagioclase and K-feldspar in this rock are highly altered to sericite. Some plagioclase grains show albite twinning. Subhedral to anhedral dark-green pleochroic hornblende grains are partially altered to chlrorite. Zircon and oxides are preserved as inclusions in hornblende. Quartz appears as anhedral intertitial grains.

Legend: Bt = biotite; Chl = chlorite; Kfs = K-feldspar; Hbl = hornblende; Opq = opaque mineral; Pl = plagioclase; Qz = quartz; Ser = sericite

APPENDIX 2.9 UTUADO PLUTON (08UP-03) - PETROGRAPHIC DESCRIPTION

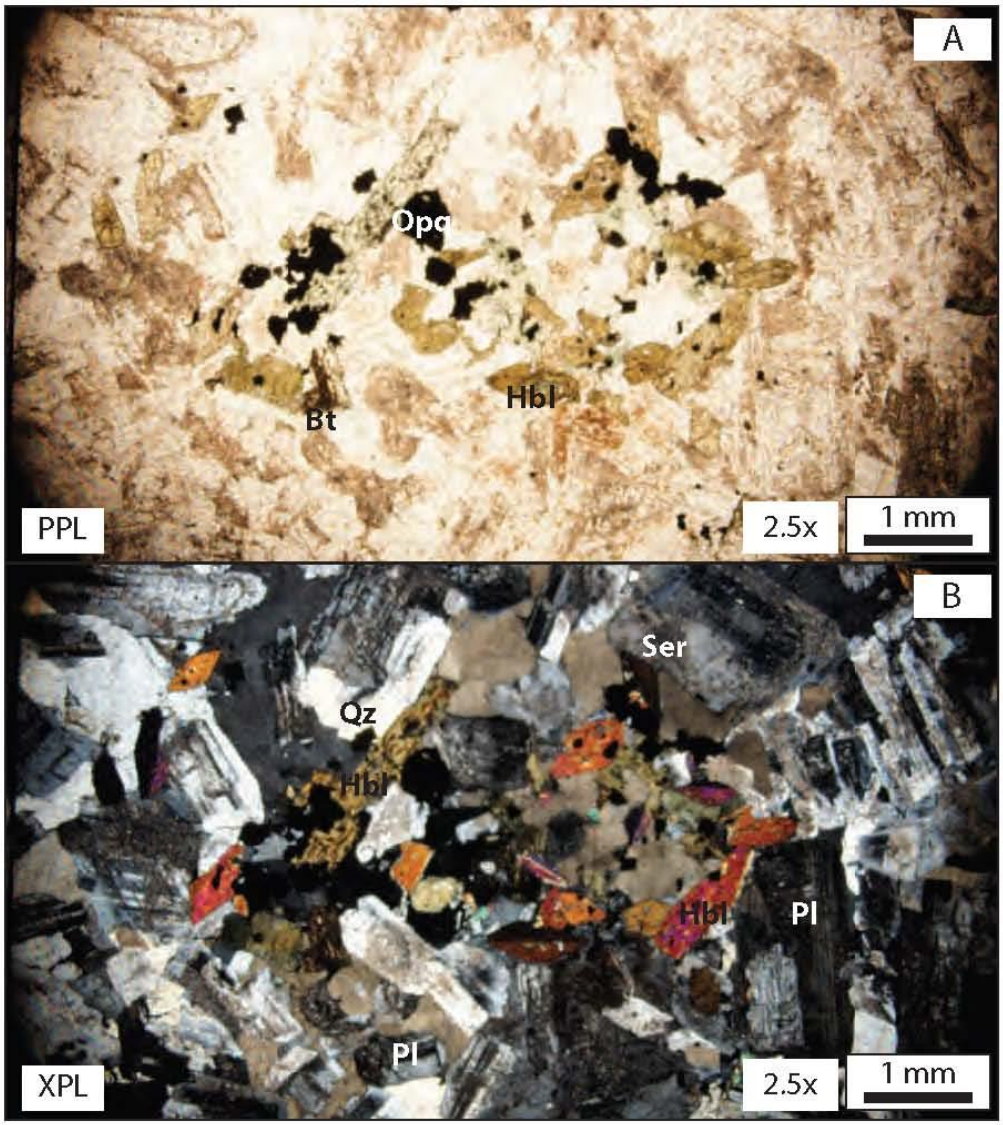

Thin section: 08UP-03
Location: Utuado Pluton
Rock name: granodiorite
Texture: holocrystalline, phaneritic
Grain size: medium-grained

Description

The mineral composition of this rock is 40% plagioclase, 22% quartz, 18% K-feldspar, 12% hornblende, 5% biotite, 2% oxides, and 1% accesory minerals (zircon and apatite). Plagioclase shows predominantly albite twinning and it is highly altered to sericite. Subhedral to euhedral hornblende grains show green pleochroism and occur as inclusions in K-feldspar. The Q-A-P modal percentage indicates the rock is a granodiorite with 50% plagioclase, 28% quatrz, and 22% K-feldspar.

Legend: Bt = biotite; Chl = chlorite; Kfs = K-feldspar; Hbl = hornblende; Opq = opaque mineral; Pl = plagioclase; Qz = quartz; Ser = sericite

APPENDIX 2.10 UTUADO PLUTON (08UP-07) - PETROGRAPHIC DESCRIPTION

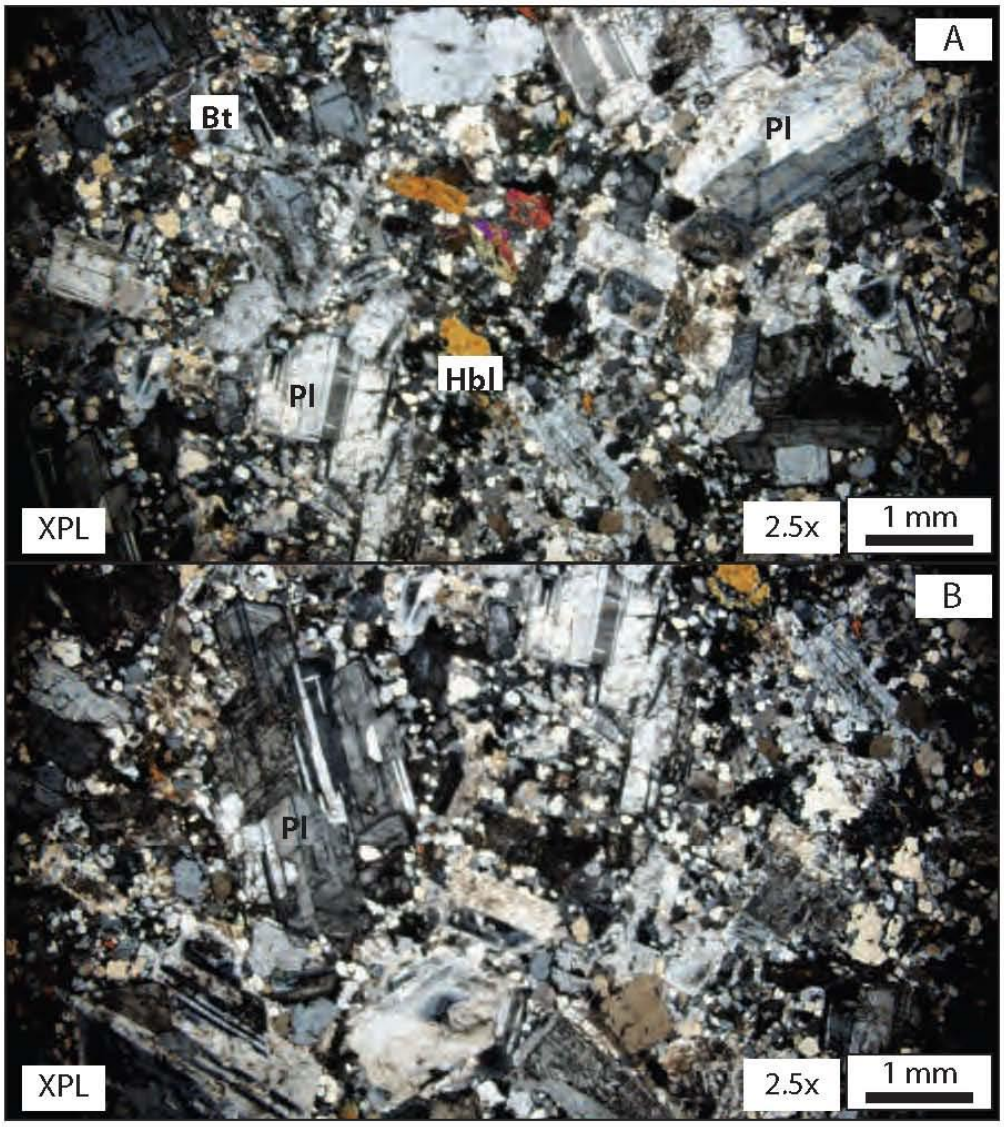

Thin section: 08UP-07
Location: Utuado Pluton
Rock name: granodiorite
Texture: holocrystalline, phenocryst
Grain size: porphyritic

Description

This rock has a mineral composition of 43% plagioclase, 23% quartz, 18% K-feldspar, 8% hornblende, 3% biotite, 2% chlorite, 2% oxides, and 1% accesory minerals (zircon and apatite). Plagioclase phenocrysts show albite twinning and alteration to sericite. The groundmass consists of equigranular grains of K-feldspar and quartz. Hornblende grains show green pleochroism, euhedral to subhedral grains. Biotite shows brown pleochroism and alteration to chlorite along its margins. Oxides occurs as inclusions in hornblende.

Legend: Bt = biotite; Chl = chlorite; Kfs = K-feldspar; Hbl = hornblende; Opq = opaque mineral; Pl = plagioclase; Qz = quartz; Ser = sericite

APPENDIX 2.11 ISLA CULEBRA (07IC-04) - PETROGRAPHIC DESCRIPTION

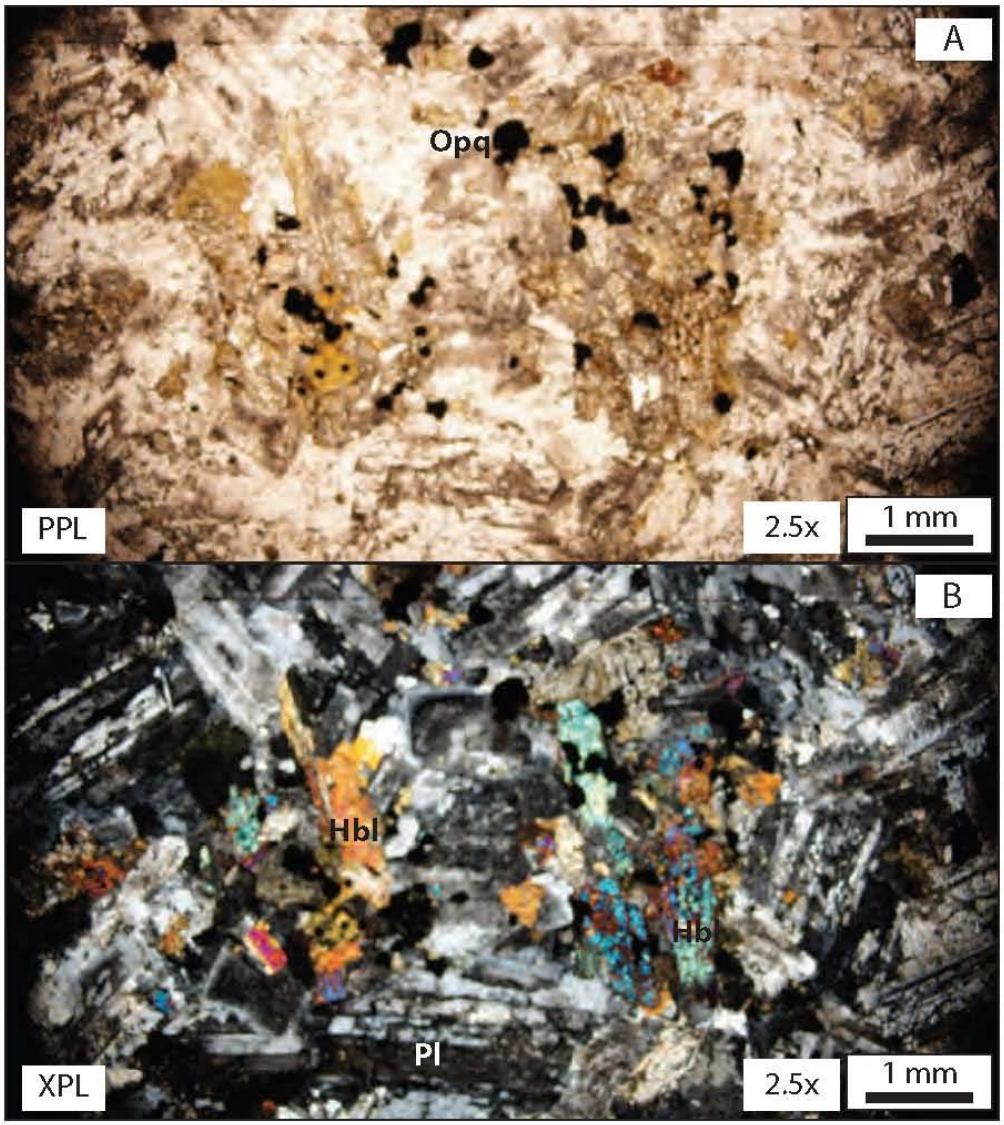

Thin section: 07IC-04
Location: Isla Culebra
Rock name: diorite
Texture: holocrystalline
Grain size: medium-grained

Description

This rock is pervasively altered. It is composed of 49% plagioclase, 15% K-feldspar, 10% quartz, 20% hornblende, 5% opaques, and 1% accesory minerales (zircon and apatite). Plagioclase are highly altered to sericite but some **albite and Carlsbad twinning can be still be identified. The Q-A-P modal percentage is 66% plagioclase,** 20% K-feldspar, and 14% quartz.

Legend: Bt = biotite; Chl = chlorite; Kfs = K-feldspar; Hbl = hornblende; Opq = opaque mineral; Pl = plagioclase; Qz = quartz; Ser = sericite

APPENDIX 2.12 ISLA CULEBRA (07IC-23) - PETROGRAPHIC DESCRIPTION

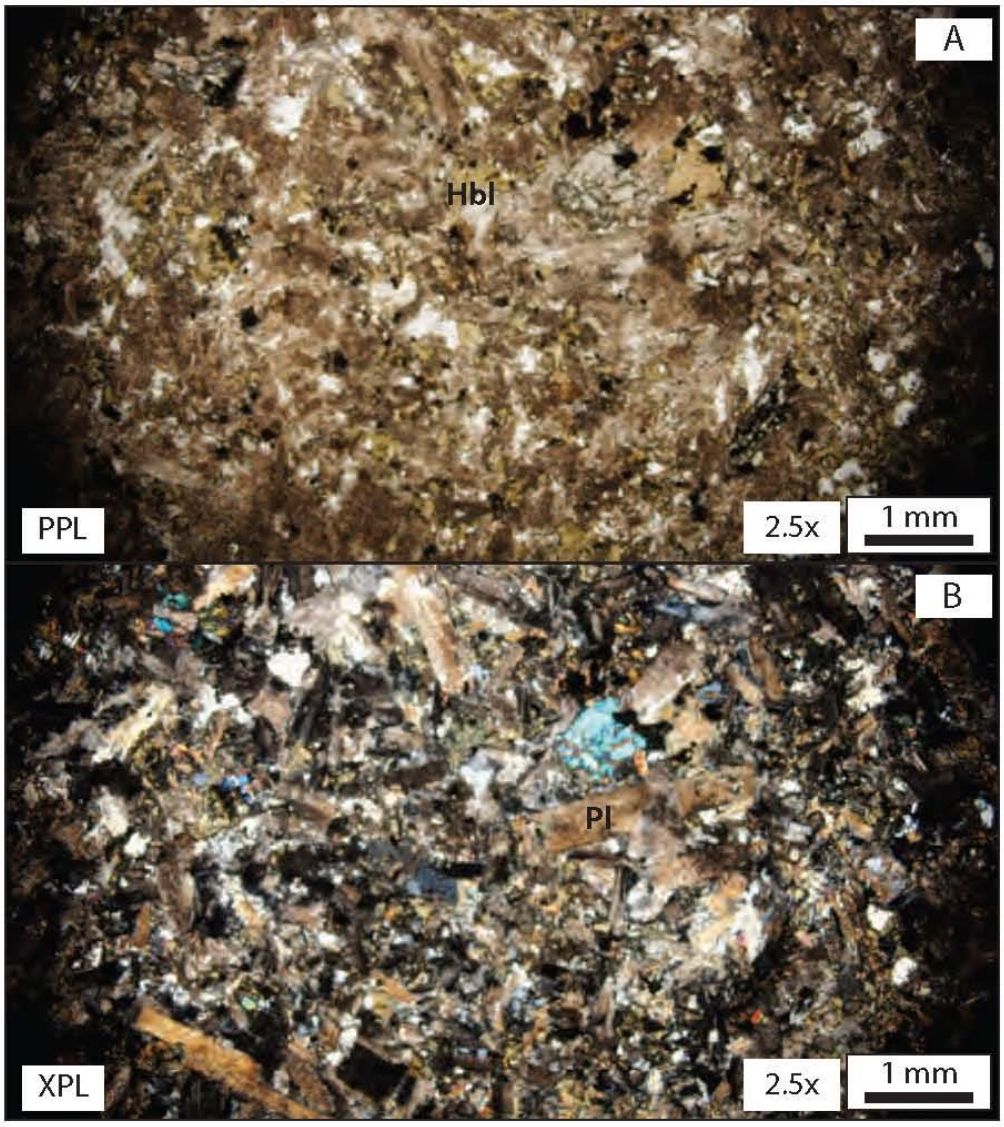

Thin section: 09IC-23
Location: Isla Culebra
Rock name: micro-diorite
Texture: holocrystalline
Grain size: porphyritic

Description

This rock is pervasively altered. It is composed of 45% plagioclase, 15% K-feldspar, 10% quartz, 20% hornblende, 5% opaques, and 1% accesory minerales (zircon and apatite). Plagioclase shows albite and Carlsbad twinning and are highly altered to sericite. The Q-A-P modal percentage is 64% plagioclase, 21% K-feldspar, and 15% quartz.

Legend: Bt = biotite; Chl = chlorite; Kfs = K-feldspar; Hbl = hornblende; Opq = opaque mineral; Pl = plagioclase; Qz = quartz; Ser = sericite

APPENDIX 2.13 TORTOLA (09VI-02) - PETROGRAPHIC DESCRIPTION

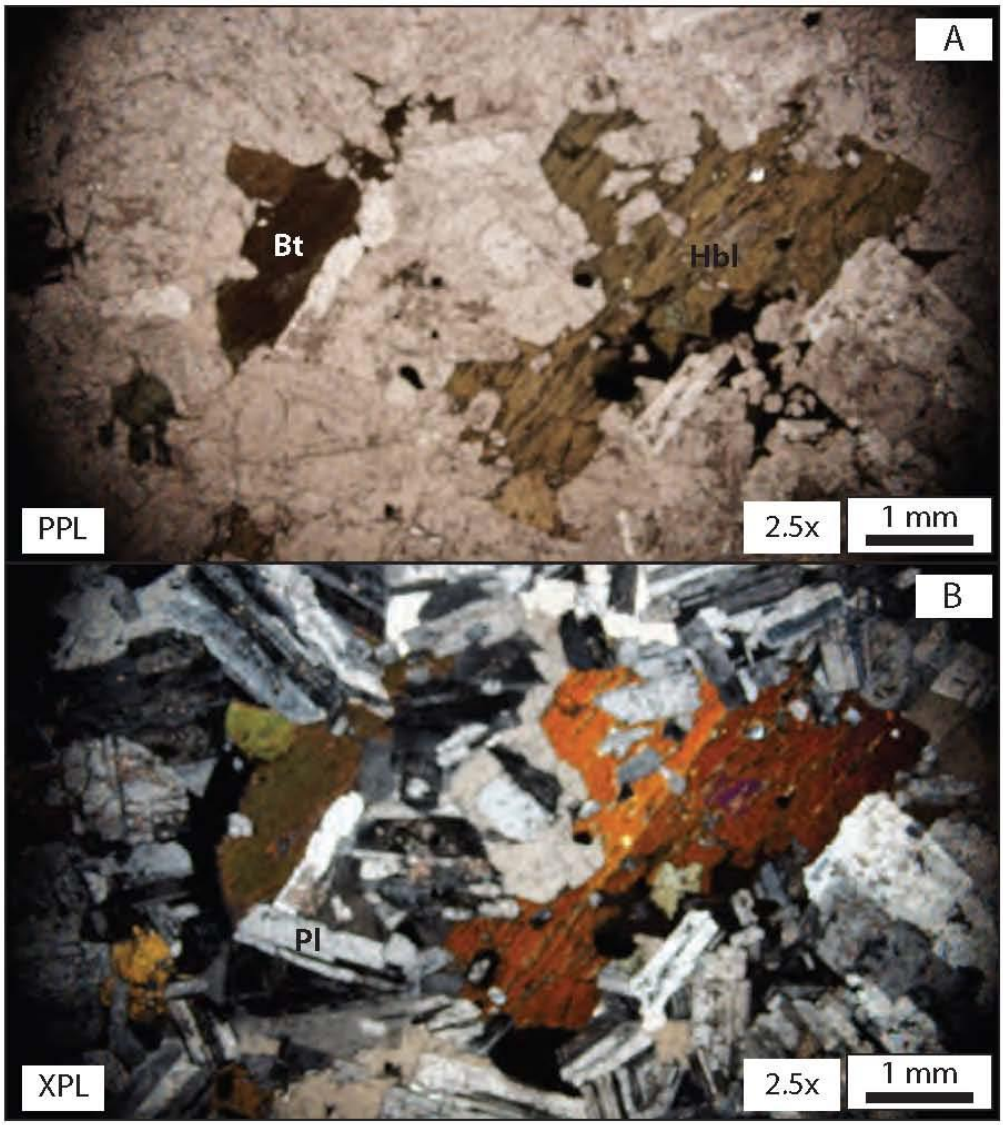

Thin section: 09VI-02
Location: Tortola
Rock name: granodiorite
Texture: holocrystalline, phaneritic
Grain size: medium-grained

Description

This rock is composed of 45% plagioclase, 12% quartz, 8% K-feldspar, 15% hornblende, 12% biotite, 5% chlorite, 2% opaques, and 1% accesory minerals. The Q-A-P modal percentage indicates the rock is a granodiorite with 69% plagioclase, 19% quartz, and 12% K-feldspar. Plagioclase occurs as euhedral grains showing albite and Carlsbad twinning. Minor alteration to sericite is also visisble and it is found as inclusions in quartz grains. Quartz occurs as anhedral grains with distinct ondulatory extinction. Hornblende shows green pleochroism and alteration **to biotite. Biotite shows brown pleochroism and secondary alteration to chlorite can identified along its boundaries.** Opaques occur as inclusions in hornblende grains.

Legend: Bt = biotite; Chl = chlorite; Kfs = K-feldspar; Hbl = hornblende; Opq = opaque mineral; Pl = plagioclase; Qz = quartz; Ser = sericite

APPENDIX 2.14 NORMAN ISLAND (09VI-05) - PETROGRAPHIC DESCRIPTION

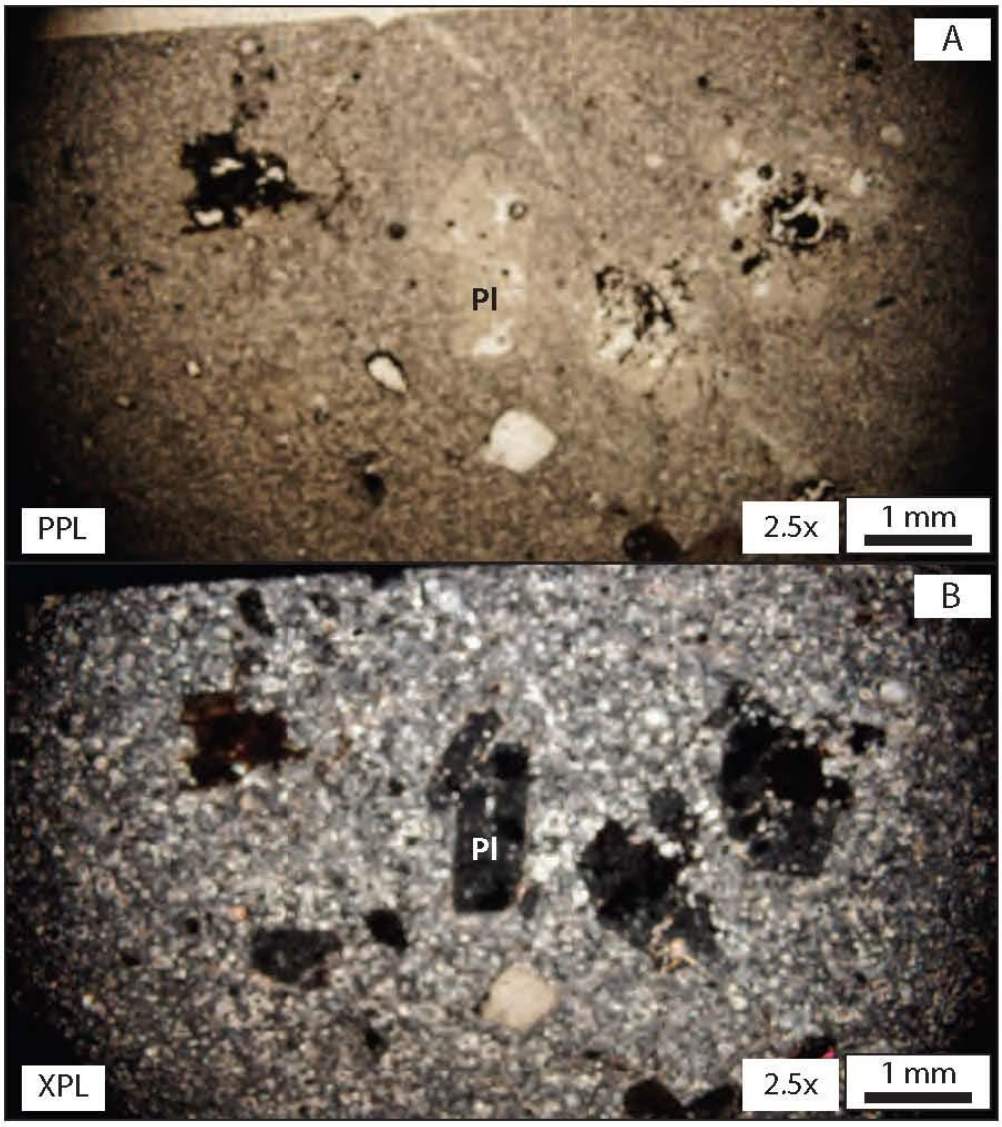

Thin section: 09VI-05
Location: Norman Island
Rock name: silicified rhyolite (keratophyre)
Texture: holocrystalline, porphyritic
Grain size:

Description

This fine-grained rock is composed of a plagioclase groundmass with large quartz and plagioclase phenocrysts.

Legend: Bt = biotite; Chl = chlorite; Kfs = K-feldspar; Hbl = hornblende; Opq = opaque mineral; Pl = plagioclase; Qz = quartz; Ser = sericite

APPENDIX 2.15 VIRGIN GORDA (09VI-06) - PETROGRAPHIC DESCRIPTION

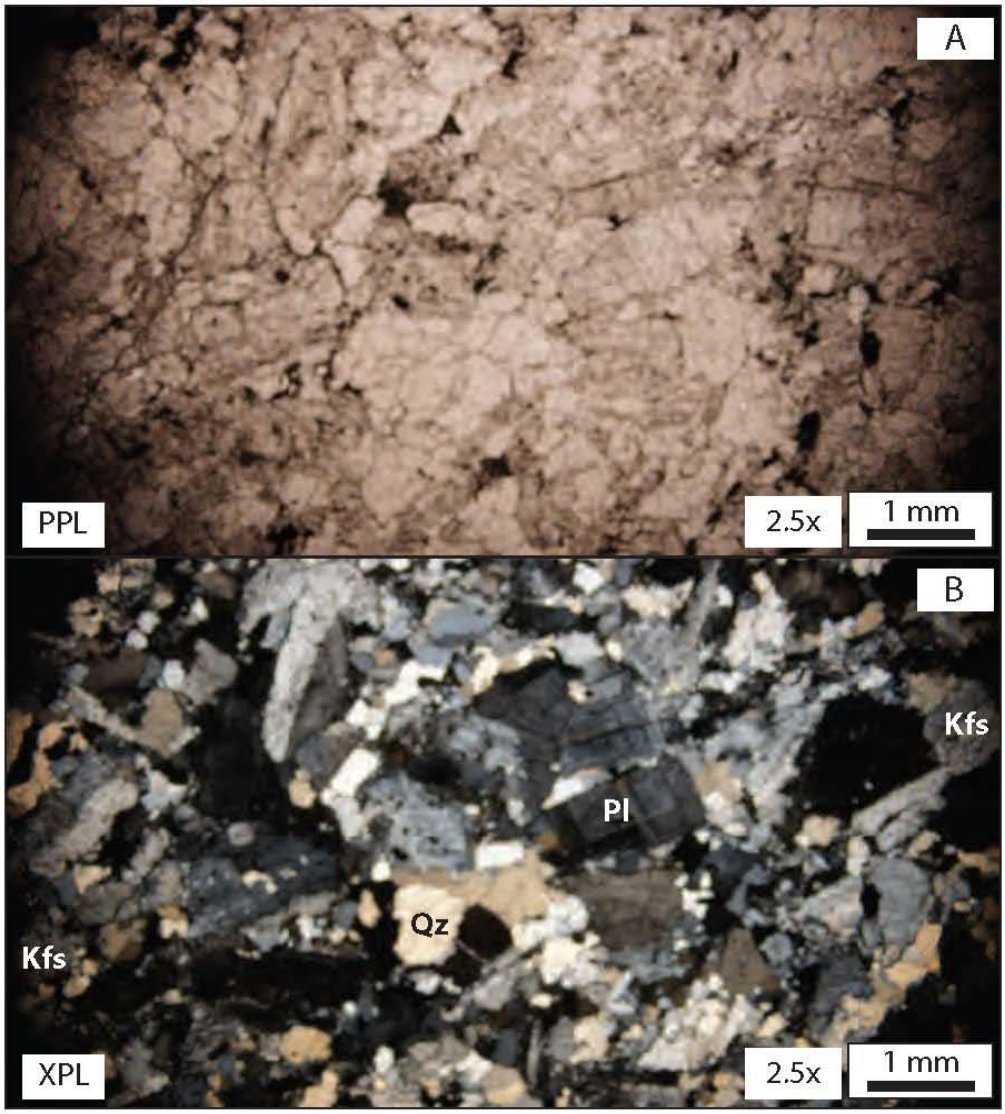

Thin section: 09VI-06
Location: Virgin Gorda
Rock name: granodiorite
Texture: holocrystalline
Grain size:

Description

This rock is composed of a 45% plagioclase, 30% quartz and 25% K-feldspar. Alteration to sericite in K-feldspar is present.

Legend: Bt = biotite; Chl = chlorite; Kfs = K-feldspar; Hbl = hornblende; Opq = opaque mineral; Pl = plagioclase; Qz = quartz; Ser = sericite

APPENDIX 2.16 VIRGIN GORDA (09VI-12) - PETROGRAPHIC DESCRIPTION

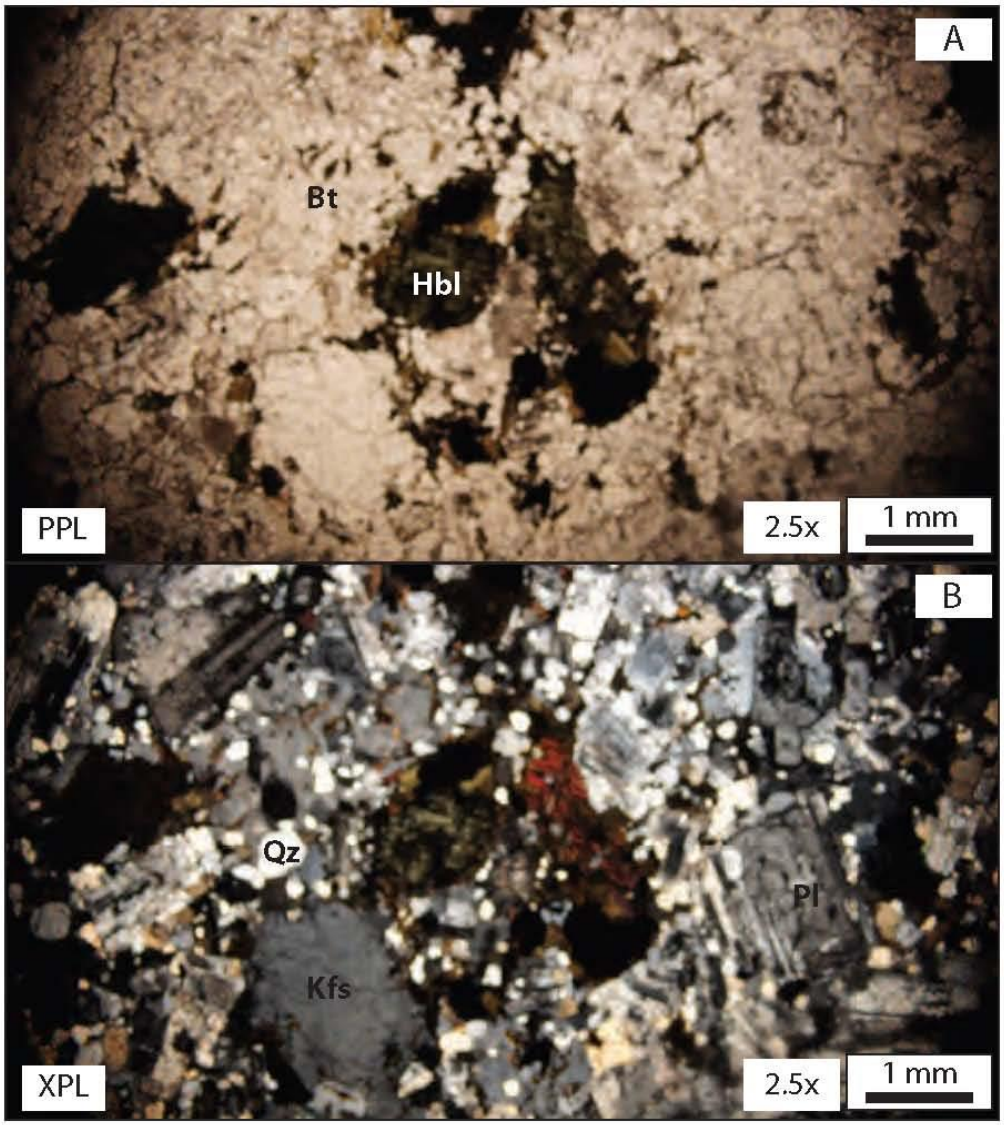

Thin section: 09VI-12
Location: Virgin Gorda
Rock name: quartz-granodiorite
Texture: holocrystalline
Grain size: porphyritic

Description

This rock is composed of 35% plagioclase, 30% quartz, 7% K-feldspar, 12% hornblende, 8% biotite, 5% chlorite, 2% opaques, and 1% accesory minerals. The Q-A-P modal percentage is 49% plagioclase, 42% quartz, 9% K-feldspar. Plagioclase occurs as large euhedral phenocrysts showing albite and Carlsbad twinning. Quartz occurs as small anhedral grains with ondulatory extinction. Green hornblende grains show secondary alteration to biotite. Biotite shows brown pleochroism and shows alteration to chlorite.

Legend: Bt = biotite; Chl = chlorite; Kfs = K-feldspar; Hbl = hornblende; Opq = opaque mineral; Pl = plagioclase; Qz = quartz; Ser = sericite

APPENDIX 3.1 (U-TH)/HE ZIRCON AGES AND GEOCHEMISTRY

Sample	Age (Ma)	Error	U (ppm)	Th (ppm)	147Sm (ppm)	[U]e	Th/U	He (nmol/g)	Mass (ug)	Ft	ESR
Rio Blanco stock											
z06RB01-01	52.4	4.19	31.7	6.3	0.1	33.1	0.20	8.0	24.96	0.85	81.08
z06RB01-02	44.8	3.58	30.7	6.1	0.1	32.1	0.20	6.3	10.81	0.81	61.81
z06RB01-03	34.5	2.76	42.4	9.4	0.1	44.6	0.22	6.7	8.85	0.81	60.04
z06RB01-04	30.4	2.43	86.0	21.6	0.2	90.9	0.25	11.4	4.66	0.76	48.77
z06RB01 (Avg.)	***40.5***	***3.2***	***47.7***	***10.9***	***0.1***	***50.2***	***0.2***	***8.1***	***12.3***	***0.8***	***62.9***
Caguas stock											
z06CG01-01	36.7	2.9	59.5	23.9	0.0	65.0	0.40	11.0	23.87	0.85	81.12
z06CG01-02	46.3	3.7	121.5	46.4	1.0	132.2	0.38	27.4	14.83	0.83	69.11
z06CG01-03	41.3	3.30	166.7	77.4	0.2	184.6	0.46	30.8	4.42	0.75	45.85
z06CG01-04	36.5	2.92	128.3	42.1	0.1	138.0	0.33	22.0	9.59	0.81	61.46
z06CG01 (Avg.)	***40.2***	***3.2***	***119.0***	***47.4***	***0.3***	***130.0***	***0.4***	***22.8***	***13.2***	***0.8***	***64.4***
Ciales stock											
z06CS-01-01	50.2	4.02	117.7	41.8	-	-	0.36	29.85	31.6	0.86	-
z06CS-01-02	47.4	3.79	29.4	13.0	-	-	0.44	7.00	19.9	0.84	-
z06CS-01-03	49.2	3.94	88.8	39.2	-	-	0.44	21.32	13.3	0.82	-
z06CS-01 (Avg.)	***49.0***	***3.9***	***78.6***	***31.3***	-	-	***0.4***	***19.4***	***21.6***	***0.8***	-

Sample	Age (Ma)	Error	U (ppm)	Th (ppm)	147Sm (ppm)	[U]e	Th/U	He (nmol/g)	Mass (ug)	Ft	ESR
Cuyon stock											
z06CY01-01	37.5	3.00	158.4	50.1	-1.0	169.9	0.32	25.5	3.74	0.74	43.94
z06CY01-02	28.3	2.26	107.2	44.9	135.6	118.2	0.42	14.0	5.10	0.77	50.41
z06CY01-03	32.4	2.60	89.0	33.5	55.7	97.0	0.38	13.4	7.22	0.79	54.90
z06CY01-04	37.2	2.98	134.8	47.6	69.8	146.2	0.35	22.7	6.20	0.77	50.78
z06CY01 (Avg.)	***33.9***	***2.7***	***122.4***	***44.0***	***65.0***	***132.8***	***0.4***	***18.9***	***5.6***	***0.8***	***50.0***
Morovis stock											
z06MS-01-01	45.4	3.63	98.0	50.9	-	-	0.5	22.90	21.7	0.85	-
z06MS-01-02	67.6	5.40	93.7	44.7	-	-	0.5	31.70	16.4	0.83	-
z06MS-01 (Avg.)	***56.5***	***4.5***	***95.8***	***47.8***	-	-	***0.5***	***27.3***	***19.1***	***0.8***	-
Rio Grade pluton											
z08RG01-01	46.4	3.71	152.0	56.7	0.4	165.1	0.37	33.8	11.33	0.82	64.36
z08RG01-02	42.0	3.36	207.4	91.3	0.3	228.4	0.44	43.0	13.93	0.83	68.93
z08RG01-03	42.2	3.37	157.1	61.8	0.4	171.3	0.39	30.9	8.43	0.79	56.30
z08RG01 (Avg.)	***43.5***	***3.5***	***172.2***	***69.9***	***0.4***	***188.3***	***0.4***	***35.9***	***11.2***	***0.8***	***63.2***
z08RG02-01	40.3	3.22	60.1	27.3	0.4	66.4	0.45	11.9	13.28	0.82	66.85
z08RG02-02	46.9	3.75	50.0	21.5	0.4	55.0	0.43	11.5	14.72	0.82	67.29
z08RG02-03	49.8	3.98	53.3	34.6	27.3	61.4	0.65	13.4	11.35	0.81	61.79
z08RG02-04	59.2	4.74	40.7	17.1	1.2	44.7	0.42	11.8	12.68	0.82	66.68

Sample	Age (Ma)	Error	U (ppm)	Th (ppm)	147Sm (ppm)	[U]e	Th/U	He (nmol/g)	Mass (ug)	Ft	ESR
z08RG02 (Avg.)	***49.0***	***3.9***	***51.1***	***25.1***	***7.3***	***56.9***	***0.5***	***12.1***	***13.0***	***0.8***	***65.7***
z08RG03-01	46.4	3.71	110.7	52.9	0.2	122.9	0.48	23.8	5.84	0.77	51.37
z08RG03-02	33.9	2.71	379.1	128.0	0.2	408.6	0.34	60.6	10.63	0.81	62.21
z08RG03-03	47.5	3.80	81.7	33.9	0.3	89.5	0.41	19.2	16.49	0.83	72.45
z08RG03-04	38.1	3.05	369.1	132.7	0.3	399.6	0.36	65.4	8.33	0.79	57.25
z08RG03 (Avg.)	***41.5***	***3.3***	***235.1***	***86.9***	***0.3***	***255.1***	***0.4***	***42.3***	***10.3***	***0.8***	***60.8***
San Lorenzo Bath.											
z06SL03-01	41.0	3.28	110.9	44.3	0.1	121.1	0.40	21.3	7.88	0.79	57.48
z06SL03-02	36.3	2.90	149.7	47.4	-0.7	160.6	0.32	23.3	3.89	0.74	44.31
z06SL03-03	24.0	1.92	2.6	4.8	3.2	3.7	1.88	0.4	6.86	0.77	54.06
z06SL03-04	37.5	3.00	148.6	52.5	0.2	160.7	0.35	24.8	5.55	0.76	48.40
z06SL03 (Avg.)	***34.7***	***2.8***	***102.9***	***37.2***	***0.7***	***111.5***	***0.7***	***17.5***	***6.0***	***0.8***	***51.1***
Utuado Batholith											
z06UP02-01	42.9	3.43	474.0	241.0	0.2	529.5	0.51	91.4	4.80	0.74	45.45
z06UP02-02*	17.4	1.39	106.6	57.9	179.5	120.8	0.54	7.9	2.09	0.69	36.84
z06UP02-03	43.7	3.50	412.9	229.9	146.5	466.6	0.56	77.6	2.66	0.70	38.51
z06UP02-04	40.2	3.22	514.9	289.9	47.3	581.8	0.56	83.8	1.73	0.66	33.35
z06UP02 (Avg.)	***42.3***	***3.4***	***467.3***	***253.6***	***64.7***	***526.0***	***0.5***	***84.3***	***3.1***	***0.7***	***39.1***

Sample	Age (Ma)	Error	U (ppm)	Th (ppm)	147Sm (ppm)	[U]e	Th/U	He (nmol/g)	Mass (ug)	Ft	ESR
z08UP03-01	50.4	4.03	219.3	135.8	-0.2	250.6	0.62	50.7	3.69	0.74	45.12
z08UP03-02*	94.2	7.54	65.1	29.2	0.4	71.9	0.45	29.7	11.63	0.81	61.85
z08UP03-03	43.1	3.45	56.4	25.0	0.3	62.2	0.44	11.4	7.16	0.78	54.38
z08UP03-04*	1092.4	87.39	3.2	10.7	-2.6	5.6	3.36	24.1	2.12	0.68	37.05
z08UP03-05	51.2	4.09	90.8	71.2	0.7	107.2	0.78	22.5	5.28	0.76	48.55
z08UP03-06	46.7	3.73	47.2	18.2	0.3	51.4	0.38	10.0	5.37	0.77	50.74
z08UP03 (Avg.)	***47.8***	***3.8***	***103.4***	***62.5***	***0.3***	***117.8***	***0.6***	***23.7***	***5.4***	***0.8***	***49.7***
z09UP07-01	43.8	3.51	112.2	38.5	0.2	121.1	0.34	22.9	8.35	0.80	57.59
z09UP07-02	42.4	3.39	108.0	32.6	0.2	115.5	0.30	19.9	4.10	0.75	46.02
z09UP07-03	38.5	3.08	218.1	90.3	0.3	238.8	0.41	39.4	8.29	0.79	56.82
z09UP07 (Avg.)	***41.6***	***3.3***	***146.1***	***53.8***	***0.3***	***158.5***	***0.4***	***27.4***	***6.9***	***0.8***	***53.5***
Cotui Limestone											
z06CL06-01	53.9	4.31	98.8	53.1	3.7	111.0	0.54	24.0	4.42	0.74	44.92
z06CL06-02	48.0	3.84	78.3	40.9	0.4	87.7	0.52	17.6	6.56	0.77	51.74
z06CL06-03	52.0	4.16	84.3	43.0	-0.9	94.2	0.51	19.0	3.13	0.72	40.56
z06CL06-04	46.7	3.73	110.3	72.2	0.5	127.0	0.65	23.4	3.67	0.73	42.88
z06CL06 (Avg.)	***50.1***	***4.0***	***92.9***	***52.3***	***0.9***	***105.0***	***0.6***	***21.0***	***4.4***	***0.7***	***45.0***

Sample	Age (Ma)	Error	U (ppm)	Th (ppm)	147Sm (ppm)	[U]e	Th/U	He (nmol/g)	Mass (ug)	Ft	ESR
Mayagüez											
z06CF06-01*	9.9	0.79	352.5	53.3	0.7	364.8	0.15	15.1	6.70	0.78	51.48
z06CF06-02*	7.6	0.61	443.7	186.1	1.2	486.5	0.42	13.2	1.54	0.66	32.71
z06CF06-03	39.2	3.13	81.8	26.9	0.2	88.0	0.33	14.1	4.27	0.75	46.95
z06CF06-04	38.7	3.09	140.7	49.4	0.0	152.1	0.35	20.5	1.16	0.64	31.18
z06CF06 (Avg.)	***38.9***	***3.1***	***111.2***	***38.1***	***0.1***	***120.0***	***0.3***	***17.3***	***2.7***	***0.7***	***39.1***
Hormigueros											
z06HP01-01	60.4	4.83	165.1	57.9	90.6	178.9	0.35	44.6	5.39	0.76	48.41
z06HP01-02	47.4	3.79	291.9	109.6	11.1	317.2	0.38	58.7	3.47	0.72	41.24
z06HP01-03	50.2	4.01	240.6	40.2	0.3	249.9	0.17	53.1	7.92	0.78	53.26
z06HP01-04	47.5	3.80	115.2	27.7	0.2	121.6	0.24	24.9	8.65	0.80	57.93
z06HP01 (Avg.)	***51.4***	***4.1***	***203.2***	***58.8***	***25.6***	***216.9***	***0.3***	***45.3***	***6.4***	***0.8***	***50.2***
Lajas											
z09LF04-01	60.5	4.84	57.3	33.6	0.3	65.0	0.59	16.6	7.61	0.78	53.44
z09LF04-02	62.0	4.96	59.3	31.1	0.6	66.5	0.52	17.3	6.88	0.77	51.75
z09LF04-03	54.4	4.35	50.6	29.9	0.2	57.5	0.59	13.7	10.22	0.81	61.97
z09LF04-04	57.0	4.56	62.6	42.9	0.4	72.5	0.69	16.5	4.37	0.74	44.80
z09LF04-05	53.9	4.32	50.0	26.5	0.3	56.1	0.53	13.2	9.32	0.80	60.80
z09LF04-06	45.3	3.63	54.4	32.5	0.6	61.9	0.60	12.0	7.02	0.79	55.89
z09LF04 (Avg.)	***55.5***	***4.4***	***55.7***	***32.7***	***0.4***	***63.3***	***0.6***	***14.9***	***7.6***	***0.8***	***54.8***

Sample	Age (Ma)	Error	U (ppm)	Th (ppm)	147Sm (ppm)	[U]e	Th/U	He (nmol/g)	Mass (ug)	Ft	ESR
Las Tunas stock											
z06LT-01-01	55.5	4.44	34.5	18.4	-	-	0.5	9.93	23.1	0.85	-
z06LT-01-02	45.7	3.66	40.4	21.3	-	-	0.5	9.66	32.3	0.86	-
z06LT-01-03	46.4	3.71	53.1	28.1	-	-	0.5	12.43	16.8	0.83	-
z06LT-01 (Avg.)	***49.2***	***3.9***	***42.7***	***22.6***	-	-	***0.5***	***10.7***	***24.1***	***0.8***	-
Maguayo											
z09MP01-01	52.3	4.19	343.8	73.9	0.5	360.9	0.22	77.7	6.67	0.76	48.02
z09MP01-02	54.9	4.39	328.5	101.7	0.4	352.0	0.31	78.4	4.38	0.75	45.92
z09MP01-03	55.6	4.45	298.9	145.0	0.9	332.3	0.49	74.9	5.11	0.75	46.19
z09MP01 (Avg.)	***54.3***	***4.3***	***323.8***	***106.9***	***0.6***	***348.4***	***0.3***	***77.0***	***5.4***	***0.8***	***46.7***
Tibes stock											
z06TS06-01	44.1	3.53	186.6	94.4	-	-	0.5	39.29	8.6	0.79	-
z06TS06-02	49.4	3.95	100.8	55.5	-	-	0.6	25.17	16.3	0.83	-
z06TS06-03	36.3	2.90	292.5	167.2	-	-	0.6	52.72	11.0	0.81	-
z06TS06 (Avg.)	***43.3***	***3.5***	***193.3***	***105.7***	-	-	***0.5***	***39.1***	***12.0***	***0.8***	-
Cayo Ratón											
z09IC23-01	33.1	2.65	0.7	1.7	17.1	1.2	2.32	0.2	5.22	0.74	46.80

Sample	Age (Ma)	Error	U (ppm)	Th (ppm)	147Sm (ppm)	[U]e	Th/U	He (nmol/g)	Mass (ug)	Ft	ESR
Isla de Vieques											
z06IV01-01	28.2	2.26	44.6	11.7	0.3	47.3	0.26	5.9	10.74	0.81	63.47
z06IV01-02	26.5	2.12	106.6	26.2	-1.2	112.6	0.25	11.1	2.21	0.69	35.97
z06IV01-03	33.7	2.70	68.3	18.6	0.2	72.6	0.27	11.2	22.45	0.84	76.01
z06IV01-04	29.1	2.32	51.4	15.1	0.0	54.9	0.29	7.3	18.47	0.84	75.41
z06IV01 (Avg.)	***29.4***	***2.3***	***67.7***	***17.9***	***-0.2***	***71.9***	***0.3***	***8.8***	***13.5***	***0.8***	***62.7***
Tortola											
z09VI02-01	22.0	1.76	354.9	99.4	0.0	377.8	0.28	33.7	4.28	0.75	46.08
z09VI02-02	30.2	2.42	66.2	18.3	0.1	70.5	0.28	8.4	3.31	0.73	42.31
z09VI02-03	22.7	1.82	53.2	14.6	0.4	56.5	0.28	5.6	9.77	0.80	60.15
z09VI02 (Avg.)	***25.0***	***2.0***	***158.1***	***44.1***	***0.2***	***168.3***	***0.3***	***15.9***	***5.8***	***0.8***	***49.5***
Norman Island											
z09VI05-01*	-74.5	-5.96	-0.1	-0.1	-0.2	-0.1	1.73	0.0	2.08	0.69	37.79
z09VI05-02	27.4	2.19	218.2	104.2	1.7	242.2	0.48	25.8	2.73	0.72	40.86
z09VI05-03	26.7	2.14	67.3	18.1	0.0	71.5	0.27	7.1	1.84	0.69	35.79
z09VI05 (Avg.)	***27.1***	***2.2***	***142.8***	***61.2***	***0.8***	***156.9***	***0.4***	***16.4***	***2.3***	***0.7***	***38.3***

Sample	Age (Ma)	Error	U (ppm)	Th (ppm)	147Sm (ppm)	[U]e	Th/U	He (nmol/g)	mass (ug)	Ft	ESR
Virgin Gorda											
z09VI06-01	26.6	2.13	137.7	48.9	1.3	148.9	0.36	15.3	2.71	0.71	39.50
z09VI06-02	24.2	1.94	122.9	39.4	1.2	131.9	0.32	13.2	4.60	0.76	48.67
z09VI06-03	23.8	1.91	207.4	60.2	1.5	221.3	0.29	20.2	2.56	0.71	39.00
z09VI06 (Avg.)	***24.9***	***2.0***	***156.0***	***49.5***	***1.3***	***167.4***	***0.3***	***16.2***	***3.3***	***0.7***	***42.4***
z09VI12-01	23.4	1.87	118.7	28.1	0.2	125.2	0.24	13.1	13.82	0.83	70.03
z09VI12-02	23.7	1.90	48.4	14.2	0.1	51.6	0.29	5.6	16.77	0.84	74.99
z09VI12-03*	48.2	3.85	410.0	152.5	0.6	445.1	0.37	83.1	3.18	0.72	40.34
z09VI12 (Avg.)	***23.5***	***1.9***	***83.6***	***21.1***	***0.2***	***88.4***	***0.3***	***9.3***	***15.3***	***0.8***	***72.5***
Bermeja Complex											
z06BC01-01	*47.6*	*3.81*	*11.8*	*2.1*	*0.2*	*12.3*	*0.17*	*2.1*	*1.61*	*0.66*	*32.73*
z06BC01-02	*40.4*	*3.23*	*6.4*	*0.6*	*0.0*	*6.5*	*0.09*	*1.1*	*5.91*	*0.78*	*51.41*
z06BC01-03	*33.3*	*2.67*	*10.7*	*0.9*	*0.1*	*10.9*	*0.09*	*1.5*	*5.88*	*0.77*	*50.16*
z06BC01 (Avg.)	***40.5***	***3.2***	***9.6***	***1.2***	***0.1***	***9.9***	***0.1***	***1.6***	***4.5***	***0.7***	***44.8***

[U]e = Effective uranium concentration

Ft = Alpha ejection correction

ESR = Equivalent spherical radio

TABLE 3.2 (U-TH)/HE APATITE AGES AND GEOCHEMISTRY DATA

Sample	Age (Ma)	Error	U (ppm)	Th (ppm)	147Sm (ppm)	[U]e	Th/U	He (nmol/g)	mass (ug)	Ft	ESR
Rio Blanco stock											
06RB01-01	23.6	1.41	6.5	4.5	21.0	7.6	0.68	0.7	9.92	0.74	57.85
06RB01-02	26.6	1.60	12.5	8.2	30.2	14.5	0.66	1.4	4.34	0.67	44.62
06RB01-03	27.4	1.64	12.4	9.3	43.7	14.8	0.75	1.6	7.18	0.71	51.50
06RB01 (Avg.)	***25.9***	***1.6***	***10.5***	***7.3***	***31.6***	***12.3***	***0.7***	***1.2***	***7.1***	***0.7***	***51.3***
Caguas stock											
06CG01-01	33.4	2.00	12.0	21.7	17.5	17.1	1.81	2.3	12.70	0.74	60.90
06CG01-02	29.3	1.76	10.0	19.6	13.9	14.6	1.95	1.7	11.13	0.73	58.56
06CG01-03	31.1	1.87	15.7	24.7	16.1	21.4	1.58	2.6	9.08	0.72	56.19
06CG01 (Avg.)	***31.3***	***1.9***	***12.6***	***22.0***	***15.8***	***17.7***	***1.8***	***2.2***	***11.0***	***0.7***	***58.6***
Ciales stock											
06CS01-01	32.1	1.92	7.9	18.6	32.7	12.4	2.35	1.5	7.36	0.70	51.17
06CS01-02	34.3	2.06	9.1	19.3	16.7	13.7	2.10	1.8	7.25	0.70	51.22
06CS01-03	28.2	1.69	8.5	18.0	38.5	12.8	2.12	1.3	5.19	0.67	46.08
06CS01 (Avg.)	***31.5***	***1.9***	***8.5***	***18.6***	***29.3***	***13.0***	***2.2***	***1.5***	***6.6***	***0.7***	***49.5***

Sample	Age (Ma)	Error	U (ppm)	Th (ppm)	147Sm (ppm)	[U]e	Th/U	He (nmol/g)	mass (ug)	Ft	ESR
Morovis stock											
06MS01-01	29.8	1.79	3.6	6.4	8.4	5.1	1.78	0.5	2.30	0.58	35.18
06MS01-02	29.1	1.74	11.8	17.8	16.4	15.9	1.51	1.6	3.61	0.64	41.42
06MS01-03	30.6	1.84	8.7	19.1	31.3	13.2	2.20	1.4	3.14	0.62	39.26
06MS01 (Avg.)	***29.8***	***1.8***	***8.0***	***14.4***	***18.7***	***11.4***	***1.8***	***1.2***	***3.0***	***0.6***	***38.6***
Rio grande pluton											
08RG01-01	24.3	1.46	16.6	20.4	16.4	21.4	1.23	1.8	1.84	0.63	40.57
08RG01-02*	69.0	4.14	18.1	30.8	18.7	25.3	1.70	5.6	1.16	0.58	35.59
08RG01-03	27.9	1.67	7.1	14.1	17.0	10.4	1.98	0.9	1.50	0.59	36.25
08RG01 (Avg.)	***26.1***	***1.6***	***11.9***	***17.3***	***16.7***	***15.9***	***1.6***	***1.4***	***1.7***	***0.6***	***38.4***
08RG02-01	17.9	1.08	9.6	15.9	27.6	13.4	1.65	0.7	2.01	0.56	33.53
08RG02-02	20.1	1.21	12.2	19.8	23.4	16.9	1.62	1.1	2.88	0.61	38.10
08RG02-03	29.7	1.78	7.8	15.5	29.1	11.5	1.98	1.1	2.38	0.59	35.88
08RG02 (Avg.)	***22.6***	***1.4***	***9.9***	***17.1***	***26.7***	***14.0***	***1.7***	***1.0***	***2.4***	***0.6***	***35.8***
08RG03-01*	7.8	0.47	-0.1	0.5	-	-	-0.5	-6.1	0.00	13.9	-
08RG03-02	22.6	1.35	1.6	4.9	-	-	5.5	3.1	0.27	9.1	-
08RG03-03*	154.3	9.26	-0.2	0.9	-	-	-0.9	-4.6	0.01	7.6	-
08RG03-04	21.2	1.27	1.6	4.3	-	-	3.4	2.6	0.24	9.0	-
08RG03 (Avg.)	***21.9***	***1.3***	***1.6***	***4.6***	-	-	***4.4***	***2.9***	***0.3***	***9.0***	-

Sample	Age (Ma)	Error	U (ppm)	Th (ppm)	147Sm (ppm)	[U]e	Th/U	He (nmol/g)	mass (ug)	Ft	ESR
San Lorenzo Bath.											
06SL01-01	14.2	0.85	20.4	29.2	21.0	27.3	1.43	1.3	3.48	0.63	40.80
06SL01-02	16.6	1.00	20.5	27.0	21.4	26.8	1.31	1.5	3.14	0.62	39.13
06SL01-03	14.3	0.86	12.0	14.8	25.5	15.6	1.23	0.7	2.83	0.61	38.33
06SL01 (Avg.)	***15.1***	***0.9***	***17.7***	***23.7***	***22.6***	***23.2***	***1.3***	***1.2***	***3.2***	***0.6***	***39.4***
06SL03-02	29.3	1.8	10.1	13.6	9.2	13.2	1.36	1.4	5.63	0.67	45.61
Utuado pluton											
06UP02-01	31.0	1.86	14.4	26.1	41.8	20.6	1.81	2.3	4.96	0.66	45.26
06UP02-02	35.0	2.10	11.6	20.9	31.5	16.5	1.81	2.1	5.74	0.67	45.65
06UP02-03	30.2	1.81	11.6	21.4	32.2	16.7	1.84	1.8	4.29	0.64	41.63
06UP02 (Avg.)	***32.1***	***1.9***	***12.5***	***22.8***	***35.2***	***17.9***	***1.8***	***2.1***	***5.0***	***0.7***	***44.2***
08UP03-01	7.1	0.43	11.9	45.3	44.0	22.6	3.79	0.5	1.92	0.56	33.78
08UP03-02	14.3	0.86	10.9	27.4	30.4	17.4	2.51	0.7	1.40	0.52	30.01
08UP03-03	9.8	0.59	13.3	32.4	34.0	20.9	2.44	0.6	1.56	0.52	30.69
08UP03 (Avg.)	***10.4***	***0.6***	***12.1***	***35.0***	***36.1***	***20.3***	***2.9***	***0.6***	***1.6***	***0.5***	***31.5***

Sample	Age (Ma)	Error	U (ppm)	Th (ppm)	147Sm (ppm)	[U]e	Th/U	He (nmol/g)	mass (ug)	Ft	ESR
09UP07-01	18.2	1.09	7.2	10.0	36.1	9.6	1.40	0.6	1.74	0.62	39.16
09UP07-02	25.6	1.54	6.4	10.2	31.0	9.0	1.58	0.7	0.79	0.54	31.30
09UP07-03	12.9	0.78	15.6	15.4	59.8	19.4	0.99	0.9	1.54	0.62	39.07
09UP07 (Avg.)	***18.9***	***1.1***	***9.7***	***11.9***	***42.3***	***12.7***	***1.3***	***0.7***	***1.4***	***0.6***	***36.5***
Mayagüez											
07CF06-01	33.8	2.03	9.5	17.0	57.9	13.7	1.79	1.6	2.33	0.64	42.59
07CF06-02	35.0	2.10	7.3	13.8	50.3	10.7	1.88	1.4	2.97	0.69	49.23
07CF06 (Avg.)	***34.4***	***2.1***	***8.4***	***15.4***	***54.1***	***12.2***	***1.8***	***1.5***	***2.7***	***0.7***	***45.9***
Hormigueros											
06HP01-01	11.1	0.67	4.0	14.8	-	-	14.2	3.7	0.33	4.7	-
06HP01-02	49.2	2.95	1.9	4.2	-	-	11.6	2.2	0.62	7.2	-
06HP01-03	29.1	1.74	1.6	5.0	-	-	9.7	3.2	0.32	4.2	-
06HP01 (Avg.)	***29.8***	***1.8***	***2.5***	***8.0***	-	-	***11.8***	***3.0***	***0.4***	***5.4***	-
Las Tunas stock											
06LT01-01	28.5	1.71	6.2	14.9	48.2	9.8	2.42	0.9	3.22	0.61	38.97
06LT01-02	32.3	1.94	6.5	15.6	40.0	10.3	2.42	1.2	3.80	0.63	41.70
06LT01-03	32.1	1.93	6.5	16.8	50.2	10.6	2.60	1.2	4.38	0.65	43.45
06LT01 (Avg.)	***31.0***	***1.9***	***6.4***	***15.8***	***46.1***	***10.2***	***2.5***	***1.1***	***3.8***	***0.6***	***41.4***

Sample	Age (Ma)	Error	U (ppm)	Th (ppm)	147Sm (ppm)	[U]e	Th/U	He (nmol/g)	mass (ug)	Ft	ESR
Maguayo											
09MP01-02	48.4	2.90	5.8	9.4	32.5	8.1	1.63	1.2	1.58	0.54	31.38
09MP01-03	56.0	3.36	5.5	7.3	33.7	7.4	1.33	1.3	1.94	0.56	33.42
09MP01 (Avg.)	***52.2***	***3.1***	***5.6***	***8.3***	***33.1***	***7.7***	***1.5***	***1.2***	***1.8***	***0.6***	***32.4***
Tea Diorite											
06TD01-01	33.9	2.03	6.6	4.9	25.0	7.9	0.74	1.1	9.28	0.73	55.63
06TD01-02	34.5	2.07	5.5	3.7	24.9	6.5	0.67	1.0	17.47	0.78	71.20
06TD01-03	33.7	2.02	5.3	4.1	22.6	6.3	0.77	0.8	5.94	0.69	48.01
06TD01 (Avg.)	***34.0***	***2.0***	***5.8***	***4.2***	***24.2***	***6.9***	***0.7***	***0.9***	***10.9***	***0.7***	***58.3***
Isla Culebra											
07IC04-01	55.1	3.31	4.5	8.5	78.4	6.9	1.89	1.5	6.48	0.70	50.88
07IC04-02	31.7	1.90	5.0	10.4	84.8	7.8	2.07	1.0	6.37	0.69	50.34
07IC04-03	27.8	1.67	3.8	7.7	66.8	5.9	2.03	0.7	12.68	0.76	64.82
07IC04 (Avg.)	***29.7***	***1.8***	***4.4***	***9.0***	***75.8***	***6.8***	***2.1***	***0.8***	***9.5***	***0.7***	***57.6***
09IC23-01	18.9	1.13	2.4	4.2	54.1	3.7	1.73	0.2	0.79	0.54	31.54
09IC23-02	17.2	1.03	3.9	4.1	47.5	5.1	1.05	0.3	1.05	0.60	36.08
09IC23-03	20.9	1.25	3.4	5.7	51.8	5.0	1.67	0.3	0.95	0.58	35.21
09IC23 (Avg.)	***19.0***	***1.1***	***3.2***	***4.7***	***51.1***	***4.6***	***1.5***	***0.3***	***0.9***	***0.6***	***34.3***

Sample	Age (Ma)	Error	U (ppm)	Th (ppm)	147Sm (ppm)	[U]e	Th/U	He (nmol/g)	mass (ug)	Ft	ESR
Tortola											
09VI02-01	18.7	1.12	20.0	21.1	31.6	25.0	1.05	1.8	6.29	0.70	50.74
09VI02-02	19.2	1.15	22.9	22.8	40.9	28.3	1.00	2.1	6.02	0.70	50.39
09VI02-03	15.1	0.90	9.2	13.6	45.8	12.5	1.49	0.6	1.31	0.60	36.64
09VI02 (Avg.)	***17.7***	***1.1***	***17.4***	***19.2***	***39.4***	***22.0***	***1.2***	***1.5***	***4.5***	***0.7***	***45.9***
Virgin Gorda											
09VI12-01	22.1	1.33	11.4	11.2	73.9	14.3	0.98	1.3	4.22	0.72	54.48
09VI12-02*	176.6	10.60	11.8	77.3	63.9	29.9	6.57	17.4	1.35	0.59	37.55
09VI12-03	21.1	1.27	8.1	8.8	63.9	10.4	1.09	0.7	1.07	0.60	36.22
09VI12 (Avg.)	***21.6***	***1.3***	***9.7***	***10.0***	***68.9***	***12.4***	***1.0***	***1.0***	***2.6***	***0.7***	***45.4***

[U]e = Effective uranium concentration

Ft = Alpha ejection factor

ESR = Equivalent spherical radio

APPENDIX 4.1 U-Pb ZIRCON AGE OF SAMPLE 06BC01, BERMEJA COMPLEX AMPHIBOLITE

Sample Name			**207Pb/235U**		**206Pb/238U**		**207Pb/206U**		**Best age**		
Grain #	[U] ppm	U/Th	Age (Ma)	2σ error	Age (Ma)	2σ error	Age (Ma)	2σ error	(Ma)	2σ error	% Discordance*
06BC01-1	14.9	13.07	140	16	131	8.3	550	110	131	8.3	6.4
06BC01-2	7.6	4.50	148	19	131.6	9.7	600	140	131.6	9.7	11.1
06BC01-3	12.8	10.36	134	11	132	6.3	480	87	132	6.3	1.5

* The percent of discordance reported is 206Pb/238U vs 207Pb/235U.

- LAICPM-MS spot size is 30 μm diameter and 16 μm deep.

Theses analyses were made at the U-Th/He laboratory in the University of Texas-Austin.